UNIVERSITY OF OKLAHOMA

GRADUATE COLLEGE

DEVELOPING A WATER BALANCE MODEL TO ESTIMATE CONSUMPTIVE USE IN THE SOUTHEAST WATERSHED PLANNING REGION OF OKLAHOMA

A THESIS

SUBMITTED TO THE GRADUATE FACULTY

in partial fulfillment of the requirements for the

Degree of

MASTER OF ENVIRONMENTAL SCIENCE

By

WALTER CHANDLER
Norman, Oklahoma
2020

Downloaded from SHAREOK. Persistent Handle URL: https://hdl.handle.net/11244/324330

DEVELOPING A WATER BALANCE MODEL TO ESTIMATE CONSUMPTIVE USE IN THE SOUTHEAST WATERSHED PLANNING REGION OF OKLAHOMA

A THESIS APPROVED FOR THE
SCHOOL OF CIVIL ENGINEERING AND ENVIRONMENTAL SCIENCE

BY THE COMMITTEE CONSISTING OF

Dr. Jason Vogel, Chair

Dr. Jeffery Basara

Dr. Jonathan Gourley

© Copyright by WALTER CHANDLER 2020
All Rights Reserved.

Acknowledgments

First, I would like to thank my advisor Dr. Vogel for believing in me and giving me this opportunity to work with him on this project and supporting my graduate education. The knowledge and experience I've gained not only from this research, but the many other opportunities I've had during my two years at the Oklahoma Water Survey have been immensely beneficial. His passion for solving water and environmental related issues is truly inspiring, and I consider myself very lucky to have worked with him these past two years. I also want to thank my other committee members, Dr. Basara and Dr. Gourley for providing their expertise and guidance throughout this project.

Next I want to thank all the current and former Water Survey employees who contributed to this project in some way or another. Special thanks to Grant Graves and Shana Mashburn for providing their expertise in helping me solve the countless problems that arose from this research, and to all my fellow student employees who helped with the tedious GIS analyses or kayaking around ponds collecting bathymetric data in the middle of summer. Their assistance was crucial to this research and I am extremely grateful.

Finally, I want to thank my family and friends for all their love and support, especially my amazing fiancé Suzie. I would not have been able to accomplish all I have the past two years without her constant encouragement and love. I thank God for surrounding me with such wonderful people who care for me deeply.

Table of Contents

List of Tables vi

List of Figures viii

List of Appendix Tables xii

Abstract xiv

Chapter 1 – Introduction 2

Chapter 2 - Background 5

2.1 Water Balance Models 5
2.2 Consumptive Use 8

Chapter 3 – Study Area 12

3.1 Physical Geography 12
3.2 Hydrology 16
3.3 Human Geography 18

Chapter 4 – Methodology 20

4.1 Precipitation 22
4.2 Streamflow 23
4.3 Surface Storage Change 27
4.3.1 Mapped Surface Waterbodies 28
4.3.2 Unmapped Surface Waterbodies 33
4.4 Sub-surface Storage 41
4.5 Evapotranspiration 44
4.6 Additional Hydrologic Components 46
4.6.1 Baseflow 46
4.6.2 Wastewater Discharges 47
4.6.3 Reservoir Discharges 48
4.7 Statistical Methods 48

Chapter 5 – Results & Discussion 51

5.1 Water Balance Model Components 51
5.2 Uncertainty 55
5.2.1 Precipitation 55
5.2.2 Streamflow 56
5.2.3 Surface Storage Change 57
5.2.4 Sub-surface Storage Change 59
5.2.5 Evapotranspiration 60
5.3 Water Balance Model Component Analysis 61
5.4 Baseflow, Wastewater Discharges, and Reservoir Discharges 69
5.5 Consumptive Use 74
5.6 Total Water Balance Model Uncertainty 79
5.7 Annual Water Balance Model 80

Chapter 6 – Conclusions & Future Research 86

References 91

Appendix 97

List of Tables

Table 1: Estimated water demand by sector (cm) in the Southeast Watershed Planning Region of Oklahoma for 2010 and projected for 2020-2060 (OWRB, 2011b). 19

Table 2: United State Geological Survey (USGS) stream gauges used to calculate net flow gains for Southeast Watershed Planning Region of Oklahoma outflow streams. 25

Table 3: Regression equations to estimate storage volume from surface area on mapped Southeast Watershed Planning Region of Oklahoma reservoirs, where *V* is storage volume in ac-ft and *A* is surface area in ac. R^2 is the coefficient of determination for each equation. 31

Table 4: Performance metrics used to evaluate regression models for predicting lentic waterbody storage volume from surface area. R^2 = coefficient of determination, nRMSE = standard deviation normalized root mean square error, NSE = Nash-Sutcliffe Efficiency, and % bias = percent bias. 37

Table 5: Regression models for predicting storage volume of small and large unmapped lentic waterbodies in the Southeast Watershed Planning Region of Oklahoma, evaluated with performance metrics. Chosen models are shown in **bold**. 38

Table 6: Minimum quantifiable uncertainty of each water balance model (WBM) component shown as an average % of the total quarterly volume. NA was given for components that had no quantifiable uncertainty. WBM components include precipitation (P), streamflow out (Q_{out}), evapotranspiration (ET), surface storage change (ΔS_{surf}), and sub-surface storage change (ΔS_{sub}). 55

Table 7: Mean (μ) in cm and coefficient of variation (CV) of precipitation (P), evapotranspiration (ET), streamflow out (Q_{out}), total surface storage (S_{surf}). For sub-surface storage change (ΔS_{sub}), the standard deviation (σ) is shown instead of CV. ... 62

Table 8: Correlation matrix with Pearson correlation coefficients (CC) between the water balance model (WBM) components and additional variables and sub-components used in analysis. The WBM components include precipitation (P), evapotranspiration (ET), streamflow out (Q_{out}), surface storage change (ΔS_{surf}), and sub-surface storage change (ΔS_{sub}). The additional sub-components and variables are solar radiation (R), baseflow (BF), wastewater discharges (WWD), and reservoir discharges (RD). * denotes significance at the 95% confidence level. 62

Table 9: Quarterly baseflow (BF) depths in cm and baseflow index (BFI) values for streams flowing out of the Southeast Watershed Planning Region of Oklahoma. Data from United State Geological Survey. 70

Table 10: Quarterly wastewater discharge (WWD) depths within the Southeast Watershed Planning Region of Oklahoma. Data from Oklahoma Department of Environmental Quality. 71

Table 11: Quarterly reservoir discharge (RD) depths from Broken Bow Lake, Hugo Lake, and Pine Creek Lake. Data from United States Army Corps of Engineers. 73

Table 12: Estimated quarterly consumptive use + error (C_{+err}) depths from the Southeast Watershed Planning Region of Oklahoma water balance model. 75

Table 13: Correlation coefficients between consumptive use + error (C_{+err}) and each of the other water balance model component for each of the four annual quarters, and for all quarters combined. The WBM components include precipitation (P), evapotranspiration (ET), streamflow out (Q_{out}), surface storage change (ΔS_{surf}), and sub-surface storage change (ΔS_{sub}). * denotes significance at the 95% confidence level. 77

Table 14: Quarterly consumptive use + error (C_{+err}) volumes with minimum uncertainty given in both cm and relative percent. 80

Table 15: Results of the annual water balance model (WBM) analysis. Annual volumes for each WBM component and consumptive use + error (C_{+err}) are given in cm along with the average annual volumes for 2007-2017. WBM components include precipitation (P), streamflow out (Q_{out}), evapotranspiration (ET), surface storage change (ΔS_{surf}), and sub-surface storage change (ΔS_{sub}). 82

Table 16: Average annual coefficient of variation (CV) values for the annual water balance model (WBM) component's, and average quarterly CV values for the quarterly WBM components. WBM components include precipitation (P), streamflow out (Q_{out}), evapotranspiration (ET), surface storage change (ΔS_{surf}), and sub-surface storage change (ΔS_{sub}). Total surface storage (S_{surf}) was used to represent ΔS_{surf} variability. * standard deviation was used to represent ΔS_{sub} variability. 85

Table 17: Limitations and suggestions for how to improve and reduce uncertainty for each water balance model (WBM) component estimation method. WBM components include precipitation (P), streamflow out (Q_{out}), evapotranspiration (ET), surface storage change (ΔS_{surf}), and sub-surface storage change (ΔS_{sub}). Some limitations are specific to the Southeast Watershed Planning Region of Oklahoma (SEWPR). 90

List of Figures

Figure 1: Visualization of the natural hydrologic cycle from the United States Geological Survey. 3

Figure 2: European Union Water Framework Directive water balance model (European Commission, 2015). 7

Figure 3: Watershed Planning Regions of Oklahoma. Map courtesy of the 2012 Oklahoma Comprehensive Water Plan from the Oklahoma Water Resources Board (OWRB, 2011a)..... 13

Figure 4: Level III Ecoregions located within the Southeast Watershed Planning Region of Oklahoma. Data from the United States Environmental Protection Agency..... 14

Figure 5: Land cover classification in the Southeast Watershed Planning Region of Oklahoma from the National Land Cover Database (NLCD 2016)..... 15

Figure 6: Topography of the Southeast Watershed Planning Region of Oklahoma. Data from United States Geological Survey Digital Elevation Model..... 15

Figure 7: Major waterbodies within the Southeast Watershed Planning Region of Oklahoma. Data from Oklahoma Water Resources Board and United States Geological Survey. 17

Figure 8: Major and minor aquifers underlying the Southeast Watershed Planning Region of Oklahoma. Map courtesy of the 2012 Oklahoma Comprehensive Water Plan – Southeast Watershed Planning Region Report from the Oklahoma Water Resources Board (OWRB, 2011b). 17

Figure 9: Precipitation accumulations from the National Centers for Environmental Prediction Stage IV Quantitative Precipitation Estimates in the Southeast Watershed Planning Region of Oklahoma for 2007 Quarter 1. 23

Figure 10: Active United States Geological Survey stream gauges within the Southeast Watershed Planning Region (USGS, 2019b)..... 24

Figure 11: Location of United States Geological Survey stream gauges on Little River, Red River, and Lower Mountain Fork River used for streamflow out (Q_{out}) estimation in the Southeast Watershed Planning Region of Oklahoma (SEWPR). 26

Figure 12: Locations of Oklahoma Water Resource Board mapped reservoirs in the Southeast Watershed Planning Region of Oklahoma. Imagery from United States Department of Agriculture National Agricultural Imagery Program..... 30

Figure 13: Contour intervals used to determine surface area to storage volume relationships for mapped Oklahoma Water Resource Board reservoirs. 5 feet intervals for Lake Nanih Waiya are shown. Imagery from United States Department of Agriculture National Agricultural Imagery Program..... 31

Figure 14: True color Red-Green-Blue (left), Modified Normal Difference Water Index (MNDWI) (middle), and binary raster (right) images of Lake Nanih Waiya derived from Landsat reflectance data. Pixels with higher MNDWI values are shown in dark blue (middle), and pixels identified as water in the binary raster are shown in light blue (right). 33

Figure 15: Bathymetric data collection on waterbody in the Southeast Watershed Planning Region of Oklahoma, including the kayak with fish finder mounted on the right side (left). Collection of shoreline global positioning system points used for bathymetric data processing (right). 35

Figure 16: Depth points collected from a bathymetric survey of a lentic waterbody in the Southeast Watershed Planning Region of Oklahoma on 10/28/2019 (left) and contour intervals and depth raster surface derived from collected depth points used to estimate storage volume (right). 37

Figure 17: Distribution of selected United States Department of Agriculture National Agricultural Imagery Program (NAIP, 2018) images for unmapped waterbody digitizing from 2015 Quarter 3. 40

Figure 18: Example of a digitized waterbody from 2008 United States Department of Agriculture National Agricultural Imagery Program imagery in the Southeast Watershed Planning Region of Oklahoma. 40

Figure 19: Operational Simplified Surface Energy Balance model actual evapotranspiration in inches for the Southeast Watershed Planning Region of Oklahoma for 2007 Quarter 1, with United State Army Corps of Engineers reservoirs removed (FEWS NET, 2019). 45

Figure 20: Trends of quarterly precipitation (P), evapotranspiration (ET), streamflow out (Q_{out}), surface storage change (ΔS_{surf}), and sub-surface storage change (ΔS_{sub}). P, ET and Q_{out} are shown on the left axis, and ΔS_{surf} and ΔS_{sub} are shown on the right axis to account for the negative values. 52

Figure 21: Trends of quarterly precipitation (P). Data from the National Centers for Environmental Prediction Stage IV Quantitative Precipitation Estimates. 52

Figure 22: Trends of quarterly streamflow out (Q_{out}). 53

Figure 23: Trends of quarterly evapotranspiration (ET). Data from the Famine Early Warning Systems Network. 53

Figure 24: Trends of quarterly surface storage change (ΔS_{surf})..... 54

Figure 25: Trends of quarterly sub-surface storage change (ΔS_{sub}). Data from the Gravity Recovery and Climate Experiment satellite mission. 54

Figure 26: Trends of quarterly precipitation (*P*) and evapotranspiration (*ET*). *P* data from the National Centers for Environmental Prediction Stage IV Quantitative Precipitation Estimates and *ET* data from the Famine Early Warning Systems Network. 64

Figure 27: Trends of quarterly evapotranspiration (*ET*) in cm (left axis) and solar radiation (*R*) in Mega Joules (MJ) (right axis). *ET* data from the Famine Early Warning Systems Network and *R* data from Oklahoma Mesonet. 64

Figure 28: Trends of quarterly precipitation (*P*) and streamflow out (Q_{out}). *P* data from the National Centers for Environmental Prediction Stage IV Quantitative Precipitation Estimates. 66

Figure 29: Trends of quarterly surface storage change(ΔS_{surf}) and sub-surface storage change (ΔS_{sub}). ΔS_{sub} data from the Gravity Recovery and Climate Experiment satellite mission. 67

Figure 30: Trends of quarterly sub-surface storage change (ΔS_{sub}) (left axis) and evapotranspiration (*ET*) (right axis). ΔS_{sub} data from the Gravity Recovery and Climate Experiment satellite mission and *ET* data from the Famine Early Warning Systems Network. 68

Figure 31: Trends of quarterly surface storage change (ΔS_{surf}) (left axis) and precipitation (*P*) (right axis). *P* data from the National Centers for Environmental Prediction Stage IV Quantitative Precipitation Estimates. 68

Figure 32: Trends of quarterly baseflow (BF) and streamflow out (Q_{out}). BF data from United States Geological Survey. 70

Figure 33: Percentage of total quarterly wastewater discharge (WWD) in the Southeast Watershed Planning Region of Oklahoma from different water use sectors (ODEQ, 2018). 72

Figure 34: Trends of quarterly streamflow out (Q_{out}) and reservoir discharges (RD). RD data from the United States Army Corps of Engineers. 73

Figure 35: Trends of quarterly consumptive use + error (C_{+err}) depths. 75

Figure 36: Trends of quarterly consumptive use + error (C_{+err}) and surface storage (ΔS_{surf}) depths. 77

Figure 37: Trends of quarterly consumptive use + error (C_{+err}) (left axis) and precipitation (P) (right axis) depths. P data from the National Centers for Environmental Prediction Stage IV Quantitative Precipitation Estimates. 78

Figure 38: Trends of quarterly consumptive use + error (C_{+err}) (left axis) and evapotranspiration (ET) (right axis) depths. ET data from the Famine Early Warning Systems Network. 78

Figure 39: Trends of quarterly consumptive use + error (C_{+err}) and net precipitation (Net P) (precipitation – evapotranspiration) depths. 79

Figure 40: Trends of annual precipitation (P), streamflow out (Q_{out}) and evapotranspiration (ET) depths. P data from the National Centers for Environmental Prediction Stage IV Quantitative Precipitation Estimates. ET data from the Famine Early Warning Systems Network. 83

Figure 41: Trends of annual surface storage change (ΔS_{surf}) and sub-surface storage change (ΔS_{sub}) depths. ΔS_{sub} data from the Gravity Recovery and Climate Experiment satellite mission. 83

Figure 42: Trends of annual consumptive use + error (C_{+err}) depths. 84

List of Appendix Tables

Table A1: Quarterly streamflow coefficients (SC) representing the proportion of long-term average (1971-2017) to observed net flow gain from 2007-2017 for the Little River and Red River. Data from the United States Geological Survey. 97

Table A2: StreamStats average annual flow in cubic feet per second (cfs), and drainage area in square kilometers (km^2) for each outflow stream in the Southeast Watershed Planning Region of Oklahoma. Streams are organized in ascending order by drainage area. Data from the United States Geological Survey. 98

Table A3: Quarterly storage in cm for United States Army Corps of Engineers (USACE) managed reservoirs within the Southeast Watershed Planning Region of Oklahoma, including Broken Bow Lake, Hugo Lake, Pine Creek Lake, and Sardis Lake. The first

day of each quarter was used as the storage depth. Data from USACE Tulsa District. 99

Table A4: Estimated quarterly storage in cm for reservoirs within the Southeast Watershed Planning Region with bathymetric data from the Oklahoma Water Resources Board (OWRB) including Lake Carl Albert, Lake Nanih Waiya, Ozzie Cobb Lake, and Schooler Lake. Storage depth was estimated on the day closest to the beginning of each quarter that a suitable Landsat image was available to estimate surface area, using equations in Table 3. 101

Table A5: Surface area in acres (ac) and storage volume in acre-feet (ac-ft) for 17 small lentic waterbodies in the Southeast Watershed Planning Region of Oklahoma, based on bathymetric data was collected between July and October, 2019. Each waterbody also includes the area and volume for each contour interval below the actual shoreline, which provided additional area-volume data to build regression equations (Table 5). 102

Table A6: Estimated total quarterly unmapped waterbody storage within the Southeast Watershed Planning Region of Oklahoma. Quarters in **bold** had available imagery from the United States Department of Agriculture National Agricultural Imagery Program used to calculate waterbody surface area. 105

Table A7: Estimated quarterly change in equivalent water thickness (EWT) in cm for the Southeast Watershed Planning Region of Oklahoma (SEWPR). EWT represents the total amount of surface-water, groundwater, and soil moisture across the SEWPR. Quarters in *italics* were estimated using linear interpolation (Equation 14). 2017 Q3 and Q4 (denoted with *) were estimated using a regression model (Equation 15) due to a lack of available data for those quarters. Data from the Gravity Recovery and Climate Experiment satellite mission. 105

Table A8: Quarterly depths in cm for all water balance model components including precipitation (P), streamflow out (Q_{out}), evapotranspiration (ET), surface storage change (ΔS_{surf}), and sub-surface storage change (ΔS_{sub}). Negative depths for ΔS_{surf} and ΔS_{sub} indicate a decrease in total storage from the previous quarter. Maximum values for each component are written in **bold**, minimum values are written in *italics*. 106

Abstract

With the passage of the Water for 2060 Act, Oklahoma established a statewide goal of consuming no more freshwater in 2060 than was consumed in 2012. However, there currently does not exist a quantifiable method to estimate consumptive water use in the long-term. A quantitative analysis of freshwater consumptive use in Oklahoma using a water balance approach would not only make it possible to gauge whether quantifiable water use goals are being met, but would also be useful for water resource managers across the state to track consumptive use and determine where and when conservation strategies may be implemented to have the most impact.

A water balance model (WBM) was developed to quantify consumptive water use at a Watershed Planning Region scale in Oklahoma. Under perfect natural conditions, the inflow and outflow water volumes in a region over a given period of time will be equal. However, humans disturb the natural conditions by removing water from the hydrologic cycle through consumptive use. Considering consumptive use as a component of the water balance, the volumes of each inflow and outflow component of the water balance were estimated, and consumptive use was estimated using a water balance equation as the residual imbalance caused by humans removing the water from the natural system. The WBM was developed for the Southeast Watershed Planning Region of Oklahoma (SEWPR) at a quarterly (3-month) temporal scale, with the goal of applying the model to other Watershed Planning Regions in the future.

The WBM results for quarterly consumptive use were unrealistically high and even negative in some cases. The likely cause of these extreme values is the large and mostly unknown uncertainty associated with the WBM component estimation methodologies. While the WBM is currently not suitable for consumptive use estimation, the gathered data, developed

methodologies, and valuable information obtained from this research provide a useful framework for future research.

Foreword

This study set out to develop and test a methodology for estimating consumptive water use on a watershed scale using a water balance model (WBM) approach. Each of the WBM components were estimated for the spatial and temporal scale of the model, and consumptive use estimates were calculated. The consumptive use estimates in this study are provided to show how the WBM functions, and to highlight current limitations in areas that require improvement. The objective of this study was to develop the methodologies for the WBM, not to provide realistic and accurate consumptive use estimates. This project was a success, because the framework for meeting the overall goal of providing water resource managers with a useful tool for tracking consumptive use through the use of the WBM was established. In addition, several methods described in this report include innovative approaches for estimating WBM components that were developed specifically for this study, but have potential applications for many different water resources related challenges.

Chapter 1 – Introduction

As populations continue to rise, the demand for water resources increases as well. Conservation initiatives to reduce human consumption of water have become an important aspect of water resource management. The state of Oklahoma passed the Water for 2060 Act in 2012, which established a statewide goal of consuming no more freshwater in 2060 than was consumed in 2012 (H.B. 3055). However, there currently does not exist a quantifiable method to estimate consumptive freshwater use on an ongoing basis that can be used to guide policy and management decisions in Oklahoma. The Oklahoma Water Resources Board (OWRB) released the Oklahoma Comprehensive Water Plan (OCWP) in 2012 which included reports for each of the 13 watershed planning regions across the state. The reports contain data for water use and demand estimates, but no direct estimate of consumption. This is often due to insufficient or unreliable water withdrawal and return data from water users. Methods for estimating consumptive freshwater use on at least an annual scale, which do not rely on estimated water use data, must be developed for Oklahoma. This would allow water resource managers to determine consumptive water use in any given year, including the 2012 target goal for 2060 and in future years to track progress towards this goal.

This study explores the method of using a water balance model (WBM) to estimate consumptive freshwater use on a watershed planning region scale in Oklahoma. A WBM is a simple and refined method for understanding hydrologic processes and interactions on some spatial scale (Martinez and Gupta 2010). The WBM developed in this study does not rely on human water use estimates, but rather uses components of the natural hydrologic cycle (Figure 1) that have already been estimated or were estimated using available data.

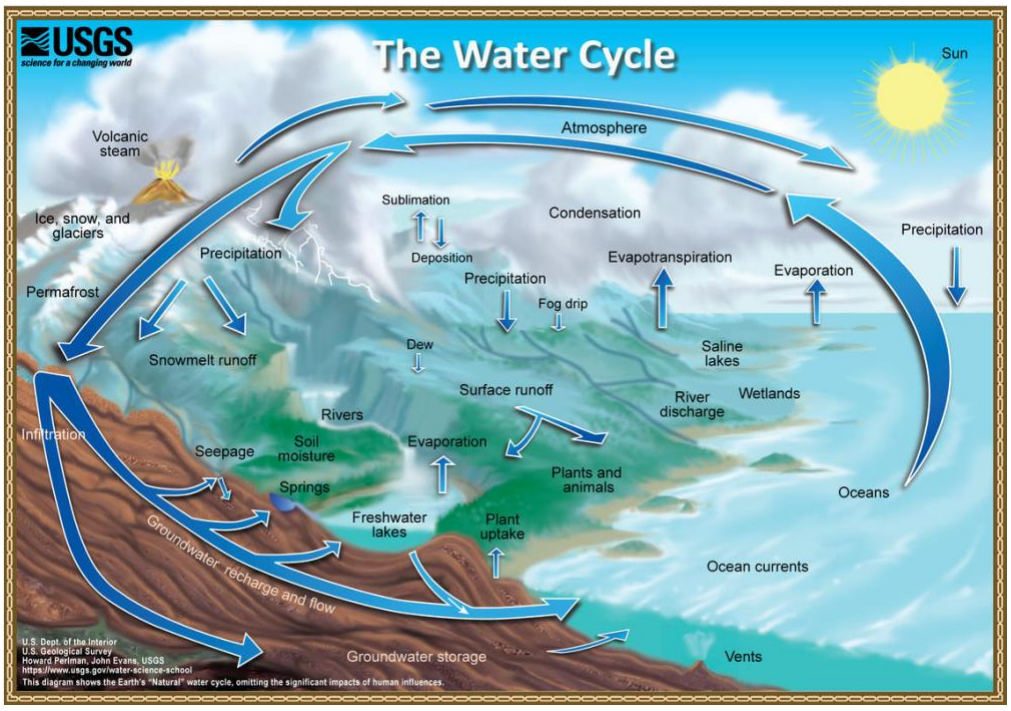

Figure 1: Visualization of the natural hydrologic cycle from the United States Geological Survey.

The overall goal of this project was to provide water resource managers in Oklahoma – and potentially other states – with a useful tool for tracking consumptive use through the use of the WBM. If the model can be successfully used to estimate consumptive use in Oklahoma, it could help facilitate more water use studies, and provide a useful way to track progress towards water use goals, such as Water for 2060.

The main objective of this project was to develop a WBM designed to estimate human consumptive water use by considering it as an output component of the water balance equation. Consumptive use was estimated by quantifying all other hydrologic inputs and outputs to a region, and solving the WBM equation for consumptive use as the residual imbalance of the natural hydrologic balance.

In addition, there were two sub-objectives. The first was to quantify the uncertainty associated with each WBM component estimation method and add up all uncertainty to calculate

the overall uncertainty of the consumptive use estimation output of the WBM. The second was to estimate other important hydrologic components within the SEWPR boundary that are incorporated into other major components. These include wastewater discharges, reservoir discharges, and baseflow.

Chapter 2 - Background

In this chapter, background information for the concepts of water balance models (WBM) and consumptive water use is provided. Information from previous studies on both the use of WBMs for hydrologic variable estimation, and on consumptive use estimation methods, are provided. This information is necessary to fully understand the need for alternative methods for consumptive use estimation, and how a WBM approach could be used for consumptive use estimation.

2.1 Water Balance Models

One of first known studies to utilize the concept of a WBM was done by Thornwaite & Mather (1955). They developed a method to estimate potential evapotranspiration (PET) using a simple mass balance equation of hydrologic inputs and outputs, solved for PET. This study is considered by many to be the first to introduce the idea of using seasonal hydrologic data in a WBM to estimate unknown components of the hydrologic cycle (Ferguson 1996). Since then, WBMs have been adopted and modified for use in numerous water-resource studies. The increased complexity has allowed WBMs to be applied to a wide range of hydrologic problems, including the impacts of climate change on hydrologic systems (Gleick, 1987; Guo et al., 2002; Wang et al., 2009), runoff estimation (Schaake et al., 1996; Arnell, 1999), and groundwater recharge (Westonboek et al., 2010).

Despite the many different applications for WBMs, most differ in details such as the input data required, the spatial and temporal scale, and scope of hydrologic processes they aim to address, but are similar in overall concept. In their review of WBMs, Xu and Singh (1998) outline some of the common features among typical WBMs: (1) they describe spatially averaged hydrologic processes, (2) they require hydrologic data at specific time scales as input parameters,

and they may utilize other non-hydrologic data inputs, and (3) the basis of the models is the water-balance equation. The water-balance equation can take many forms depending on the objectives of the research and the intended output of the WBM. However, all water-balance equations take the same general form of the continuity equation, where:

$$Change\ in\ storage = Inflow - Outflow$$

A simple form of the equation above, in which major outflow and inflow components of the water balance for a watershed are represented, is written as:

$$\Delta S = P + Q_{in} - ET - Q_{out} \quad (1)$$

where P is precipitation, Q_{in} is streamflow into the watershed, ET is actual evapotranspiration (the sum of evaporation from soils, surface-water bodies, and plants), ΔS is change in water storage over time, and Q_{out} is streamflow out of the watershed (Healy et al., 2007). The number of water balance components differs depending on the complexity and intended output of the WBM. Equation 1 employs only the basic hydrologic components, with groundwater interactions ignored. More complex models may contain additional components such as soil moisture change (Xu and Chen, 2005; Saravanane et al., 2014), infiltration or groundwater recharge (Alemaw and Chaoka, 2003; Martinez and Gupta, 2010), or even irrigation (Andales et al., 2011). Figure 2 shows the components of a moderately complex WBM developed by the European Commission for the European Union Water Framework Directive (European Commission, 2015). In some models, ΔS is considered negligible and ignored, or left as the remaining component for which to solve the WBM equation for. This depends on the objective and spatial/temporal scale of the WBM. ΔS is usually ignored in mean annual or interannual WBM calculations, but even then, some temporal variability is lost by ignoring ΔS (Wang, 2012).

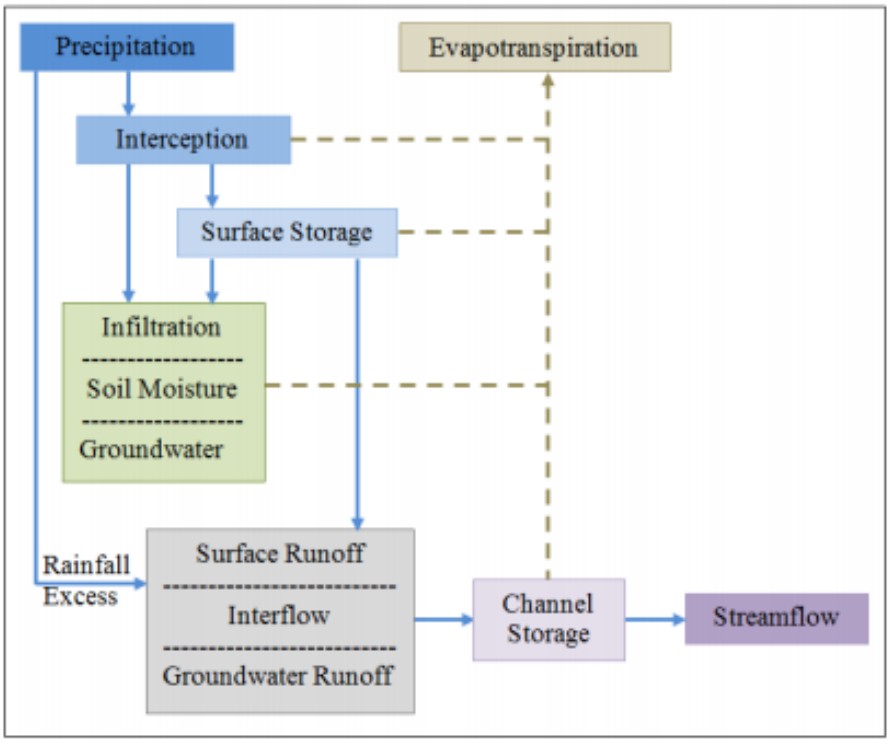

Figure 2: European Union Water Framework Directive water balance model (European Commission, 2015).

For typical WBMs, any component can be estimated provided that all other components can be calculated or estimated from available data. For example, the United State Geological Survey (USGS) developed a method for estimating groundwater recharge within a watershed. The model estimates precipitation, surface water inflow/outflow, interception, evapotranspiration, and change in soil moisture by using data inputs of climate, land use, hydrologic soil group, flow direction, and soil-water capacity data (Westonboek et al. 2010). Most WBMs are used to estimate historical fluxes or predict future fluxes in natural hydrologic processes. However, with growing populations creating a greater demand for water resources, there is an apparent need for evaluation of human impact on the water balance.

2.2 Consumptive Use

One way to measure the impact of humans on the natural water balance is by estimating human consumptive water use. USGS defines consumptive water use as "water that is evaporated, transpired, incorporated into products or crops, consumed by humans or livestock, or otherwise removed from an immediate water environment" (Shaffer, 2008). A distinction is also made between consumptive water use and water withdrawals. Water withdrawals refer to the total water withdrawn from surface or groundwater systems. Much of that water is returned to the hydrologic systems immediately or after a short period of time. This portion can be considered non-consumptive water use. Major non-consumptive water uses include industrial or domestic water uses that are captured as wastewater, treated, and discharged back in the system. Withdrawn water that is not returned back to the system is considered consumptive use. For the US, irrigation and thermoelectric power are the largest consumptive uses of water (Maupin et al. 2014). Estimating consumptive use and understanding its role in the water balance is critical for water resources management.

Consumptive use is commonly estimated in one of two ways: (1) by application of consumptive use coefficients; and (2) using a water balance equation (Shaffer, 2008). For the consumptive use coefficient method, the coefficients are calculated by subtracting total withdrawn water returned from total water withdrawn, and then dividing by total water withdrawn. Typically, the coefficients are represented as a percent. Coefficients calculated for a specific area where withdrawal and return flow data is available are typically applied to larger areas where return flow data may not be available. At a minimum, complete water withdrawal data for the entire area and time interval of interest is required to use the consumptive use coefficient method.

A USGS study estimated consumptive water use in the Great Lakes Basin using the

consumptive use coefficient method. Coefficients calculated or referenced in other studies conducted for the Great Lakes Basin, or climatically similar areas, were compiled for different water use categories: domestic and public supply, industrial, thermoelectric power, irrigation, livestock, commercial, and mining. The coefficients for each water use category were statistically analyzed to determine the appropriate consumptive use coefficient to apply to the Great Lakes Basin (Shaffer and Runkle, 2007). The major limitation of this study was the sources of the consumptive use coefficients. Some of previous studies from which coefficients were taken were over 10 years old at the time of the study. Many studies were also listed as secondary sources for the coefficients they provided, meaning they were calculated even earlier. Even if the USGS study utilized current water withdrawal data in their calculation of consumptive use, the older coefficients used in the analysis could lead to an inaccurate representation of current consumptive water use patterns.

Another USGS study utilized similar methods to estimate consumptive use for irrigation and thermoelectric power for each US state in 2015 (Dieter et al., 2018). One limitation of this consumptive use data is that it does not include all major water use categories, only irrigation and thermoelectric power. While these were the largest two categories for the entire US in 2015 (41% and 37% respectively) this may not be the case in all areas. Another limitation is the infrequency of estimation. 2015 was the first year since 1995 that consumptive use estimates were included in the USGS water use report. Even if they continue to include the data in future reports, new data will only be available every five years. The data is also only available at the state level, so additional assumptions must be made to use the data for areas smaller than statewide scale.

Another method for consumptive use estimation, the water balance method, may provide

a way to estimate consumptive use in a more complete and frequent manner than previously used methods. The water balance method equation for estimating consumptive use can take several forms. The simplest form is the same basic equation for calculating consumptive use when total withdrawal and return flow data is known (Shaffer and Runkle, 2007).

$$Consumptive\ use = Withdrawal - Return\ flows$$

Similar to the consumptive use coefficient method, successful use of this form of a water balance equation is limited to areas where withdrawal and return flow data is available. These areas may include individual commercial, industrial, or agricultural operations, municipalities, states, or even nations. It is rare to find applications on a watershed scale, since water use data is typically organized based on private or political boundaries, rather than by watershed boundaries. A study by Tidwell et al. (2014) estimated water availability and future consumptive use for 17 western states in the US. Consumptive water use was estimated with a simple water balance equation using historical water use data from each state's water plan. The consumptive use projections for 2030 were estimated using linear extrapolation from current consumptive use estimates and population growth estimates (Tidwell et al., 2014). While this study provided important information for future water resource management, the methods relied on the availability of statewide water withdrawal data, which may not be available at different spatial or temporal scales. The study also did not incorporate their estimations into the overall water balance, such as the one shown in Figure 2.

To the author's knowledge, there are no studies which employ a holistic water balance approach to estimating consumptive water use on a watershed scale. The consumptive water use studies reviewed here are dependent on the availability of water withdrawal data, and/or previously calculated consumptive use coefficients. These studies also do not provide

consumptive use data in a frequent or semi-frequent time frame (e.g. monthly or quarterly). An important factor in watershed management is knowing the quantity of water flowing in and out of the watershed over a certain period of time, and how much is available for human use. The need for an integrated WBM approach for estimating human water use is apparent. The WBM approach proposed in this study utilizes readily and frequently available hydrologic data and validated estimation methods for the calculation of water balance components. In order for water use goals such as the state of Oklahoma's Water for 2060 Act to be met, timely water use estimations are needed.

Chapter 3 – Study Area

This chapter describes the physical geography, hydrology, and human geography of the project study area which is the Southeast Watershed Planning Region (SEWPR) of Oklahoma as defined by OWRB (OWRB, 2011a). There are 13 different watershed planning regions across Oklahoma separated by both watershed and state boundaries (Figure 3). The SEWPR was chosen as the initial study area because it has one of the lowest water demands of the 13 planning regions (OWRB, 2011a). Selecting a region with lower demand simplified the WBM analysis so the methods could be developed and tested more easily.

3.1 Physical Geography

The SEWPR encompasses almost 11,500 square kilometers (km^2) located in the southeastern corner of the state and includes all of McCurtain County, and portions of Atoka, Choctaw, Latimer, Le Flore, Pittsburg, and Pushmataha Counties. The SEWPR is located within two different United States Environmental Protection Agency (US EPA) Level III Ecoregions (Woods et al., 2005), the Ouachita Mountains in the north, and the South Central Plains in the south (Figure 4). The primary land cover types within the SEWPR are Deciduous Forest and Evergreen Forest covering 27.5% and 26.2% of the region respectively, followed by Pasture/Hay covering 15.3% (NLCD, 2016). The region contains only 4.2% developed land, with 89% of that being open space developed (Yang et al., 2018) (Figure 5). The topography of the SEWPR varies greatly, from the Kiamichi Mountains in the north which reach heights of over 820 meters (m) above sea level, to the alluvial plains and hardwood wetlands near the Red River in the south with minimum elevations of approximately 40 m. The total relief within the SEWPR is

approximately 780 m with elevation generally increasing going from south to north with the exception of a few valleys between mountain ranges in the north (Figure 6).



Figure 3: Watershed Planning Regions of Oklahoma. Map courtesy of the 2012 Oklahoma Comprehensive Water Plan from the Oklahoma Water Resources Board (OWRB, 2011a).

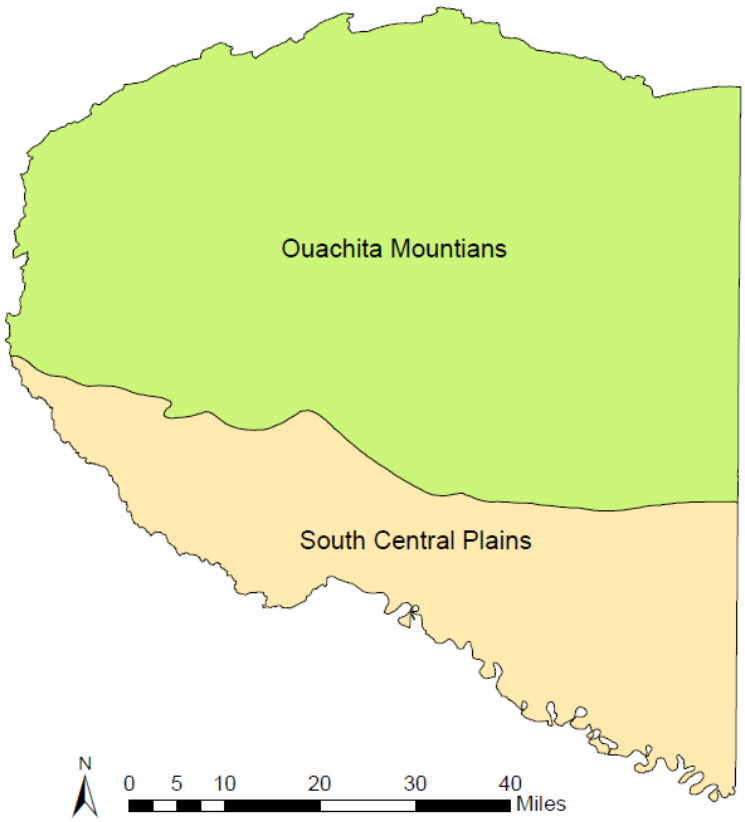

Figure 4: Level III Ecoregions located within the Southeast Watershed Planning Region of Oklahoma. Data from the United States Environmental Protection Agency.

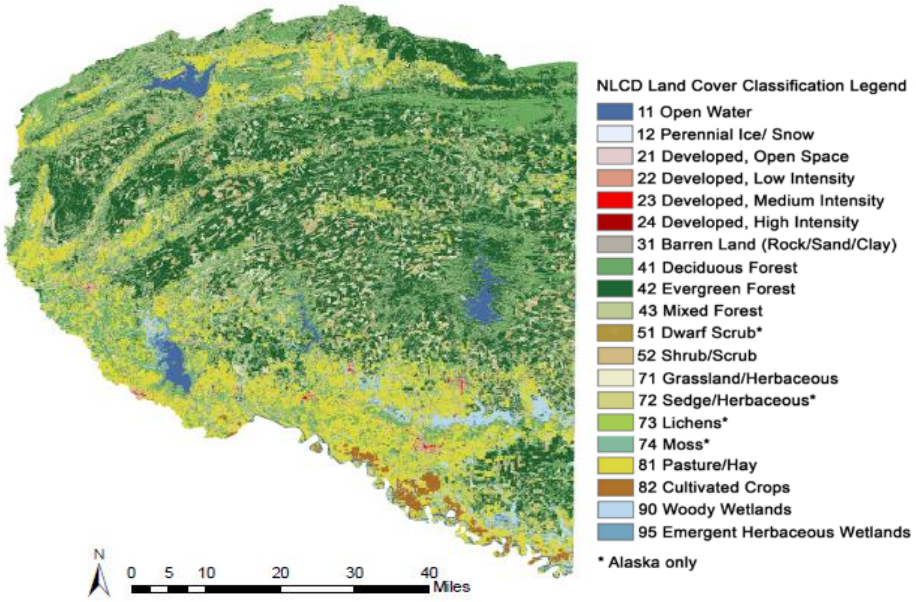

Figure 5: Land cover classification in the Southeast Watershed Planning Region of Oklahoma from the National Land Cover Database (NLCD 2016).

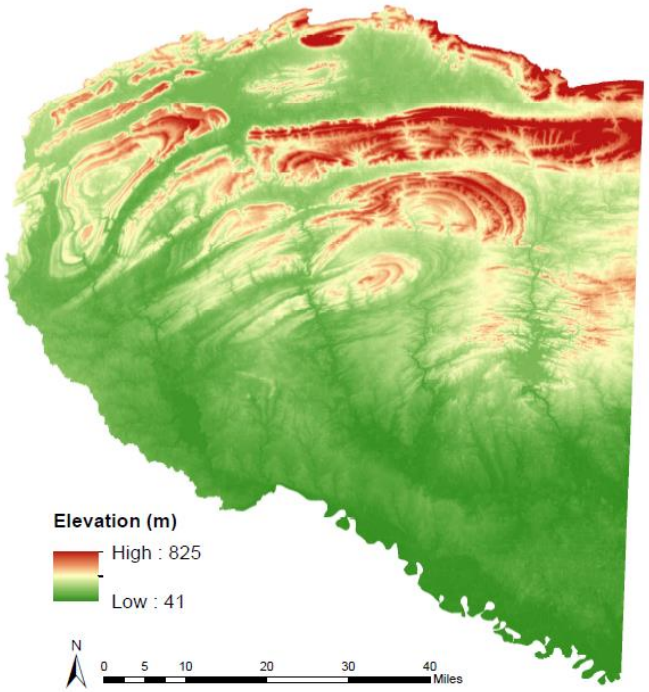

Figure 6: Topography of the Southeast Watershed Planning Region of Oklahoma. Data from United States Geological Survey Digital Elevation Model.

3.2 Hydrology

The topography of the region results in a general flow of major streams from east to west in the north, and north to south/east in the south. The major lotic water bodies include the Glover, Kiamichi, Little, and Mountain Fork Rivers, and the major lentic waterbodies include Broken Bow, Hugo, Pine Creek, and Sardis Lakes (Figure 7). The Red River flows along most of the southern boundary of the SEWPR, but the water within the Red River was not considered part of the SEWPR's hydrologic system for this project. There are two major aquifers within the SEWPR, the Antlers and Red River aquifers, that underlie the southern portion of the region. The Antlers aquifer is a major bedrock aquifer which stretches east to west and underlies approximately 3,370 km^2 across the region. The Red River aquifer is a major alluvial aquifer extending north from the Red River and underlies approximately 870 km^2 of the region. There are several other minor bedrock and alluvial aquifers across the region, the largest being the Kiamichi bedrock aquifer which underlies approximately 7,070 km^2 (61%) of the SEWPR (OWRB, 2011b) (Figure 8). Major aquifers are defined by OWRB as having an average annual water well yield of at least 568 liters per minute (150 gallons per minute) for alluvial aquifers and at least 189 liters per minute (50 gallons per minute) for bedrock aquifers, and minor alluvial and bedrock aquifers do not meet those thresholds (OWRB, 2011b). The region receives an average of 125 centimeters (cm) in annual precipitation which is about 34 cm more than the statewide average (Oklahoma Mesonet, 2019).

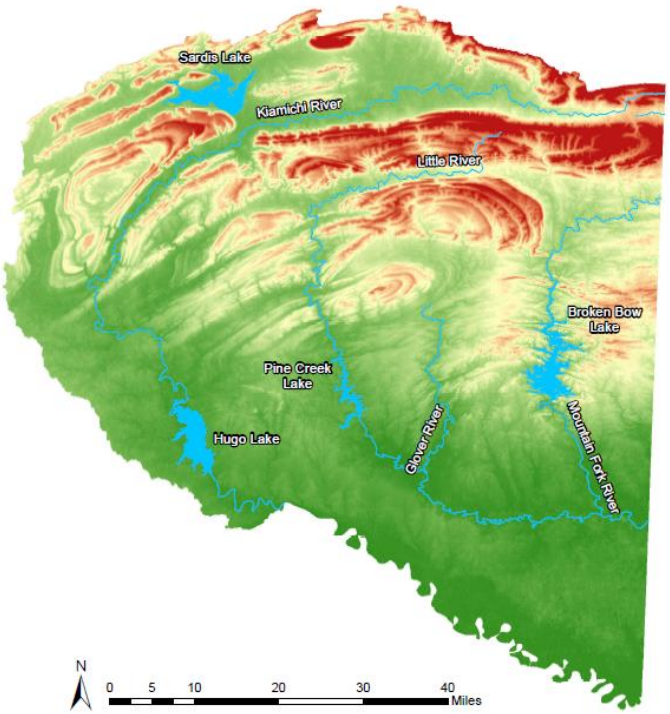

Figure 7: Major waterbodies within the Southeast Watershed Planning Region of Oklahoma. Data from Oklahoma Water Resources Board and United States Geological Survey.

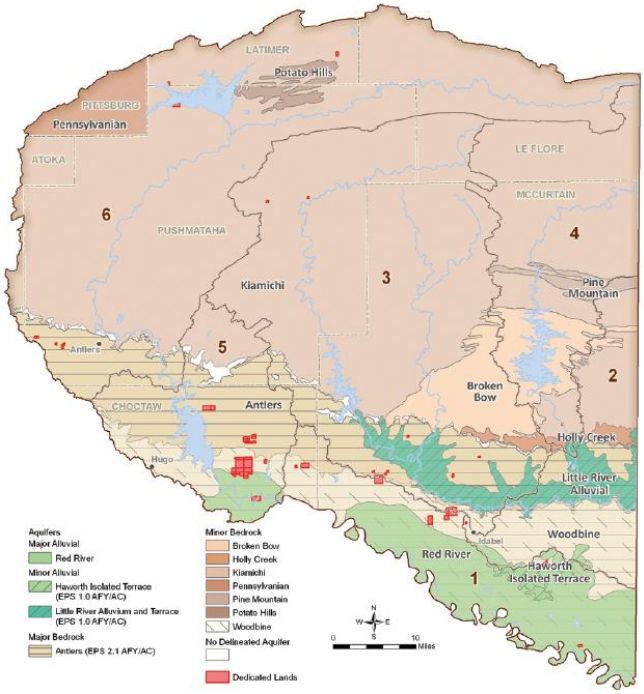

Figure 8: Major and minor aquifers underlying the Southeast Watershed Planning Region of Oklahoma. Map courtesy of the 2012 Oklahoma Comprehensive Water Plan – Southeast Watershed Planning Region Report from the Oklahoma Water Resources Board (OWRB, 2011b).

3.3 Human Geography

Estimated population in the SEWPR was approximately 59,400 as of 2010 (US Census, 2010). The largest town in the SEWPR is Idabel with a 2010 population of 7,010. Other major towns within the region include Hugo (5,310), Broken Bow (4,120), and Antlers (2,450). To estimate population projections in the SEWPR for 2060, county population projections from an Oklahoma Department of Commerce study (Barker, 2012) were weighted by the percentage of each county that falls within the SEWPR. The projected 2060 population for the SEWPR was estimated to be 64,500, an 8.6% increase from 2010.

In the 2012 OCWP SEWPR report, the total annual water demand for the SEWPR was estimated at 0.62 cm in 2010 and was estimated to grow by about 26% by 2060. The 2010 estimate accounted for approximately 3% of the state's total estimated water demand, with 96% supplied by surface water and 4% from groundwater. The sector that contributed to the largest demand was industrial which includes water demands from large industries that do not depend on public water supply. This accounted for about 60% of the total estimated water demand in 2010 (Table 1). Water use data is also estimated in USGS reports published every five years, and data is available for 2010 and 2015 at the statewide level (Maupin et al., 2014; Dieter et al., 2018). Assuming the same 3% share of the state's water demand for the SEWPR from OWRB, the total freshwater withdrawals for the SEWPR were 0.64 and 0.65 cm for 2010 and 2015 respectively. These values were consistent with the OCWP water demand estimates. The same report also estimated consumptive use from irrigation and thermoelectric power at the statewide level in 2015. The total consumptive use for these two water use categories in the SEWPR would be 0.29 cm assuming the 3% share for the SEWPR again, which is 45% of 2015 estimated total withdrawals.

The values for both water demand and withdrawals from OWRB and USGS represent the amount of water pumped or diverted to meet user needs. The OWRB report does not include any estimates for the water returned to the hydrologic system post-use, so consumptive use cannot be estimated using this data. The USGS report includes these return estimates for irrigation and thermoelectric power, but not for the other water use sectors. A consumptive use estimation in the SEWPR can be made for 2015 using the USGS data, but major assumptions must be made to separate the SEWPR from the entire state. However, this 2015 consumptive use estimate was a useful baseline to compare to WBM consumptive use estimations. It is also important to note that the OWRB and USGS water use estimates are projections based partially on self-reported survey data from water users. While this data is useful, it may not accurately represent the true amount of water used by humans in the SEWPR.

Table 1: Estimated water demand by sector (cm) in the Southeast Watershed Planning Region of Oklahoma for 2010 and projected for 2020-2060 (OWRB, 2011b).

	Crop Irrigation	Livestock	Municipal & Industrial	Oil & Gas	Self-Supplied Industrial	Self-Supplied Residential	Thermoelectric Power	Total
Year	Depth in cm							
2010	0.027	0.043	0.076	0.001	0.374	0.014	0.089	0.624
2020	0.033	0.044	0.080	0.002	0.374	0.015	0.099	0.647
2030	0.040	0.045	0.084	0.003	0.374	0.016	0.111	0.672
2040	0.046	0.045	0.088	0.004	0.380	0.016	0.124	0.704
2050	0.051	0.046	0.092	0.005	0.392	0.017	0.138	0.741
2060	0.059	0.047	0.096	0.007	0.402	0.018	0.154	0.783

Chapter 4 – Methodology

A WBM has been developed with the goal of estimating consumptive use on a quarterly basis within the SEWPR. For the purposes of this study, consumptive use was defined as the volume of freshwater removed from a watershed that is not included in natural hydrologic processes, and generally contributed to human activities. The WBM estimates consumptive use by estimating all input and output components of the natural hydrologic balance and solves for consumptive use as the remaining output component. The hydrologic zone of analysis includes both surface water and groundwater within the boundaries of the SEWPR. The surface water system is considered to be all water sources above ground, including all lentic and lotic waterbodies, water stored in plants, and any volume of water held in man-made water supply systems. The groundwater system is considered to be all below ground water sources, including soil moisture and any confined or unconfined aquifers.

To understand the interactions between each input and output component of surface water and groundwater, it is helpful to first consider both the surface and sub-surface regions as their own separate water balance. The equations for the surface water and groundwater balances are written as Equations 2 and 3 respectively:

$$\Delta S_{sw} = P + Q_{in} + G_{wd} + G_w S_w - ET_{sw} - Q_{out} - R_e - S_w G_w - C_{sw} \quad (2)$$

$$\Delta S_{gw} = R_e + S_w G_w - ET_{gw} - G_w S_w - G_{wd} - C_{gw} \quad (3)$$

where ΔS_{sw} is the change in surface-water storage, ΔS_{gw} is the change in groundwater storage, R_e is groundwater recharge, G_{wd} is groundwater withdrawals, $G_w S_w$ is groundwater to surface-water flow, $S_w G_w$ is surface-water to groundwater flow, ET_{sw} is surface water actual evapotranspiration,

ET_{gw} is groundwater actual evapotranspiration, C_{sw} is surface water consumptive use, and C_{gw} is groundwater consumptive use. Since the hydrologic zone of analysis includes both the surface water and groundwater systems, the two equations were combined. Several components which are inputs to the surface water system are also outputs to the groundwater system, and vice versa. These components cancel out, leaving only components that contribute as net inputs or outputs to the overall system. The assumption was made that all groundwater inputs and outputs take place within the SEWPR, and there are no groundwater exchanges to or from other regions. Thus, the water balance equation for the overall system becomes

$$\Delta S = P + Q_{in} - ET - Q_{out} - C \quad (4)$$

where ΔS is total change in water storage, ET is total actual evapotranspiration, and C is total consumptive use.

The final water balance equation designed to estimate consumptive use in the SEWPR takes a similar form to equation 3, with several changes made for reasons specific to the SEWPR and the chosen methods of this study. The Q_{in} component is considered negligible for the SEWPR, since there are almost no streams that flow into the region, and was omitted from the final equation. This is further explained in Section 4.2. The ΔS component is divided into surface and sub-surface storage change due to the confidence in the developed estimation methods and available data. This is further explained in Sections 4.3 and 4.4. Finally, the equation is rearranged to solve for consumptive use, and is written as:

$$C = P - \Delta S_{surf} - \Delta S_{sub} - Q_{out} - ET \quad (5)$$

where ΔS_{surf} is change in surface water storage, and ΔS_{sub} is change in sub-surface water storage.

The volume of water for each of these components was estimated on a quarterly (3-month) timescale from 2007-2017. This time period was chosen because it includes five years before and after the Water for 2060 baseline year of 2012. Throughout this document, when the terms "quarters" or "quarterly" are used, they refer to the 44 3-month periods between 2007 and 2017. The abbreviation "Q" followed by the numbers 1 – 4 were used to denote each of the four annual quarters, where Q1 is January, February and March, Q2 is April, May, and June, Q3 is July, August, and September, and Q4 is October, November and December. The following sections describe the different estimation methods used for each WBM component.

4.1 Precipitation

Quarterly precipitation for the SEWPR was estimated using the National Centers for Environmental Prediction (NCEP) Stage IV Quantitative Precipitation Estimates (QPE) from the National Weather Service. This data product includes monthly gridded precipitation (*P*) estimates from radar and rain gauge measurements. Each cell has a 4 kilometer (km) spatial resolution and contains a value for monthly *P* accumulation depth in inches. Monthly gridded raster files for 2007-2017 were downloaded and processed using ESRI™ ArcGIS software (ESRI, 2018). A subset was made for each monthly *P* raster file by removing all pixels not included in the SEWPR boundary (Figure 9). Next, the monthly rasters were summed into quarters using the Raster Calculator spatial analyst tool (ESRI, 2018) (e.g., Q1 = Jan + Feb + Mar). Finally, the Surface Volume 3D analyst tool (ESRI, 2018) was used to estimate the volume of *P* across the SEWPR for each quarter.

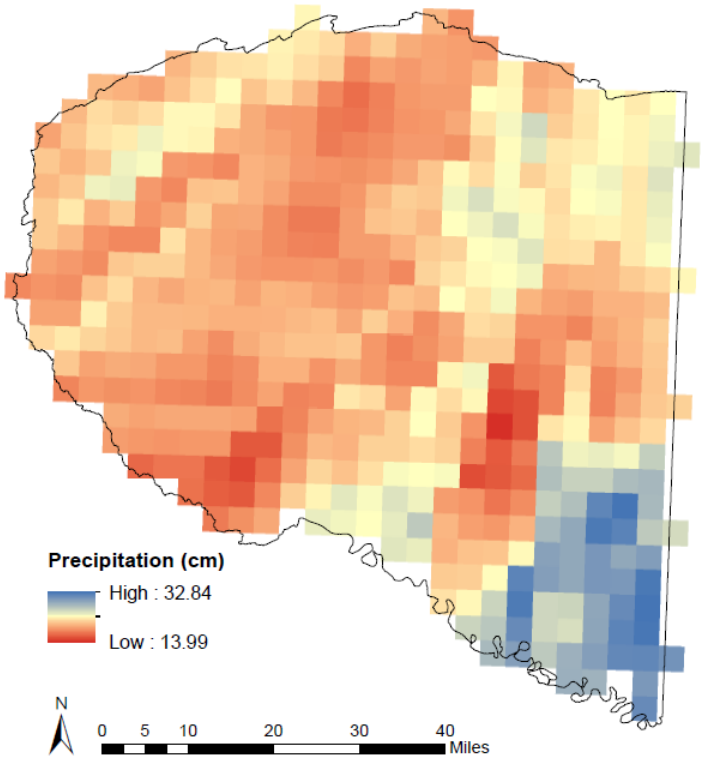

Figure 9: Precipitation accumulations from the National Centers for Environmental Prediction Stage IV Quantitative Precipitation Estimates in the Southeast Watershed Planning Region of Oklahoma for 2007 Quarter 1.

4.2 Streamflow

The SEWPR is a unique region in that there are essentially no streamflow input sources. There are several minor streams that enter the region along the Arkansas border, however, these streams exit the region shortly after entering and without converging with other streams, so their inflow contribution can be considered negligible for the WBM. All streamflow volumes were estimated as the Q_{out} component of the WBM. The USGS National Water Information System (USGS, 2019b) provides streamflow data as daily mean discharge in cubic feet per second (cfs) from seven active stream gauge stations across the SEWPR (Figure 10). To directly measure the total Q_{out} volume for the SEWPR for each quarter, stream gauges would need to exist at locations

where each stream exits the SEWPR. Since this is not the case, alternative methods were used to estimate Q_{out} for each outflow stream at the point where it exited the SEWPR.

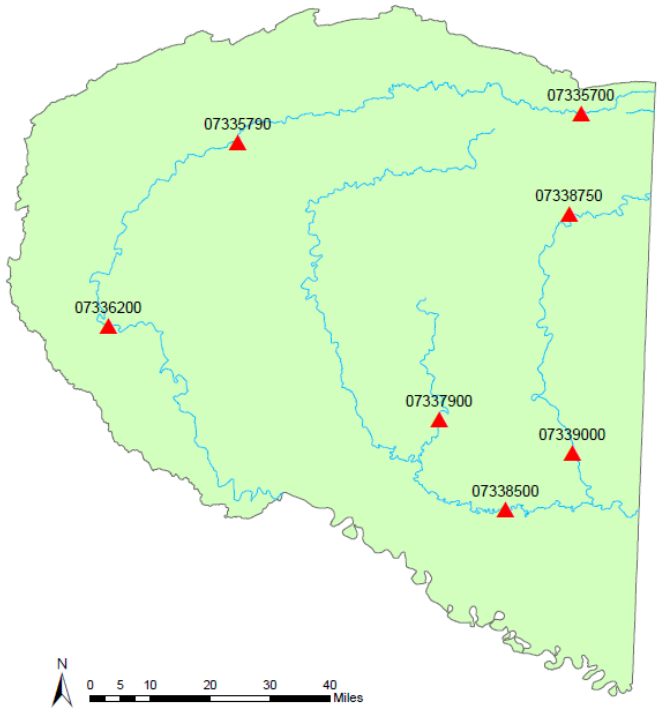

Figure 10: Active United States Geological Survey stream gauges within the Southeast Watershed Planning Region (USGS, 2019b).

Average daily discharge in cfs at ungauged locations can be estimated using the USGS StreamStats web application. StreamStats uses regional regression equations with contributing drainage area and mean annual *P* from 1971-2000 as input parameters to estimate a long-term average daily discharge rate (Esralew and Smith, 2010). However, the discharge estimation from StreamStats cannot be directly used to estimate the quarterly Q_{out} component of the WBM, since it only provides the long-term average. To account for the temporal variability in streamflow between quarters, a streamflow coefficient (SC) method was developed. This method uses a proportional SC based on observed USGS stream gauge discharge data to estimate mean quarterly streamflow at ungauged locations where each stream exits the SEWPR.

Streams that exit the SEWPR either flow south into the Red River at the Oklahoma-Texas border, or flow east across the Oklahoma-Arkansas border where they flow into either the Little River or Red River. Both rivers have multiple USGS stream gauges located within or near the SEWPR. Mean quarterly discharge data from the closest gauge upstream and downstream of the reach where the SEWPR outflow streams join their respective river was used to calculate the quarterly net streamflow gains caused by the SEWPR outflow streams (Table 2). The net flow gains were calculated by subtracting upstream gauge discharge measurements from downstream gauge discharge measurements (Figure 11). For the Little River however, discharge from USGS gauge 07339000 – Mountain Fork near Eagletown, OK was also subtracted from downstream gauge discharge to exclude the possibility of anthropogenic influence flows from the Broken Bow Lake dam releases (Figure 11).

Table 2: United State Geological Survey (USGS) stream gauges used to calculate net flow gains for Southeast Watershed Planning Region of Oklahoma outflow streams.

River	USGS Gauge	Location
Red River	07335500 at Arthur City, TX	Upstream
Red River	07337000 at Index, AR	Downstream
Little River	07338500 near Idabel, OK	Upstream
Little River	07340000 near Horatio, AR	Downstream

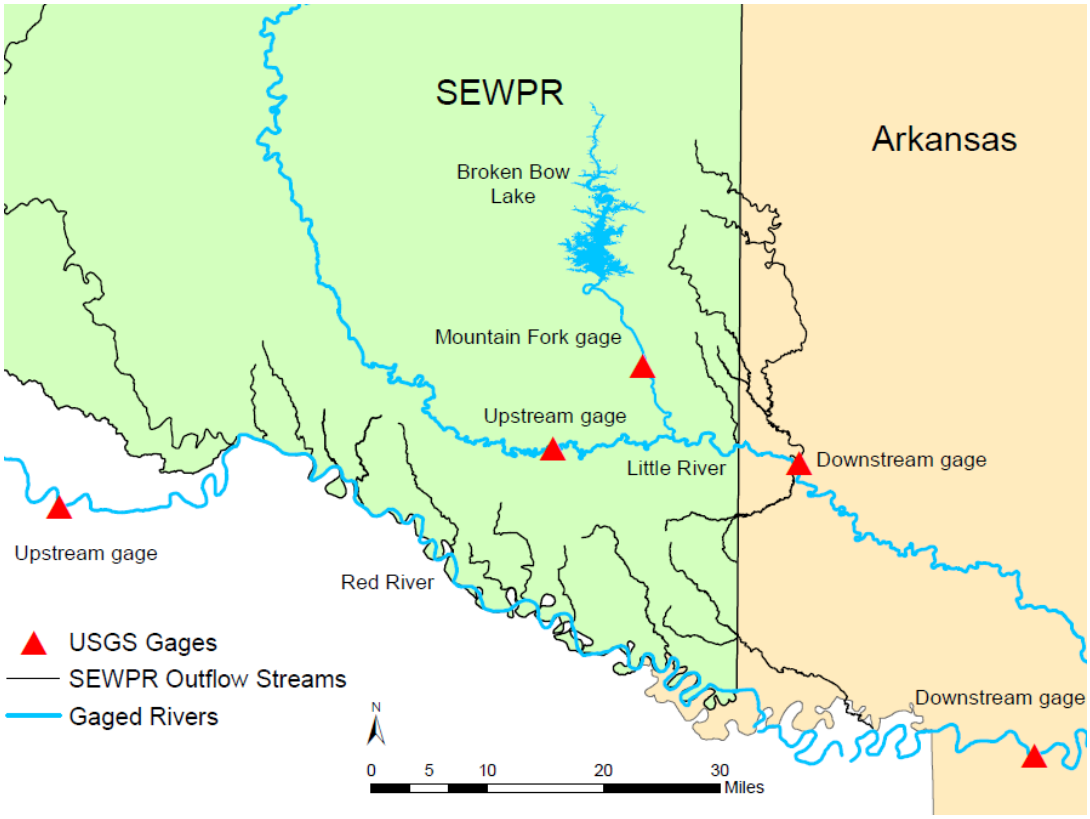

Figure 11: Location of United States Geological Survey stream gauges on Little River, Red River, and Lower Mountain Fork River used for streamflow out (Q_{out}) estimation in the Southeast Watershed Planning Region of Oklahoma (SEWPR).

Once quarterly net streamflow gains were calculated for both rivers, the average net streamflow gains between upstream and downstream gauges on both rivers for the period of 1971-2017 were calculated using available USGS gauge data. This time period includes the 11-year period for this study and is representative of the long-term average data provided by StreamStats (1971-2000) assuming mean annual *P* has not changed significantly since 2000. Next, the SC for each quarter was calculated for both the Little River and Red River (Table A1) using the following equation:

$$SC_i = \frac{Q_i}{Q_{avg}} \tag{6}$$

where SC_i is the streamflow coefficient for any quarter i (dimensionless), Q_i is the average streamflow gain for any quarter i (cfs), and Q_{avg} is the average streamflow gain from 1971-2017 (cfs). Since the streams flowing out of the SEWPR are a major source of the streamflow gains between gauges, it was assumed that each quarter's SC was representative of the relationship between the average streamflow for the quarter and the average streamflow from 1971-2000 (from StreamStats) at the location where the stream exits the SEWPR. Average quarterly streamflow in cfs for each outflow stream was estimated using the following equation

$$Q_{cfs} = SC_i * SS_{avg} \quad (7)$$

where Q_{cfs} is the average quarterly streamflow for a particular outflow stream in cfs, and SS_{avg} is the average streamflow for the same outflow stream in cfs given by StreamStats (Table A2). Quarterly outflow volumes for each stream were then converted from cfs to total volume units by extrapolating the average flow rate for each quarter and summed to estimate the Q_{out} component of the WBM for the entire SEWPR.

4.3 Surface Storage Change

To determine the ΔS_{surf} component of the WBM, storage volume of lentic surface waterbodies across the SEWPR were estimated for each quarter. Lentic surface waterbodies in the SEWPR are divided into two categories: mapped and unmapped waterbodies. The mapped waterbodies include United States Army Corps of Engineers (USACE) managed reservoirs and other reservoirs mapped by OWRB. The unmapped waterbodies include the remaining waterbodies which consist mostly of small public or privately-owned ponds for which no known bathymetric data exists. Since the methods for estimating storage volume differ for mapped and

unmapped waterbodies, this section is divided into two parts describing the methods for each category.

4.3.1 Mapped Surface Waterbodies

The USACE manages four reservoirs within the SEWPR as part of the Lower Red River Basin, managed by the Tulsa District in the Southwestern Division. These reservoirs include Broken Bow Lake, Hugo Lake, Pine Creek Lake, and Sardis Lake (Figure 7). The USACE Tulsa District reports daily data for each of their reservoirs including storage volume. Storage volumes were calculated using area-capacity curves which were developed from bathymetric survey data collected by USACE. Relationships between elevation depth, surface area, and storage volume or capacity were developed using the curves, which were then used to calculate storage volume from the reservoir pool elevation that is monitored hourly at USACE reservoirs (USACE, 2013).

Only the change in reservoir storage volume over the course of each quarter was needed to calculate the ΔS_{surf} component of the WBM. The general equation for calculating quarterly change in any variable is written as:

$$\Delta X = X_{i+1} - X_i \tag{8}$$

where ΔX is the change in variable X, Xi is the value of X for quarter i, and X_{i+1} is the value of X for the following quarter. Since ΔX represents the change from one quarter to the next, values may be positive or negative. The storage volume of each reservoir on the first day of the quarter of interest was used in Equation 7 to calculate storage change (Table A3). For example, the change in storage volume for 2007 Q1 is the difference between storage volumes on 04/01/2007 and 01/01/2007. Storage volume change was calculated for all quarters on each of the four

reservoirs, and each corresponding quarter for each reservoir was summed together to yield the total USACE reservoir quarterly storage volume change values for the SEWPR.

There are four additional mapped reservoirs within the SEWPR that are not managed by USACE. These include Lake Carl Albert, Lake Nanih Waiya, Lake Ozzie Cobb, and Schooler Lake (Figure 12). Bathymetric data exists for these reservoirs from previously conducted OWRB surveys, but the pool elevations are not frequently monitored like the USACE reservoirs. To estimate storage volume from surface area like is done in the USACE methods, surface area must be estimated using alternative methods. Reservoir storage volumes have been estimated from remote sensing-based surface area data with overall success in previous studies (Liebe et al., 2005; Rodrigues et al., 2012). Bathymetric data was used to develop a relationship between a reservoir's surface area and storage volume, and surface area was estimated from Landsat satellite imagery. This same approach was used to estimate storage volumes for the four reservoirs mapped by OWRB.

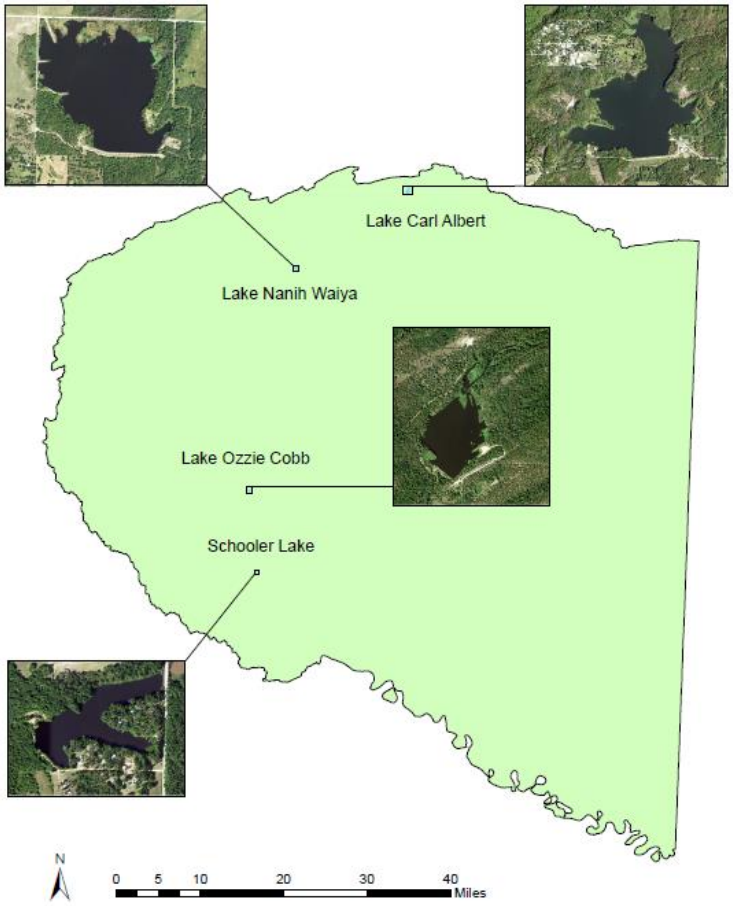

Figure 12: Locations of Oklahoma Water Resource Board mapped reservoirs in the Southeast Watershed Planning Region of Oklahoma. Imagery from United States Department of Agriculture National Agricultural Imagery Program.

The available bathymetric data for the four reservoirs included contour lines created from measured depth points representing the underwater topography for each reservoir. The storage volume and surface area of each contour interval along with the remaining intervals of greater depth included within (Figure 13) was estimated using ArcGIS 3D Analyst tools (ESRI, 2018). The resulting area and volume data was used to develop a regression model to represent the relationship between area and volume for each reservoir. Each reservoir's regression equation was used as an empirical method for estimating volume in acre-feet (ac-ft) when area in acres (ac) is known (Table 3).

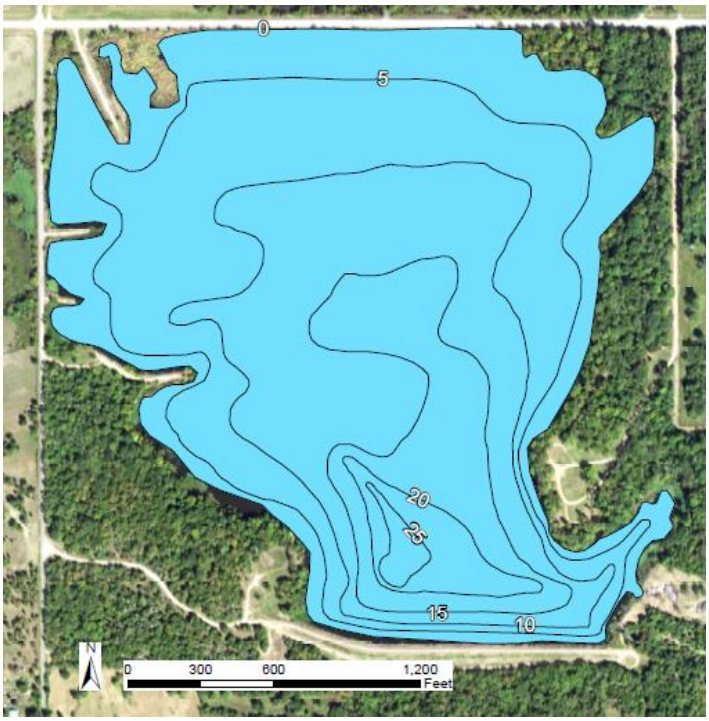

Figure 13: Contour intervals used to determine surface area to storage volume relationships for mapped Oklahoma Water Resource Board reservoirs. 5 feet intervals for Lake Nanih Waiya are shown. Imagery from United States Department of Agriculture National Agricultural Imagery Program.

Table 3: Regression equations to estimate storage volume from surface area on mapped Southeast Watershed Planning Region of Oklahoma reservoirs, where V is storage volume in ac-ft and A is surface area in ac. R^2 is the coefficient of determination for each equation.

Reservoir	Regression Equation	R^2
Carl Albert	$V = 0.0768A^2 + 4.0356A$	0.998
Nanih Waiya	$V = 0.0860A^2 + 0.5685A$	0.992
Ozzie Cobb	$V = 0.1024A^2 + 1.9326A$	1.000
Schooler	$V = 0.3287A^2 + 2.0094A$	0.998

Next, the quarterly surface area of each reservoir was estimated from Landsat satellite imagery. Landsat TM, ETM+, and OLI sensors, which provide the appropriate temporal data coverage for this study, measure surface reflectance from discrete wavelength ranges at 30 m

spatial resolution with a 16-day return interval. Images from the days closest to the beginning of each quarter with the least amount of cloud cover over the reservoirs were selected.

To distinguish surface water from other land surfaces, a spectral index called the Modified Normal Difference Water Index (MNDWI) was applied. The MNDWI is an algorithm designed to distinguish open water from other land surfaces based on the different light wavelengths absorbed or reflected by water compared to other surfaces (Xu, 2006). The formula for MNDWI is written as:

$$MNDWI = \frac{Green - MIR}{Green + MIR} \tag{9}$$

where *Green* is the Landsat band for green light reflectance (0.52-0.60 µm wavelength), and *MIR* is the Landsat band for middle infrared reflectance (1.55-1.75 µm wavelength). Values of MNDWI range from -1 to 1. Water reflects a similar amount of green light as other surface types but reflects much less MIR light. Applying the MNDWI to a water pixel should produce a positive value, while pixels of other surface types should produce a negative value.

ArcGIS Spatial Analyst tools (ESRI, 2018) were used to apply the MNDWI to Landsat images (USGS, 2019a) for each quarter. A conditional binary raster was then created which assigns all positive MNDWI pixels a value of 1, and all negative pixels a value of 0 (Figure 14). Pixels not in close proximity to the shoreline of each reservoir were removed from the rasters, and the number of water pixels associated with each reservoir was calculated within ArcGIS for each quarter. The surface area was calculated by multiplying the number of water pixels by the area of each pixel (900 m_2), and then converted to ac and used in the appropriate regression equation for each reservoir to estimate storage volume for each quarter. Storage volumes for the

four reservoirs were summed together and used in Equation 7 to calculate quarterly storage change (Table A4).

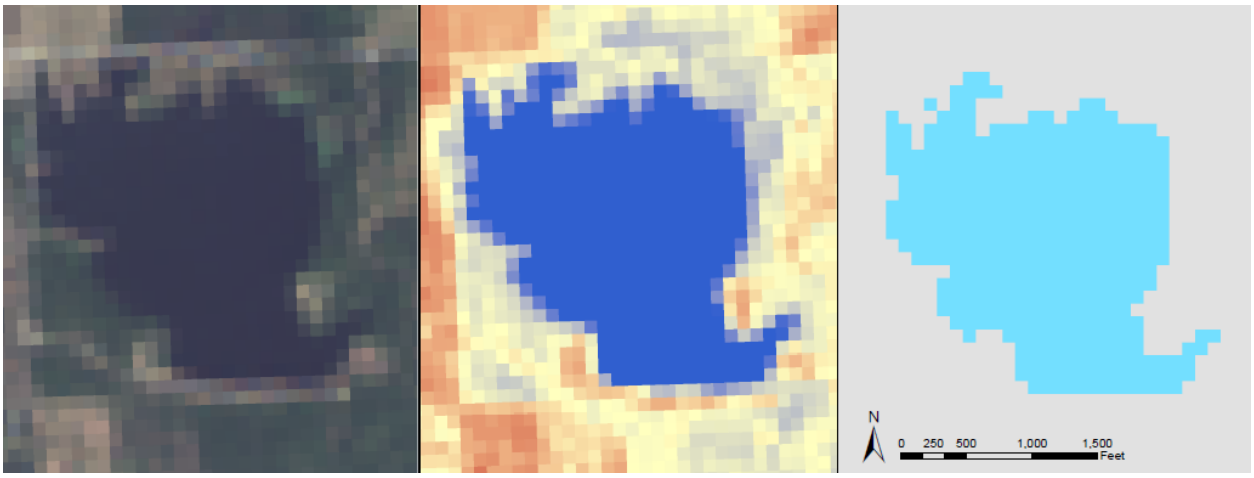

Figure 14: True color Red-Green-Blue (left), Modified Normal Difference Water Index (MNDWI) (middle), and binary raster (right) images of Lake Nanih Waiya derived from Landsat reflectance data. Pixels with higher MNDWI values are shown in dark blue (middle), and pixels identified as water in the binary raster are shown in light blue (right).

4.3.2 Unmapped Surface Waterbodies

Estimating storage for unmapped surface waterbodies in the SEWPR requires an alternative approach than used for mapped surface water bodies, since bathymetric data is not available for these waterbodies, and most are too small in area to be accurately represented by Landsat pixels. To address this issue, bathymetric data was manually collected from small lentic waterbodies in the SEPWR by the author and several other employees and students from the Oklahoma Water Survey.

Bathymetric surveys were conducted on 17 small lentic waterbodies within the SEWPR on three separate trips between July and October of 2019, totaling 7 days, consisting of travel

and field work. The surveys were conducted using simple and low-cost equipment including a kayak, a Deeper Pro+ Smart Sonar portable fish finder (Deeper, UAB, Vilnius, Lithuania) and a Garmin GPSMAP 78s handheld global positioning system (GPS) unit (Garmin International, Inc., Olathe, Kansas, USA). The fish finder was mounted to the side of the kayak with a flexible arm mount and positioned so the sonar sensor was submerged and facing towards the bottom of the waterbody (Figure 15). The device was controlled by a tablet using an application and continuously measured waterbody depth and coordinate location with a built in GPS as the kayak traveled across the waterbody. The collected depth and coordinate location data was stored in a cloud data base and automatically appeared on a map interface within the application as the person operating the kayak and fish finder traveled across the waterbody. The kayak was guided across the waterbody in evenly spaced transects until the waterbody was sufficiently covered in data points. One limitation of the Deeper fish finder was its inability to measure depth and coordinate location data in water less than 1 foot deep. For this reason, the coordinate location of the shoreline could not be collected using the built in GPS of the fish finder. Instead, a Garmin handheld GPS unit was used to collect waypoints spaced every 10 feet around the shoreline of the waterbody (Figure 15). This allowed an accurate shoreline to be delineated to serve as the boundary during post-processing of the bathymetric data.



Figure 15: Bathymetric data collection on waterbody in the Southeast Watershed Planning Region of Oklahoma, including the kayak with fish finder mounted on the right side (left). Collection of shoreline global positioning system points used for bathymetric data processing (right).

The areas of these waterbodies ranged from <0.1 to 60.3 ac and were chosen to be representative of the remaining unmapped waterbodies across the SEWPR. The waterbodies were located on both public and private land owned by several different, local, state, federal, and tribal agencies including the City of Broken Bow, Oklahoma State University, Oklahoma Department of Wildlife Conservation, Oklahoma Tourism and Recreation Department, USACE, US Forest Service, and Choctaw Nation. Representatives from each of these agencies were contacted and asked for permission to conduct the bathymetric surveys on their property. Once the bathymetric data was processed, informational maps of each waterbody were created and sent to their respective agency representatives, courtesy of the Oklahoma Water Survey.

The collected data was processed using ArcGIS software (ESRI, 2018) to calculate the storage volume of each full waterbody, along with decreasing contour intervals for each waterbody, as was done with the mapped reservoirs. First, the waterbody shoreline was

delineated from the collected GPS points. This made it possible to estimate the surface area of each waterbody at the time of the bathymetric survey. Then the collected points from the fish finder with depth and coordinate location data were used to create an interpolated raster surface and contour lines that represent the underwater topography of each waterbody (Figure 16). The storage volume for each waterbody was then estimated using 3D Analyst tools built in to ArcGIS. This process was repeated for each contour interval within the waterbody to represent the area and volume of the waterbodies if the water level dropped to each specific contour interval.

In addition to the collected bathymetric data (Table A5), contour interval areas from reservoirs mapped by OWRB and USACE that were less than 100 acres were selected to represent smaller waterbodies. Contour lines from shallower depths were removed from each reservoir until the total area was less than 100 ac. Then the volume was estimated as if the water level had dropped to the contour interval. This additional area and volume data was added to the collected bathymetric data, and used to develop regression models that predict storage volume from surface area. Separate models were fit for small (0 to 5 ac) and large (5 to 100 ac) waterbodies to more accurately estimate waterbody volumes of different sizes. A single model trained with data that included large waterbodies predicted small waterbodies with less accuracy than a model trained only with small waterbody data. Because small waterbodies make up over 99% of the sample of digitized waterbodies, accurately modeling these waterbodies was crucial. Different types of regression models including linear, quadratic, and power models using different surface area thresholds were trained and tested with independent datasets from the bathymetric data. The performance of each model was evaluated using four different performance metrics which compare modeled values to observed values (Table 4). Within the 0

to 5 ac and 5 to 100 ac thresholds, none of the different types of regression models (linear, quadratic, or power) performed significantly better than one of the other, so the model with the highest NSE value was chosen for each area threshold (Table 5).

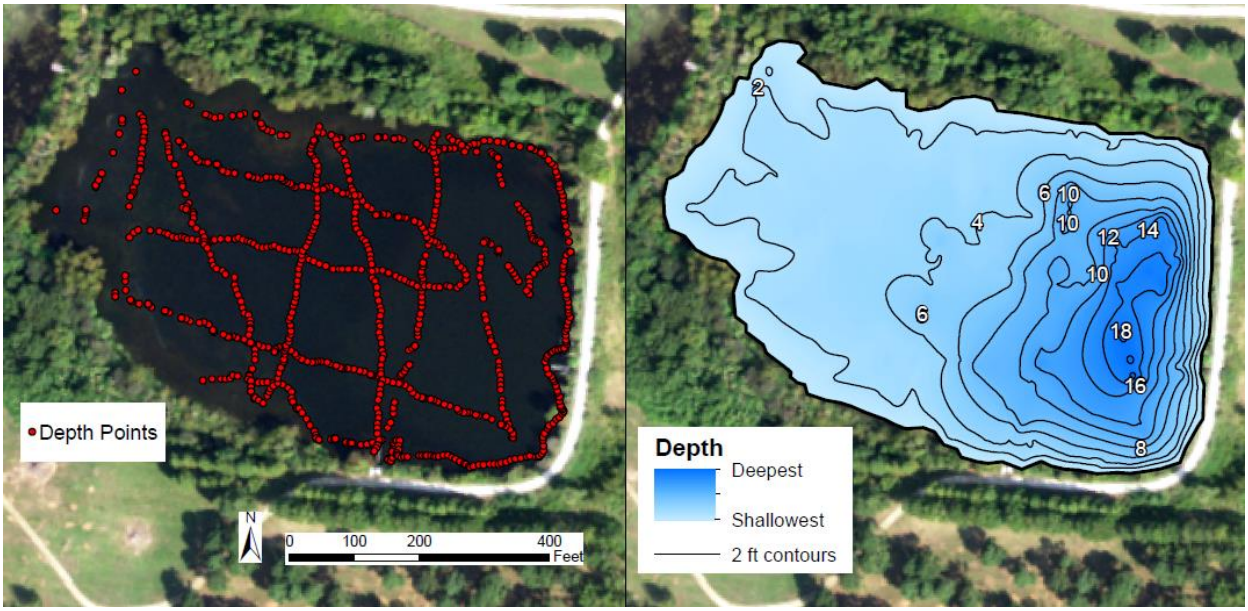

Figure 16: Depth points collected from a bathymetric survey of a lentic waterbody in the Southeast Watershed Planning Region of Oklahoma on 10/28/2019 (left) and contour intervals and depth raster surface derived from collected depth points used to estimate storage volume (right).

Table 4: Performance metrics used to evaluate regression models for predicting lentic waterbody storage volume from surface area. R_2 = coefficient of determination, nRMSE = standard deviation normalized root mean square error, NSE = Nash-Sutcliffe Efficiency, and % bias = percent bias.

Performance Metric	Range	Target Value
R_2	-1 to 1	1
nRMSE	0 to 1	0
NSE	-∞ to 1	1
% bias	-100 to 100	0

Table 5: Regression models for predicting storage volume of small and large unmapped lentic waterbodies in the Southeast Watershed Planning Region of Oklahoma, evaluated with performance metrics. Chosen models are shown in **bold**.

Area Range (acres)	Model Type	Equation	R^2	nRMSE	NSE	% bias
0-5	Linear	$V = 3.044A$	0.833	0.432	0.808	-8.6
0-5	Quadratic	$V = 1.464A^2 + 2.080A$	0.836	0.426	0.813	-10.5
0-5	**Power**	$\mathbf{V = 3.333A^{1.260}}$	**0.836**	**0.424**	**0.814**	**-7.5**
5-100	**Linear**	$\mathbf{V = 7.154A}$	**0.992**	**0.201**	**0.955**	**-5.0**
5-100	Quadratic	$V = 0.068A^2 + 3.275A$	0.979	0.330	0.879	-28.0
5-100	Power	$V = 1.099A^{1.470}$	0.975	0.326	0.882	-32.7

The spatial resolution of Landsat imagery is too low to accurately estimate many of the small unmapped surface waterbody areas. To address this issue, high resolution (1 m) aerial imagery from the United States Department of Agriculture National Agricultural Imagery Program (USDA NAIP) was used (NAIP, 2018). While the spatial resolution of the NAIP imagery is much higher than Landsat, images are taken only once every 2 to 3 years, which limits the availability to only 5 out of 44 quarters. However, NAIP was the only imagery source with high enough spatial resolution that was available at no charge. Sets of images covering at least 96 km^2 and evenly spaced across the SEWPR, were chosen for each available quarter (Figure 17). The minimum number of km^2 of images required to represent the entire SEWPR was determined using the following equations

$$n = \frac{N \times X}{X + N + 1} \tag{10}$$

where,

$$X = \frac{z^2 \times 0.5 \times (1 - 0.5)}{\varepsilon} \tag{11}$$

and N is the population size, z is the critical value of a normal distribution at the desired confidence level, ε is the margin of error, and n is the minimum sample size. The sample size required to represent all 11,500 km^2 within the SEWPR with a confidence level of 95% and a margin of error of 10% was 96 km^2.

All lentic surface waterbodies greater than 10 square meters (m^2) within the images were manually digitized using ArcGIS Editor tools. Digitizing creates a polygon for each waterbody and allows surface area to be directly calculated (Figure 18). Digitizing the entire extent of the SEWPR would be far too time consuming, so the data collected from the sample images was extrapolated across the entire SEWPR.

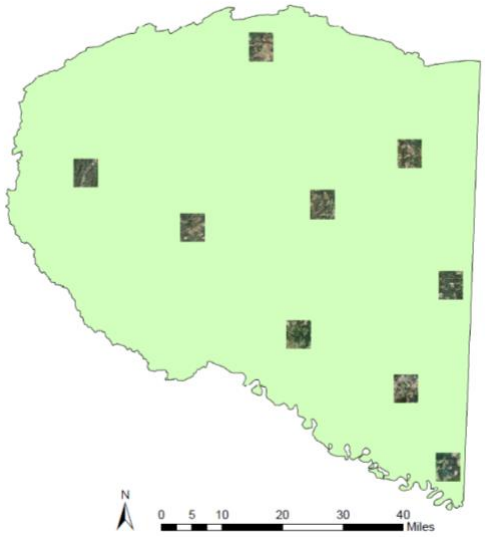

Figure 17: Distribution of selected United States Department of Agriculture National Agricultural Imagery Program (NAIP, 2018) images for unmapped waterbody digitizing from 2015 Quarter 3.

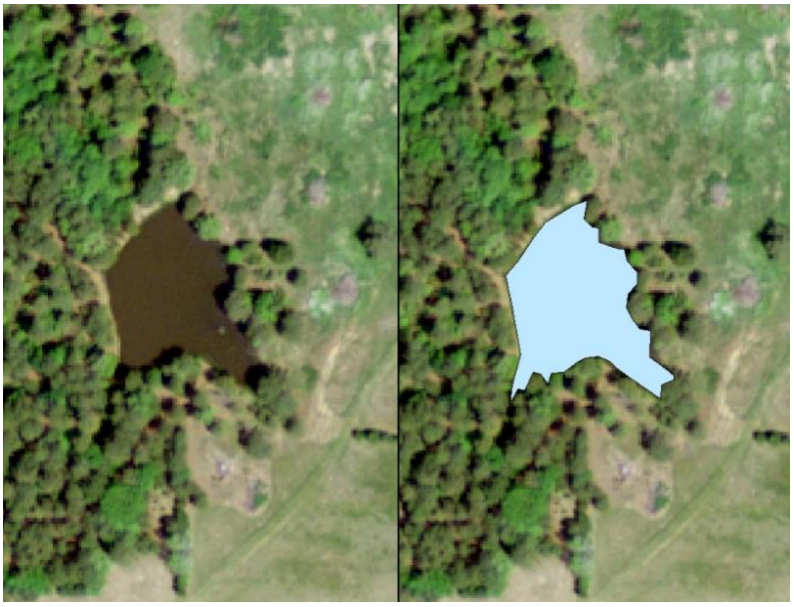

Figure 18: Example of a digitized waterbody from 2008 United States Department of Agriculture National Agricultural Imagery Program imagery in the Southeast Watershed Planning Region of Oklahoma.

The appropriate regression model was applied to the surface area data from the digitized waterbodies to estimate their storage volume. The storage volume was then summed for each

km^2 of digitized area during that quarter, and the mean storage volume per km^2 was extrapolated across the entire SEWPR to estimate total storage volume for the quarter. For quarters where imagery is not available, a multiple linear regression model was developed to estimate the quarterly total storage volume of unmapped lentic waterbodies using hydrologic input variables that were available for all quarters. Since there was only 5 quarters of digitized waterbody data to train the model on, the model could not be tested with an independent sample or evaluated with performance metrics. Instead, the model was chosen based on which variables had a coefficient and intercept that were significant at the 95% confidence level. The equation is written as:

$$V = -0.015ET + 0.022P + 42{,}603 \quad (12)$$

where V is total unmapped waterbody storage volume, ET is evapotranspiration, and P is precipitation. Each parameter volume is in ac-ft. Once each quarter had an estimated storage volume for unmapped waterbodies across the entire SEWPR, quarterly storage change was calculated using Equation 7 (Table A6).

Finally, to calculate the total ΔS_{surf} component for each quarter, the three different estimated values for storage change were summed together

$$\Delta S_{surf} = \Delta S_1 + \Delta S_2 + \Delta S_3 \quad (13)$$

where ΔS_1, ΔS_2, and ΔS_3 are the storage changes on USACE reservoirs, OWRB mapped reservoirs, and unmapped waterbodies, respectively.

4.4 Sub-surface Storage

Sub-surface storage change (ΔS_{sub}) is difficult to estimate in Southeast Oklahoma because groundwater and soil moisture monitoring networks are much more limited than those of surface

water. Even when sub-surface water monitoring data exists, there are often spatial and temporal limitations that prevent quarterly sub-surface storage change from being estimated. A common solution to the lack of ground sourced environmental data is the use of remote sensing, specifically Gravity Recovery and Climate Experiment (GRACE) satellite data for sub-surface water storage (Swenson, 2012; Landerer and Swenson, 2012; Swenson and Wahr, 2006). GRACE consists of two satellites that orbit Earth at approximately 140 miles apart. The satellites measure monthly changes in Earth's gravity field caused by changes in mass over land and in the atmosphere, relative to a time-mean baseline. Changes in atmospheric mass are removed during processing, leaving only changes in mass over land. Since most monthly gravity changes over land are due to changes in water storage, GRACE data is reported as equivalent water thickness (EWT) in cm, which represents a theoretical height of water gained or lost required to produce mass based monthly gravity changes (Wahr et al. 1998). The total EWT includes changes in surface water storage, groundwater storage, soil moisture storage, and snow water equivalent storage. Previous studies have used GRACE EWT data to estimate soil moisture and groundwater storage changes by removing the other water storage changes contributing to the EWT total (Rodell et al., 2007; Scalon et al., 2012; Swenson et al., 2008).

There are several periods of 1 to 2 months with missing EWT data throughout the WBM study period due to satellite operational errors. To estimate the EWT for the missing months with the GRACE period of record, linear interpolation was used. In this case, the equation for linear interpolation is written as:

$$EWT_i = \frac{EWT_2 - EWT_1}{n} + EWT_{i-1} \tag{14}$$

where EWT_i is the EWT for the month of interest, EWT_1 is the EWT of the closest known month

before EWT_i, EWT_2 is the EWT of the closest known month after EWT_i, n is the number of months between EWT_1 and EWT_2, and EWT_{i-1} is the EWT of the month previous to EWT_i. Equation 7 was used with the measured and estimated EWT for the first month of each quarter to estimate the quarterly change in EWT. Then each quarter's ΔS_{surf} volume was subtracted from the EWT change, and the remaining volume of water lost or gained was assumed to be due to soil moisture and groundwater storage changes, or ΔS_{sub}. Snow water equivalent storage is negligible for the SEWPR and can be ignored.

No EWT data is available for July-December 2017 as a result of the two GRACE satellites being decommissioned after June 2017. To estimate ΔS_{sub} for 2017 Q3 and Q4 which fall outside of the GRACE period of record, a multiple linear regression model was developed to estimate quarterly change in EWT using quarterly EWT change based on only observed GRACE data and not interpolated quarters, and other known quarterly hydrologic variables. Different models were trained and tested with independent data sets using different combinations of independent variables. The regression model with significant (95% confidence level) variable coefficients and intercept was chosen and is written as:

$$EWT_{(2017\ Q3,4)} = -0.328ET_{(2017\ Q3,4)} + 1.830\ \Delta S_{surf(2017\ Q3,4)} + 8.242 \quad (15)$$

where $EWT_{(2017\ Q3,4)}$ is the equivalent water thickness for 2017 Q3 and Q4, $ET_{(2017\ Q3,4)}$ is evapotranspiration for 2017 Q3 and Q4, and $\Delta S_{surf(2017\ Q3,4)}$ is surface storage change for 2017 Q3 and Q4. The model performed reasonably well when compared with observed data, with an R_2 of 0.72, nRMSE of 0.54, NSE of 0.67, and % bias of 23.7%. The ΔS_{surf} for 2017 Q3 and Q4 was subtracted from the model estimated EWT to calculate ΔS_{sub} for those quarters. Estimated change in GRACE EWT for each quarter is shown in Table A7 in the Appendix.

4.5 Evapotranspiration

The evapotranspiration (*ET*) component of the WBM was estimated using a similar procedure to *P*. Actual evapotranspiration (ET_a) data is available from the Famine Early Warning Systems Network (FEWS NET, 2019). The data product is a raster surface with 1 km resolution pixels containing monthly ET_a volumes in millimeters (mm), estimated using the Operational Simplified Surface Energy Balance (SSEBop) model (Senay et al., 2013). The SSEBop model is a modified version of the SSEB approach developed by Senay et al., where ET_a is estimated by temperature differences based on two reference *hot* and *cold* land surface temperature pixels. The *hot* pixel represents bare land, while the *cold* pixel represents wet and well vegetated land. The difference between the near-surface temperature and the land surface temperature is assumed to be the latent heat flux, or the energy consumed by evapotranspiration. Therefore, the *hot* pixel has the lowest latent heat flux and minimum ET_a, while the *cold* pixel has the highest latent heat flux and maximum ET_a. The remaining pixels have ET_a estimates proportional to their land surface temperature in relation to the *hot* and *cold* pixels (Senay et al. 2007). The way the SSEBop differs from SSEB is the unique parameterization for operational applications that uses seasonally dynamic pre-defined boundary conditions for *hot* and *cold* reference points that are unique to each pixel, improving local ET_a estimates (Senay et al., 2013).

Because the SSEBop model is designed for land pixels, it may not be as accurate over large bodies of water compared to open water evaporation estimation methods. The USACE Tulsa District reports daily evaporation data for each of their managed reservoirs that is available to the public online (USACE, 2020). They use a set of empirical equations that estimate daily reservoir evaporation (E_r) using environmental input parameters including temperature, wind speed, relative humidity, and solar radiation (Harwell, 2012). The daily E_r depths in inches were

summed into quarterly E_r depths for each reservoir and multiplied by its surface area to convert from depth to volume. This made it possible to sum the E_r volumes of all four USACE reservoir for each quarter.

Since E_r was estimated separately, SSEBop ET_a pixels for the four USACE reservoirs were removed from the analysis within the SEWPR. The monthly ET_a rasters with the reservoirs removed were summed into quarters, and ArcGIS 3D analyst tools were used to estimate the volume of ET_a across the SEWPR for each quarter (Figure 19). E_r and ET_a were added together for each quarter to calculate the *ET* component of the WBM.

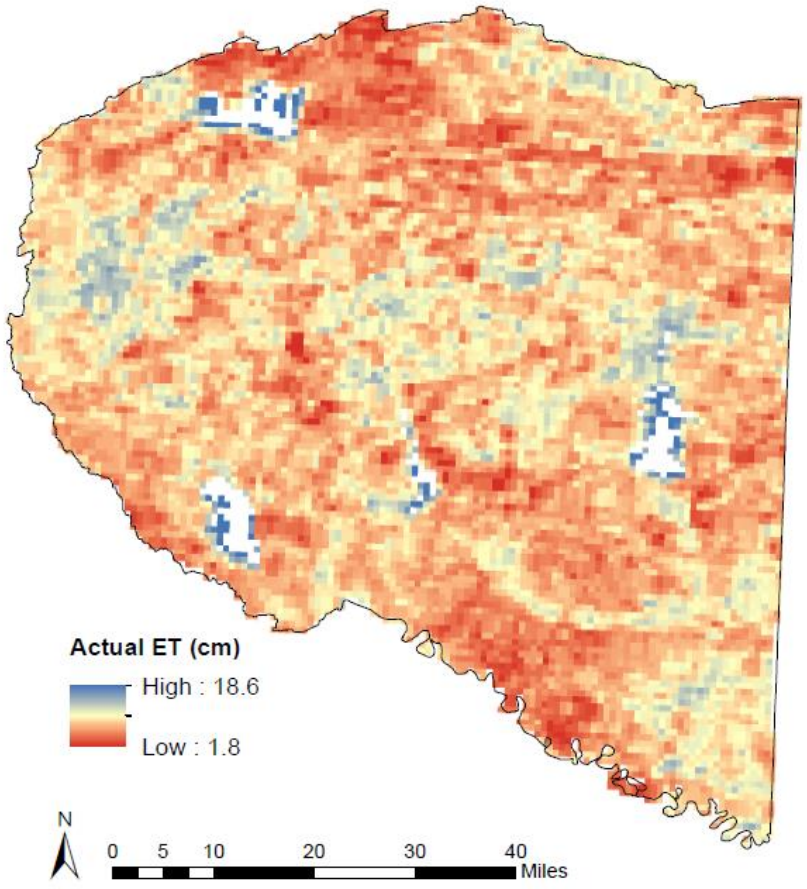

Figure 19: Operational Simplified Surface Energy Balance model actual evapotranspiration in inches for the Southeast Watershed Planning Region of Oklahoma for 2007 Quarter 1, with United State Army Corps of Engineers reservoirs removed (FEWS NET, 2019).

4.6 Additional Hydrologic Components

This section describes the methods used to estimate two additional hydrologic components on a quarterly basis within the SEWPR that are not separate components of the WBM. These include baseflow (BF), wastewater discharges (WWD), and reservoir discharges (RD) from USACE managed reservoirs within the SEWPR. All three of these sub-components are accounted for within the main components of the WBM. While they are not necessary for estimating consumptive use within the WBM, their volume and magnitude relative to each other, and the rest of the main WBM components could potentially be of interest to water managers.

4.6.1 Baseflow

Baseflow (BF) is the component of streamflow that is sustained in the absence of direct runoff, largely due to groundwater discharges (USGS, 2017). While BF is not a separate component of the WBM, it is an important parameter for understanding the hydrologic patterns of a watershed, including groundwater-surface water interactions. The PART program within the USGS Groundwater Toolbox software was used to estimate quarterly BF discharge at all stream sites leaving the SEWPR. PART uses streamflow partitioning to estimate a daily BF record from the streamflow record. PART equates BF to streamflow on days that fit an antecedent recession requirement of being unaffected by runoff or interflow, and linearly interpolates BF on other days (Rutledge, 1998).

Observed discharge data from all USGS gaging stations within the SEWPR was imported into Groundwater Toolbox. Data from several other stations with small drainage areas (less than 830 km^2) nearby but outside the SEWPR was also imported. Importing these additional stations helps increase the sample of observed discharge from small drainage areas, which were used to estimate BF on the small ungauged tributaries that exit the SEWPR. The PART program within

Groundwater Toolbox estimates the BF discharge rate and volume, along with the baseflow index (BFI) which is the ratio of BF to total stream discharge. For the two larger rivers flowing out of the SEWPR (Kiamichi River and Little River), the quarterly estimated BFI from the station nearest to the point where each river exits the SEWPR was multiplied by the estimated discharge out at the ungauged point from Section 4.2, which yields the estimated quarterly BF volume. For the smaller ungauged streams exiting the SEWPR, with drainage areas ranging from 23 to 190 km^2, the mean of quarterly BFI from the five gaging stations with the smallest drainage areas (103 to 829 km^2) was multiplied by estimated ungauged discharge on each outflow stream from Section 4.2.

4.6.2 Wastewater Discharges

It is useful to quantify wastewater discharges (WWD) within the SEWPR and the proportion that WWD contribute to the Q_{out} component of the WBM. Quantifying WWD provides water managers with an estimation of the amount of water being used, but not consumed, for industrial, municipal, or private purposes. Quarterly WWD were estimated using Oklahoma Department of Environmental Quality (ODEQ) Discharge Monitoring Report (DMR) data from National Pollutant Discharge Elimination System (NPDES) permits (ODEQ, 2018). The discharge data for each outfall location at wastewater treatment facilities within the SEWPR is reported each month as an average daily flow rate and is available by water year (October 1 – September 30) beginning in 2010. The daily flow rates were multiplied by the number of days in the respective month to calculate the monthly discharge volume, and monthly total volumes were summed into quarters for each reporting facility within the SEWPR.

4.6.3 Reservoir Discharges

Water released from the dams of three of the four USACE managed reservoirs in the SEWPR (Broken Bow, Hugo, and Pine Creek) into the receiving rivers below each reservoirs dam are referred to as reservoir discharges (RD). The RD from Sardis Lake were excluded because water discharged from the lake eventually flows into Hugo Lake further downstream via the Kiamichi River. The USACE Tulsa District reports daily RD data for each of their managed reservoirs that is available to the public online (USACE, 2020). Daily RD data for Broken Bow, Hugo, and Pine Creek reservoirs was summed into quarterly total RD volume, and then converted into relative depth in cm over the entire SEWPR.

4.7 Statistical Methods

Various statistical methods were used to analyze the relationships between the different WBM components. These included the coefficient of variation (CV), Pearson correlation coefficient (CC), and the independent two sample t-test. The CV is a standardized measurement of variability, or dispersion, in a distribution and is calculated as the ratio of standard deviation (σ) to the sample mean (μ).

$$CV = \frac{\sigma}{|\mu|} \tag{16}$$

The CV can range from 0 to $\sqrt{n - 1}$, where n is the sample size. A CV close to 0 indicates the values in the sample have a low variability, while a CV close to $\sqrt{n - 1}$ indicates the values in the sample have high variability. The CV is useful for comparing the variability among the WBM components with different sample means. However, CV can only be used for components with absolute zeros such as P, ET, and Q_{out}, and not for ΔS_{surf} and ΔS_{sub} which can have negative or positive values. The presence of both negative and positive values causes the mean to approach

0, while the σ does not change whether the values are negative or positive. This leads to misleadingly large CV values.

Another statistical metric used to analyze the WBM components was the Pearson CC, which represents the degree of correlation between two samples. The equation for the Pearson CC is written as:

$$CC = \frac{n(\sum x_1 x_2) - (\sum x_1)(\sum x_2)}{\sqrt{[n\sum x_1^2 - (\sum x_1)^2][n\sum x_2^2 - (\sum x_2)^2]}} \quad (17)$$

where n is the number of pairs between the two samples, $\Sigma x_1 x_2$ is the sum of the product of the pairs, Σx_1 is the sum of the values in the first sample, and Σx_2 is the sum of the values in the second sample. The "Hmisc" statistical analysis package (Harrell et al., 2019) written within the R programing language (R Core Team, 2018) was used to calculate the CCs between the different WBM components, and test for statistical significance at the 95% confidence level. A CC of 1 indicates perfect positive correlation between the two samples, a CC of 0 indicates no correlation between the two samples, and a CC of -1 indicates perfect negative correlation between the two samples.

The last type of statistical test used for WBM component analysis was the independent two sample t-test. This test determines whether the means of two samples are significantly different based on a selected confidence level. To perform the test, first the *t* statistic is computed as:

$$t = \frac{\mu_1 - \mu_2}{\sqrt{\frac{\sigma_1^2}{n_1} + \frac{\sigma_2^2}{n_2}}} \tag{18}$$

where μ_1 is the mean of the first sample, μ_2 is the mean of the second sample, σ_1 is the standard deviation of the first sample, σ_2 is the standard deviation of the second sample, n_1 is the sample size of the first sample, and n_2 is the sample size of the second sample. The computed *t* statistic is then compared to the critical value for the chosen confidence level. For this study, the chosen confidence level for independent two sample t-tests was 95%. Therefore, if the probability (*p*), of the *t* statistic being greater than the critical value was less than 0.05, the means of the two samples were determined to be statistically different.

Chapter 5 – Results & Discussion

In this chapter, the results for each part of the SEWPR WBM analysis are presented along with statistical analysis and discussion of the noteworthy findings. The following sub-sections provide estimated quarterly volumes of WBM components, estimated uncertainty associated with each WBM component estimation method and the overall model, quarterly consumptive use volumes and uncertainty of the entire WBM, and results of the WBM on an annual basis to compare with the quarterly results. Water volumes are given as a representative depth in cm across the entire SEWPR for the purposes of simpler reporting and analysis. The volumes can be converted to representative depths in other units or to different volume units by applying the appropriate conversion factors and multiplying by the SEWPR area.

5.1 Water Balance Model Components

The estimated quarterly volumes for the components of the SEWPR WBM are shown in Figure 20 and in Table A8 in the Appendix. Trends for each component are shown in Figures 21, 22, 23, 24, and 25 for P, Q_{out}, ET, ΔS_{surf}, and ΔS_{sub} respectively. The results illustrate both the seasonal variability of the WBM components and the magnitude of each component during the different quarters from 2007-2017.

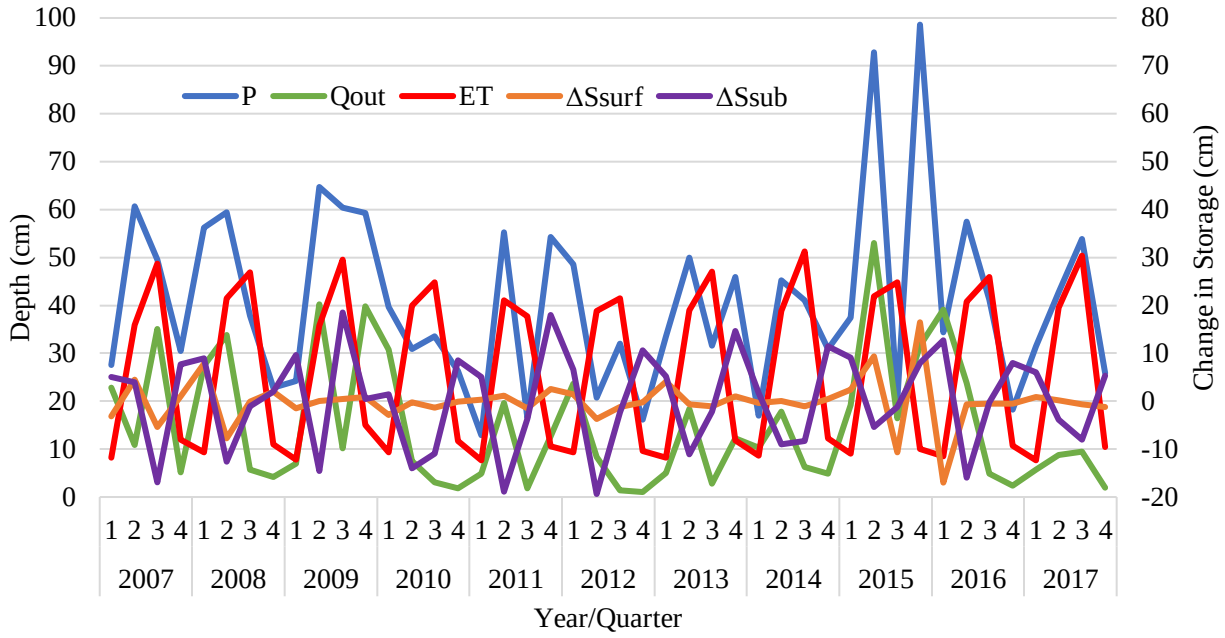

Figure 20: Trends of quarterly precipitation (*P*), evapotranspiration (*ET*), streamflow out (Q_{out}), surface storage change (ΔS_{surf}), and sub-surface storage change (ΔS_{sub}). *P*, *ET* and Q_{out} are shown on the left axis, and ΔS_{surf} and ΔS_{sub} are shown on the right axis to account for the negative values.

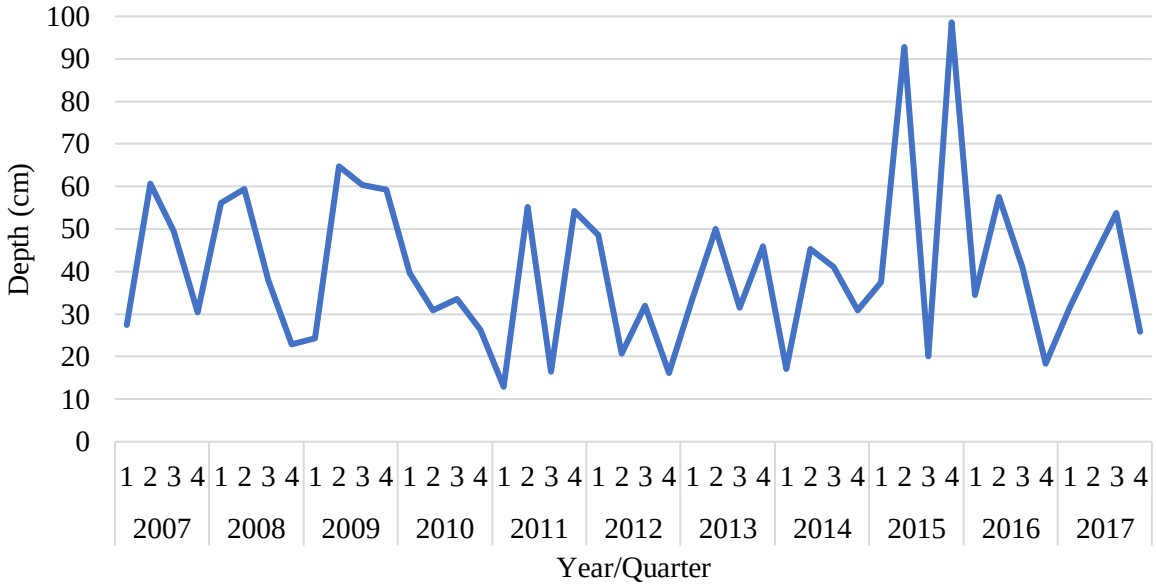

Figure 21: Trends of quarterly precipitation (*P*). Data from the National Centers for Environmental Prediction Stage IV Quantitative Precipitation Estimates.

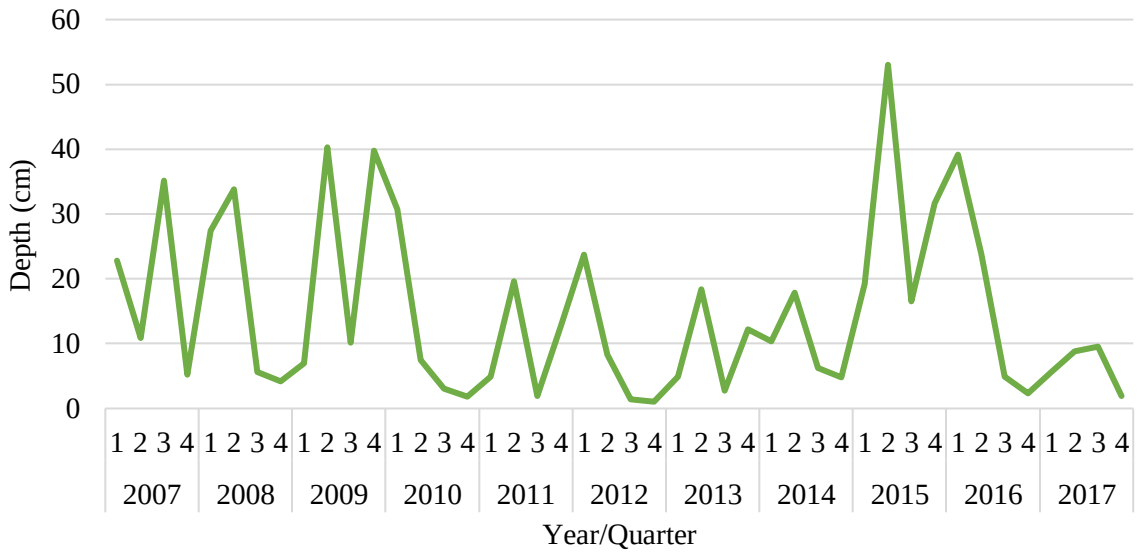

Figure 22: Trends of quarterly streamflow out (Q_{out}).

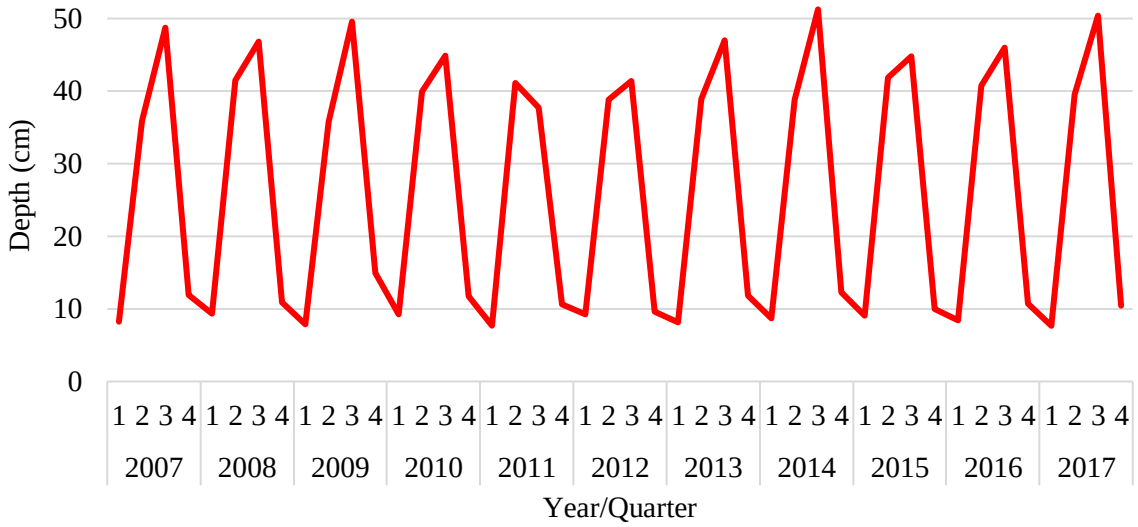

Figure 23: Trends of quarterly evapotranspiration (*ET*). Data from the Famine Early Warning Systems Network.

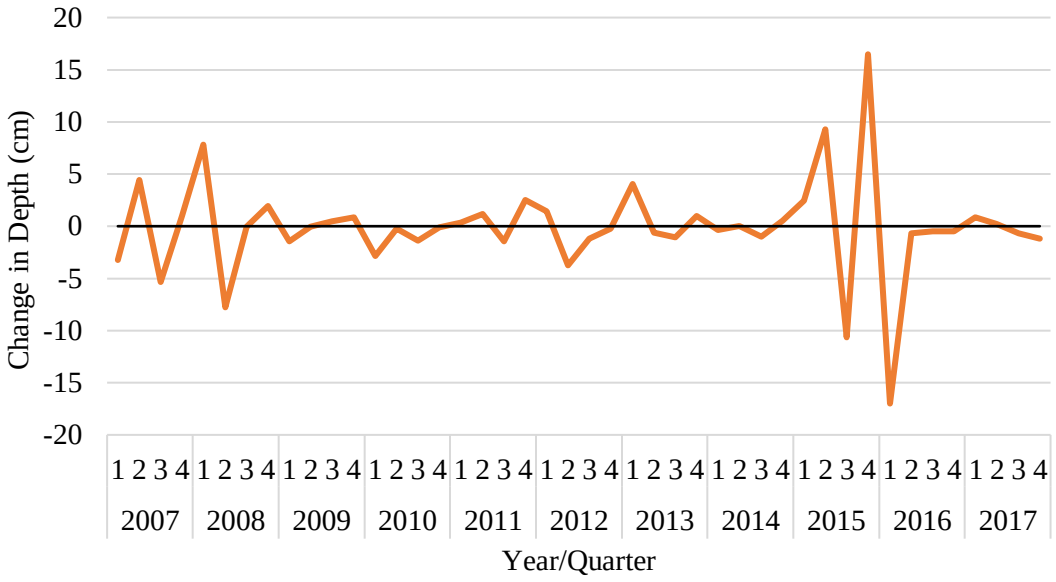

Figure 24: Trends of quarterly surface storage change (ΔS_{surf}).

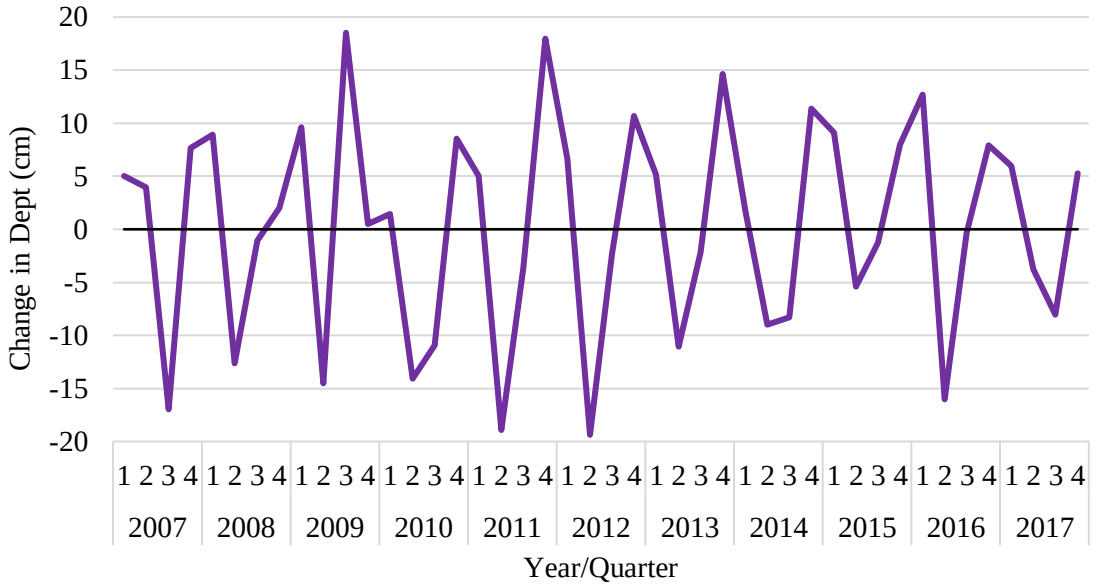

Figure 25: Trends of quarterly sub-surface storage change (ΔS_{sub}). Data from the Gravity Recovery and Climate Experiment satellite mission.

5.2 Uncertainty

The uncertainty associated with each WBM component estimation method or data set used were quantified wherever it was feasible to do so. The combined uncertainty of each component represents the uncertainty of the quarterly consumptive use estimation from the WBM. The following sub-sections describe the uncertainty estimation for each WBM or explain why an uncertainty could not be quantified for certain components. The minimum total quantifiable uncertainty for each WBM component is shown in Table 6. It is extremely important to note that these quantified uncertainties do not fully represent the total uncertainty of any WBM component, but simply represent the minimum quantified uncertainty. The true uncertainty of each component and the overall WBM was not quantifiable within the scope of this study but is likely much larger than the given minimum values.

Table 6: Minimum quantifiable uncertainty of each water balance model (WBM) component shown as an average % of the total quarterly volume. NA was given for components that had no quantifiable uncertainty. WBM components include precipitation (P), streamflow out (Q_{out}), evapotranspiration (ET), surface storage change (ΔS_{surf}), and sub-surface storage change (ΔS_{sub}).

WBM Component	Minimum Uncertainty
P	NA
Q_{out}	>18%
ET	>17%
ΔS_{surf}	>13%
ΔS_{sub}	NA

5.2.1 Precipitation

The uncertainty associated with the NCEP Stage IV QPE used to estimate quarterly P volumes in the SEWPR cannot be estimated in the scope of this study due to the manual quality control that is performed in post-processing of the observation data. NCEP Stage IV QPE is the

latest precipitation accumulation data product available from the National Weather Service, with an hourly temporal resolution. The data product was used in a study that estimated the uncertainty of another QPE rainfall product, using NCEP Stage IV QPE as reference data (Chen et al., 2013). Any uncertainty associated with the NCEP Stage IV QPE data product is likely relatively small and was considered negligible for the WBM.

5.2.2 Streamflow

Several potential sources of uncertainty associated with the streamflow estimation methods could be resulting from many different factors, such as flow contributions to the Little and Red Rivers from additional streams outside the SEWPR, different groundwater-surface water interactions among streams, or human withdrawals. The complexity of the different factors potentially contributing to this uncertainty make it infeasible to quantify within the scope of this study. To quantify this uncertainty in the future, stream gauges would need to be installed on several SEWPR outflow streams that are representative of the type present in the watershed to gather discharge observations. There are 19 total streams that exit the SEWPR (Table A2). Using the calculation steps for minimum sample size (Equation 10 and 11), along with a 95% confidence level and a 10% margin of error, stream gauges should be installed on a minimum of 17 streams to be representative of the 19 total outflow streams. Discharge observations should be recorded at each gauge. After the gauges have periods of observed discharge that are representative of both wet and dry years within the SEWPR, Q_{out} could then be estimated at each gauge site using the WBM methods and compared to observed streamflow data from the new gauge stations.

The estimated long-term average flow rates at ungauged locations from USGS StreamStats are another source of uncertainty associated with the Q_{out} estimation methods. The

StreamStats estimated flow rate for each outflow stream was multiplied by each quarter's SC (Equation 6) and summed to calculate quarterly Q_{out} volumes. A study from USGS quantified the uncertainty of the regional regression equations used by StreamStats to estimate long-term average flow rates at ungauged sites in Oklahoma, and the relative standard error as percent was used as an estimate of uncertainty (Esralew and Smith, 2010). The uncertainty of the regression equation for Region 3, which includes the SEWPR, was 18%. This uncertainty estimate was used for Q_{out}, with the assumption that there is additional unquantifiable uncertainty also associated with the quarterly Q_{out} estimates.

5.2.3 Surface Storage Change

The separate methods for ΔS_{surf} volumes estimation for mapped and unmapped surface waterbodies both have associated uncertainty that contributes to the overall uncertainty of the quarterly ΔS_{surf} volume estimates. The mapped waterbody ΔS_{surf} estimation methods include uncertainty from both USACE and OWRB mapped reservoirs, and the unmapped waterbody methods include uncertainty for the remaining lentic waterbodies within the SEWPR. The USACE reservoirs account for the largest percentage of average quarterly ΔS_{surf} in the SEWPR (73.8%) followed by unmapped waterbodies (25.9%) and OWRB mapped reservoirs (0.3%). These percentages were used to proportionally weight the uncertainty from each type of waterbody.

The USACE Tulsa District has not quantified the uncertainty of the storage volume data they report for each reservoir, but there is likely some uncertainty from human and instrumental measurement error for the bathymetric data used to develop the area-capacity curves, and from the area-capacity curve method for estimating storage volume from reservoir pool elevation.

The uncertainty of the OWRB reservoir methods potentially comes from errors in the bathymetric data collection, the MNDWI methods for identifying surface water pixels from Landsat data to estimate quarterly surface area of each reservoir, and the area-volume regression models for each waterbody (Table 2). The bathymetric data collection uncertainty comes from human and instrumental measurement errors and could not be quantified but is expected to be relatively small. The range of accuracy of the MNDWI method for identification of surface water pixels from Landsat data was estimated to be 94-99% with an average of 95% in previous studies (Rokni et al., 2014; Xu, 2006). An uncertainty of 5% was used for the number of surface water pixels identified using MNDWI.

Additional uncertainty came from the spatial resolution of the Landsat pixels. The Landsat pixel resolution of 30 m potentially causes over/underestimation of waterbody surface area along the shoreline. To estimate this uncertainty, each OWRB mapped waterbody was manually digitized using USDA NAIP aerial images to calculate the surface area. The NAIP based surface areas were compared to Landsat based areas, calculated using Landsat images from the date closest to the NAIP aerial imagery date and the MNDWI analysis. The average uncertainty of the Landsat based area compared to the NAIP based area for each reservoir was calculated and added to the 5% uncertainty from MNDWI water pixel identification. The uncertainty of the area-volume regressions models for each waterbody could not be quantified due to lack of reference data. The average known quarterly uncertainty for the OWRB mapped waterbodies was estimated to be 11%.

The unmapped surface waterbody ΔS_{surf} method uncertainty potentially comes from several sources including: bathymetric data collected for the sample of small lentic waterbodies in the SEWPR, human measurement error from manual digitization of waterbodies from aerial

images, regression models that estimate storage volume from surface area based on the bathymetric data (Table 4), extrapolation of an estimated storage volume per km^2 to the entire SEWPR, and the regression model to estimate quarterly ΔS_{surf} for unmapped waterbodies for quarters with no available aerial imagery based on other quarterly WBM components (Equation 9). Uncertainty from the bathymetric data collection and manual digitization is not quantified but assumed to be relatively small. The RMSE of the regression models used to estimate unmapped waterbody volume from surface area was considered the uncertainty. This uncertainty was weighted based on the percentage of digitized ponds each model's area threshold included. Both weighted model uncertainties were added to calculate the uncertainty of a single modeled waterbody volume, which was then extrapolated to the entire SEWPR based on estimated waterbody density per km^2. An estimated uncertainty of 52% was used for this portion of the methodology. The uncertainty of Equation 9 could not be quantified due to the lack of reference data.

Most of the uncertainty associated with the ΔS_{surf} methods was not quantifiable in the scope of this study, including the USACE reservoirs which account for 74.7% of total ΔS_{surf} volume, and portions of other mapped and unmapped waterbody methods. The minimum known uncertainty is 13%, but this includes only a small portion of the potential uncertainty, which is likely considerably larger.

5.2.4 Sub-surface Storage Change

The total uncertainty of the ΔS_{sub} component comes from the uncertainty of the monthly GRACE EWT measurements, and the large spatial resolution of the GRACE pixels. To the author's knowledge, there are no previous studies where the uncertainty of GRACE EWT data or its application for sub-surface storage change estimation has been quantified. Previous studies

have shown GRACE EWT can be suitable for estimating groundwater storage changes over large areas (Rodell et al., 2007; Scalon et al., 2012; Swenson et al., 2008), but these studies removed soil moisture from the analysis, and were conducted over much larger areas than the SEWPR (160,000 to 900,000 km^2). A common recommendation is to use a minimum study area of 200,000 km^2 when using GRACE data for hydrologic applications, which is approximately 17 times greater than the SEWPR area. The resolution of a single GRACE pixel is approximately 90,000 km^2, compared to the SEWPR area of 11,500 km^2. This means that over 87% of the land area contributing to each EWT value is outside the SEWPR. Using GRACE data at such a small scale means there are likely large uncertainties associated with the quarterly ΔS_{sub} volumes derived from the GRACE EWT values that are not quantifiable in the scope of this study. However, for this project, using GRACE was the only feasible option for estimating ΔS_{sub}.

5.2.5 Evapotranspiration

The total uncertainty of the quarterly *ET* volume estimates comes from two separate sources, the SSEBop model used to estimate actual ET for the entire SEWPR except for the four USACE reservoirs, and the USACE evaporation estimates for each reservoir. The USACE reservoir evaporation accounts for about 11% of the of the total quarterly ET volume on average, so the uncertainty of the reservoir evaporation methods contributes less to the overall uncertainty of the *ET* component estimation than the SSEBop method.

For the SSEBop model uncertainty, data from a previous study that estimated the uncertainty of the SSEBop model by comparing its results with measured actual ET from AmeriFlux tower sites located within different land cover types was used (Chen et al., 2016). The relative error of the SSEBop model for forest and grassland sites, the most predominant land cover types in the SEWPR, ranged from 18-19%, so an uncertainty of 19% was used for

quarterly SSEBop actual ET estimates in the SEWPR. The USACE Tulsa District has not quantified uncertainty for its reservoir evaporation estimates, but it was assumed that a small amount of unknown additional uncertainty from the USACE reservoir evaporation data also contributes to the quarterly *ET* volume estimates for the WBM. The proportionally weighted uncertainty of the SSEBop estimated ET_a volumes provides a minimum known uncertainty of 17% for the *ET* component.

5.3 Water Balance Model Component Analysis

In this section, relationships and trends between the quarterly WBM components were analyzed, and notable similarities and differences between the components were shown. The mean (μ) and coefficient of variation (CV) of each WBM component for each of the four quarters and for all quarters combined from 2007-2017 are shown in Table 7. The CV for ΔS_{surf} and ΔS_{sub} are not shown because the existence of both positive and negative values leads to the mean to be closer to zero than the other components. This causes misleadingly large or negative CV values when the standard deviation is divided by the mean (Equation 16). Instead the CV of total surface storage (S_{surf}) is shown, which is representative of the variability of ΔS_{surf} since ΔS_{surf} value are calculated from S_{surf} values. Total sub-surface storage data was not available, because GRACE equivalent water thickness data is only reported as a change in storage. Instead, the standard deviation (σ) is shown for ΔS_{sub} as a measure of variability, but cannot be compared to other components.

The strengths of the relationships between WBM components and some additional variables were measured using Pearson correlation coefficients (CC) (Equation 17). A correlation matrix with the CC values between each pair of WBM components, the three sub-

components (BF, WWD, and RD), and an additional variable solar radiation (R), is shown in Table 8.

Table 7: Mean (μ) in cm and coefficient of variation (CV) of precipitation (*P*), evapotranspiration (*ET*), streamflow out (Q_{out}), total surface storage (S_{surf}). For sub-surface storage change (ΔS_{sub}), the standard deviation (σ) is shown instead of CV.

	P		Q_{out}		*ET*		S_{surf}		ΔS_{sub}	
Quarter	μ	CV	μ	CV	μ	CV	μ	CV	μ	σ
1	33.0	0.4	17.8	0.6	8.5	<0.1	17.8	0.3	6.5	3.2
2	52.7	0.3	22.0	0.6	39.4	<0.1	17.1	0.2	-11.0	6.7
3	38.0	0.3	8.8	1.1	46.2	<0.1	17.3	0.2	-3.3	8.5
4	39.0	0.6	10.7	1.2	11.4	0.1	15.2	0.1	8.6	4.9
All	40.7	0.5	14.8	0.9	26.4	0.6	16.8	0.2	0.2	10.0

Table 8: Correlation matrix with Pearson correlation coefficients (CC) between the water balance model (WBM) components and additional variables and sub-components used in analysis. The WBM components include precipitation (*P*), evapotranspiration (*ET*), streamflow out (Q_{out}), surface storage change (ΔS_{surf}), and sub-surface storage change (ΔS_{sub}). The additional sub-components and variables are solar radiation (R), baseflow (BF), wastewater discharges (WWD), and reservoir discharges (RD). * denotes significance at the 95% confidence level.

	P	Q_{out}	*ET*	ΔS_{surf}	ΔS_{sub}	*R*	*BF*	*WWD*	*RD*
P	-	0.69*	0.25	0.53*	-0.14	0.14	0.45*	0.72*	0.61*
Q_{out}	0.69*	-	0.02	0.04	-0.20	-0.01	0.93*	0.78*	0.95*
ET	0.25	0.02	-	-0.20	-0.69*	0.95*	-0.03	0.13	0.04
ΔS_{surf}	0.53*	0.04	-0.20	-	0.17	-0.27	-0.24	0.13	-0.10
ΔS_{sub}	-0.14	-0.20	-0.69*	0.17	-	-0.75*	-0.20	-0.14	-0.20
R	0.14	-0.01	0.95*	-0.27	-0.75*	-	0.00	0.06	0.05
BF	0.45*	0.93*	-0.03	-0.24	-0.20	0.00	-	0.68*	0.93*
WWD	0.72*	0.78*	0.13	0.13	-0.14	0.06	0.68*	-	0.76*
RD	0.61*	0.95*	0.04	-0.10	-0.20	0.05	0.93*	0.76*	-

Precipitation (*P*) was the largest component in 34 of 44 quarters, while *ET* was larger in the remaining ten quarters, eight being in Q3 and two being in Q2 (Figure 26). *ET* displayed a very consistent cyclical pattern that was unlike the other four components. Average Q2 and Q3 *ET* volumes were approximately 3 to 5 times larger than Q1 and Q4, and variability within each quarter over the 11-year period was the lowest for *ET* than any other component, with the exception of S_{surf} in Q4 (Table 7). The mean quarterly *ET* was significantly lower in Q1 and Q4 than in Q2 and Q3 ($p < 0.01$), while the same cannot be said for the mean quarterly *P* during the same quarters ($p = 0.10$).

An additional correlation analysis was performed between *P* and *ET* to determine if *P* had a delayed effect on *ET* in the following quarter. Quarterly *P* was compared to *ET* with a one quarter delay, meaning *ET* from Q2 was compared to *P* from Q1, and so on for the remaining quarters. If correlation between quarterly *P* and the next quarter's *ET* was stronger positive than a direct quarterly comparison, it would indicate that quarterly *ET* was more dependent on the previous quarter's *P* than the same quarter's *P*. However, the CC for quarterly *P* and *ET* with a one quarter delay (0.18) was lower than the CC for a direct quarterly comparison between *P* and *ET* (0.25). These results suggest that the amount of *ET* across the SEWPR each quarter was not dependent on the amount of *P*. For example, 2015 Q4 received the most *P* of any quarter with 98.6 cm, yet only lost 10.0 cm to *ET*. While in, 2014 Q3 had the highest *ET* with 51.3 cm, and *P* was just 41.1 cm. *ET* was much more dependent on energy availability than water availability in the SEWPR, because energy from solar radiation (*R*), which is the main energy source that drives the *ET* process, is greater during Q2 and Q3 than in Q1 and Q4 in the SEWPR ($p < 0.01$) (Mesonet, 2018). *R* exhibited a very similar cyclical quarterly pattern to *ET* (Figure 27) and the CC between quarterly *R* and *ET* for all quarters is much greater than for *P* and *ET* (Table 8).

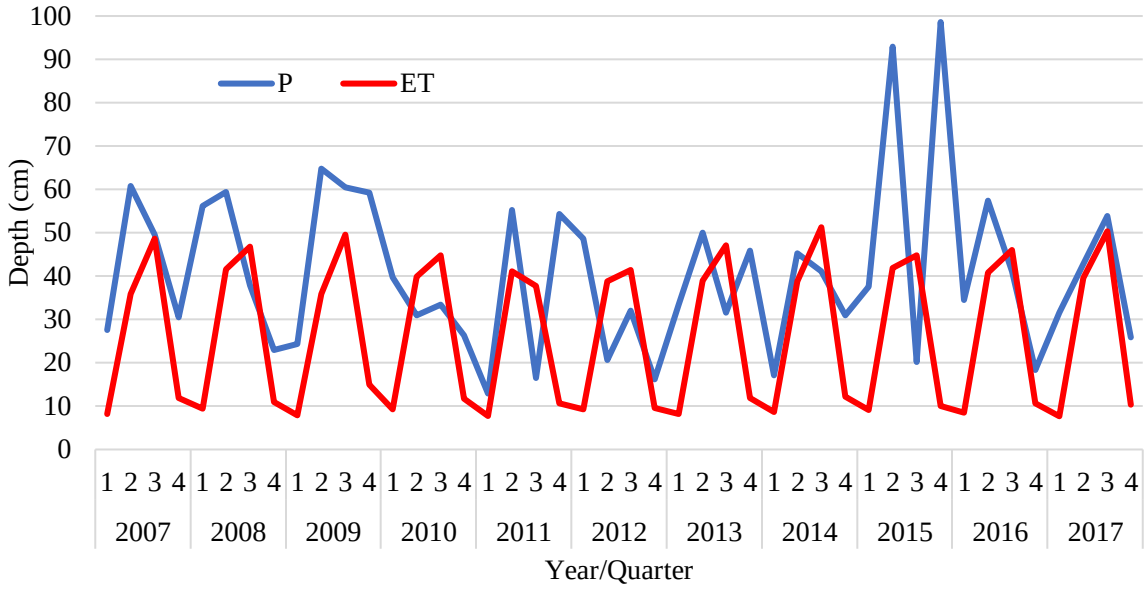

Figure 26: Trends of quarterly precipitation (*P*) and evapotranspiration (*ET*). *P* data from the National Centers for Environmental Prediction Stage IV Quantitative Precipitation Estimates and *ET* data from the Famine Early Warning Systems Network.

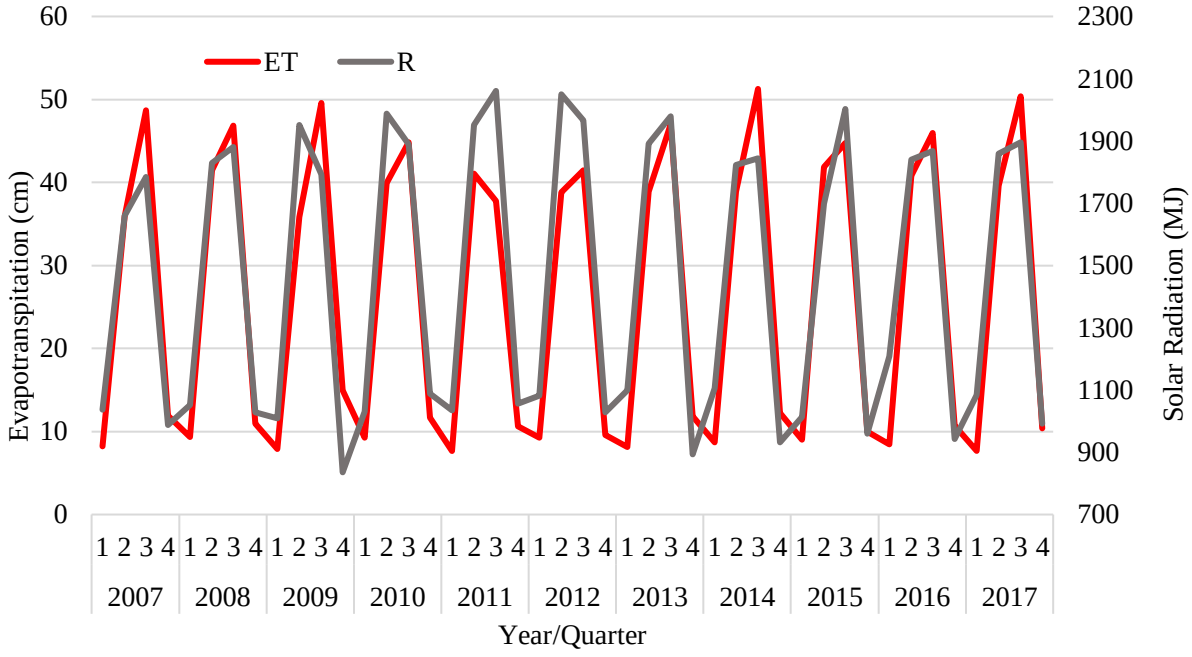

Figure 27: Trends of quarterly evapotranspiration (*ET*) in cm (left axis) and solar radiation (*R*) in Mega Joules (MJ) (right axis). *ET* data from the Famine Early Warning Systems Network and *R* data from Oklahoma Mesonet.

While *ET* is not strongly correlated with *P* (Table 8), Q_{out} showed a positive correlation with *P* (Table 8) and follow similar quarterly trends (Figure 28). These trends are typical for a rainfall-streamflow relationship where greater rainfall leads to greater streamflow, and less rainfall leads to less streamflow. However, there are several quarters that are exceptions to this general trend for the SEWPR. For example, from 2007 Q1 to 2007 Q2, *P* increased by 121%, while Q_{out} decreased by 52%. Conversely, in 2007 Q3, *P* decreased by 18%, while Q_{out} increased by 224%. There are several other quarters where a similar trend is seen. This negative relationship could potentially have been due to delayed releases from the USACE managed reservoirs following periods of heavy precipitation when water was held in the reservoirs to avoid excess flooding and then released slowly once downstream flow returned to normal levels. This was likely the case in 2016 Q1 when Q_{out} exceeded *P* by 4.7 cm following 2015 Q4 which received the most *P* of any quarter. High flows may still have been present in early 2016 Q1 causing that quarter to be the only one where Q_{out} exceeded *P*. Uncertainty associated with the Q_{out} estimation methods is likely also playing a role in the inverse relationship.

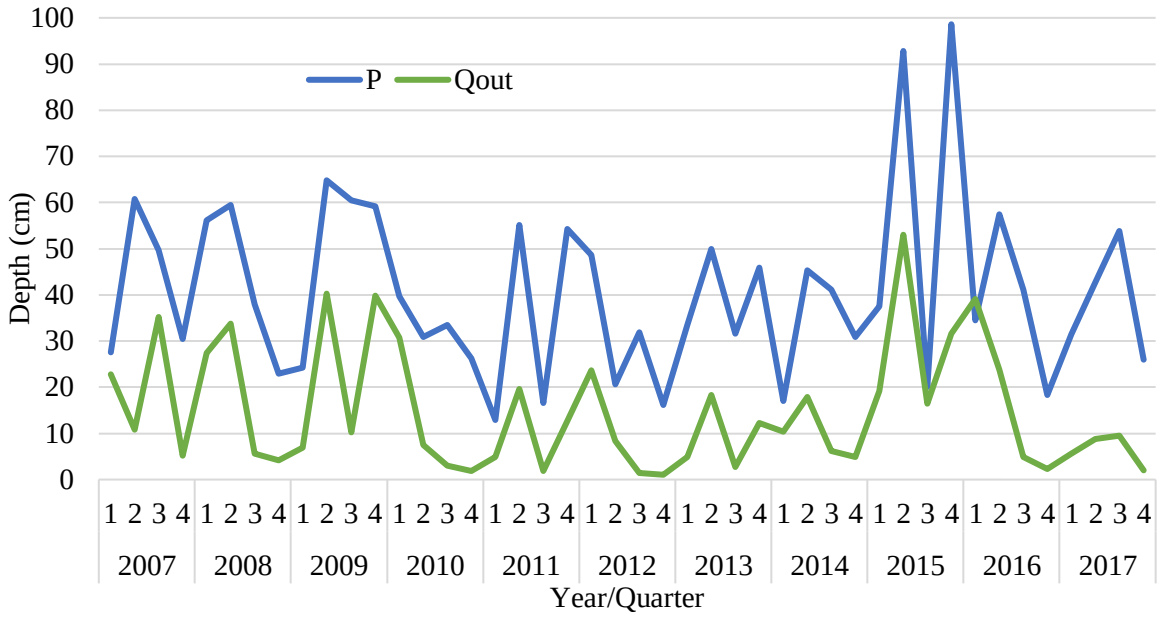

Figure 28: Trends of quarterly precipitation (*P*) and streamflow out (Q_{out}). *P* data from the National Centers for Environmental Prediction Stage IV Quantitative Precipitation Estimates.

The relationship between the two storage change components (ΔS_{surf} and ΔS_{sub}) was also analyzed. ΔS_{sub} had a greater magnitude than ΔS_{surf} in 36 of 44 quarters (Table A8) and the average quarterly magnitude of ΔS_{sub} was greater than ΔS_{surf} for all quarters (p <0.01). This could mean that there is much greater sub-surface storage capacity than surface storage capacity in the SEWPR, but there is no known way to test that theory. Regarding the trends of ΔS_{surf} and ΔS_{sub} (Figure 29), in 12 out of 44 quarters there was an opposite trend for the two storage change components. For example, in 2007 Q1 ΔS_{surf} was -2.9 cm while ΔS_{sub} was 5.0 cm. These occurrences could be due to a number of different factors, but it is most likely due to differences in surface and sub-surface hydrology, and associated uncertainty of estimation methods that is still mostly unknown.

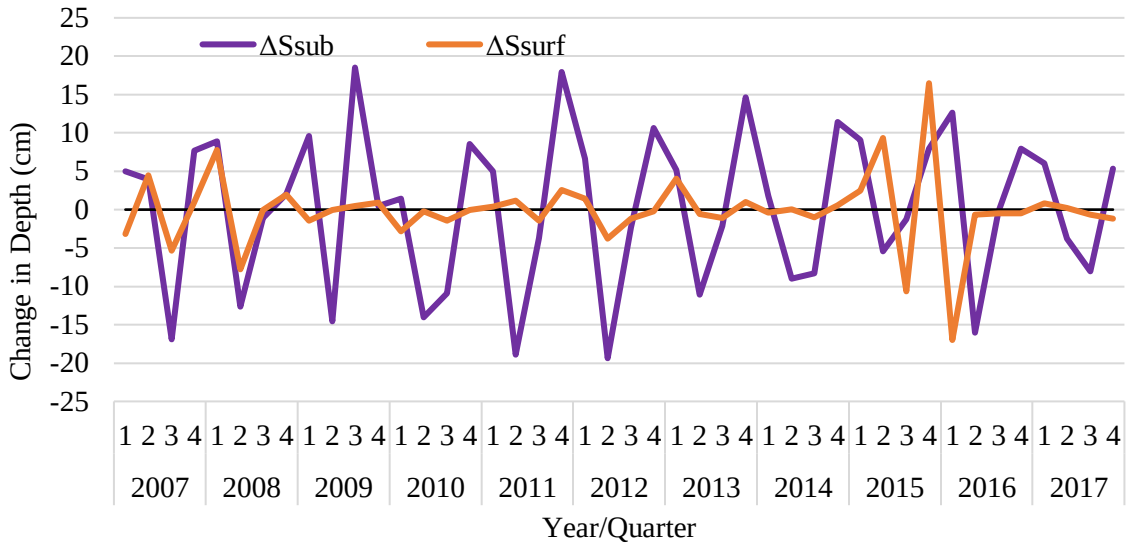

Figure 29: Trends of quarterly surface storage change (ΔS_{surf}) and sub-surface storage change (ΔS_{sub}). ΔS_{sub} data from the Gravity Recovery and Climate Experiment satellite mission.

There were also several noteworthy relationships between *P*, *ET* and storage change. *P* and *ET* are the main input and output components in the WBM, so it is expected that they appear to influence storage change. ΔS_{sub} displays a somewhat cyclical pattern which was opposite to *ET* for nearly all quarters (Figure 30). This pattern, along with a CC of -0.69 between ΔS_{sub} and *ET* (Table 8), suggests that higher *ET* volumes led to more negative ΔS_{sub}, and lower *ET* volumes led to more positive ΔS_{sub}. The was no strong correlation between ΔS_{sub} and *P* (Table 8), suggesting that ΔS_{sub} is more dependent on *ET* than *P* in the SEWPR. However, the unknown uncertainty of the ΔS_{sub} estimation methods make it difficult to draw meaningful conclusions from these relationships. For ΔS_{surf}, there was a positive correlation with *P* and a negative correlation with *ET* (Table 8). Even though the magnitude of ΔS_{surf} is much smaller than *P* for nearly every quarter (Table A6), some similar trends can be seen between the two components (Figure 31). The relationship can clearly be seen in the years 2015 and 2016, where 2015 Q2 and Q4

experienced both the largest amount of *P* and the largest positive ΔS_{surf}. The two following quarters, (2015 Q3 and 2016 Q1) had the largest negative ΔS_{surf} and below average *P*.

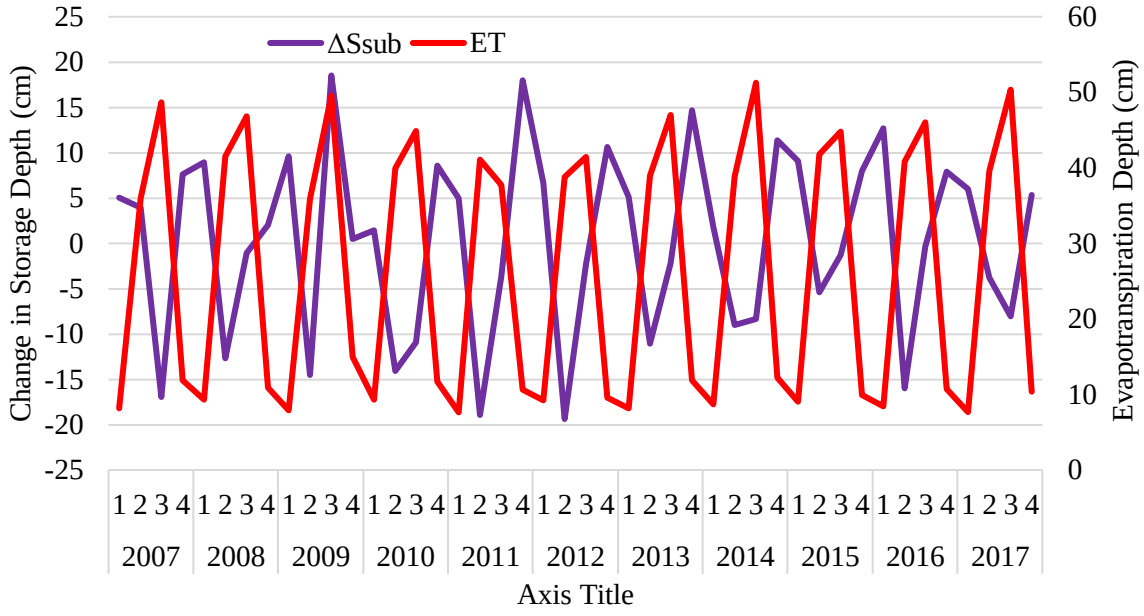

Figure 30: Trends of quarterly sub-surface storage change (ΔS_{sub}) (left axis) and evapotranspiration (*ET*) (right axis). ΔS_{sub} data from the Gravity Recovery and Climate Experiment satellite mission and *ET* data from the Famine Early Warning Systems Network.

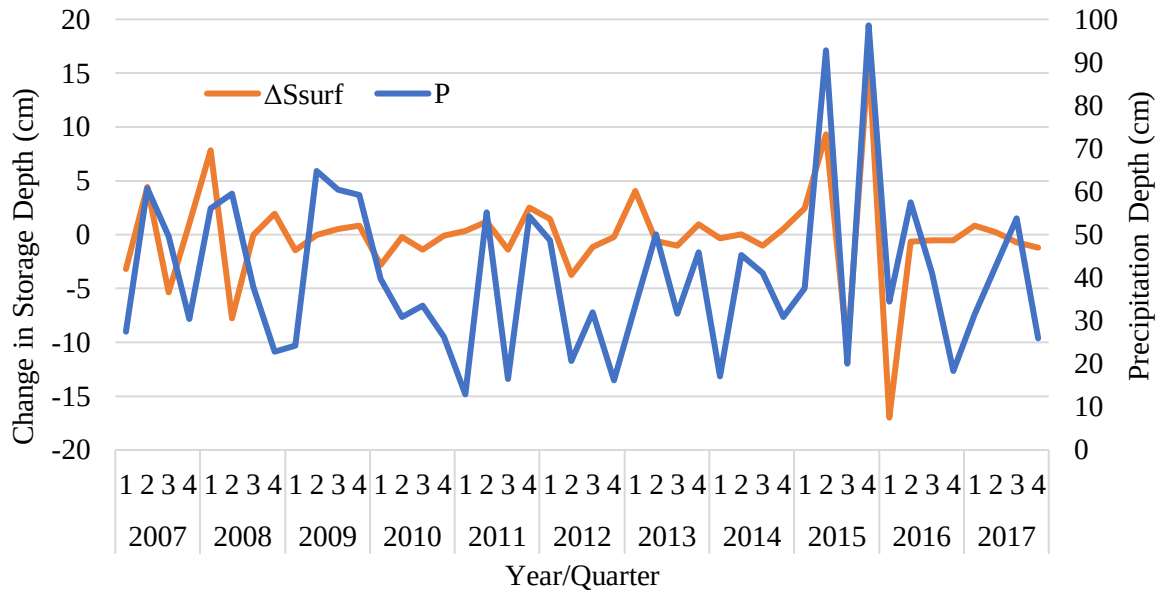

Figure 31: Trends of quarterly surface storage change (ΔS_{surf}) (left axis) and precipitation (*P*) (right axis). *P* data from the National Centers for Environmental Prediction Stage IV Quantitative Precipitation Estimates.

5.4 Baseflow, Wastewater Discharges, and Reservoir Discharges

Quarterly baseflow (BF), wastewater discharges (WWD), and reservoir discharges (RD) for the SEWPR are provided in this section. These sub-components are included in the main WBM components, but their proportions and relationships to each other, and the main WBM components can be useful information for water managers. The estimated quarterly depths for BF are shown in Table 9, which also includes BFI values that represent the proportion that BF contributes to the total streamflow. The remaining streamflow volume is assumed to be from runoff. On average, Q1 and Q2 had higher BF volumes than Q3 and Q4, which was also the case with Q_{out} volumes. BF was estimated using Q_{out}, so the quarterly trends between the two components are similar, with BF having smaller magnitudes (Figure 32). The larger the gap was between BF and Q_{out}, the smaller the BFI was, and more of the total streamflow was due to runoff. The average BFI value was 0.49 for all quarters, and the average BFI for individual quarters ranged from 0.47 for Q2 to 0.51 for Q1. This means the outflow streams typically had a fairly even mix of BF and runoff contributing to total flow, with an average of 1% more BF in Q1, and an average of 1-3% more runoff in Q2-Q4.

Table 9: Quarterly baseflow (BF) depths in cm and baseflow index (BFI) values for streams flowing out of the Southeast Watershed Planning Region of Oklahoma. Data from United States Geological Survey.

Quarterly BF volumes and BFI values								
	Q1		Q2		Q3		Q4	
Year	BF	BFI	BF	BFI	BF	BFI	BF	BFI
2007	12.9	0.57	2.7	0.25	11.7	0.33	2.3	0.44
2008	9.6	0.35	18.3	0.54	1.9	0.33	2.5	0.59
2009	3.4	0.49	17.0	0.42	1.2	0.12	19.5	0.49
2010	12.2	0.40	3.8	0.51	1.6	0.53	0.7	0.40
2011	3.3	0.67	9.4	0.48	2.1	1.12	3.3	0.26
2012	10.7	0.45	7.5	0.90	1.0	0.69	0.7	0.70
2013	2.4	0.48	8.0	0.43	1.2	0.43	4.6	0.38
2014	5.5	0.53	7.6	0.43	2.5	0.41	2.5	0.52
2015	8.6	0.45	24.1	0.45	10.4	0.63	7.7	0.24
2016	26.8	0.68	7.9	0.33	2.6	0.53	2.4	1.05
2017	3.3	0.59	3.5	0.40	2.8	0.29	0.7	0.34
Avg.	9.0	0.51	10.0	0.47	3.5	0.49	4.3	0.49

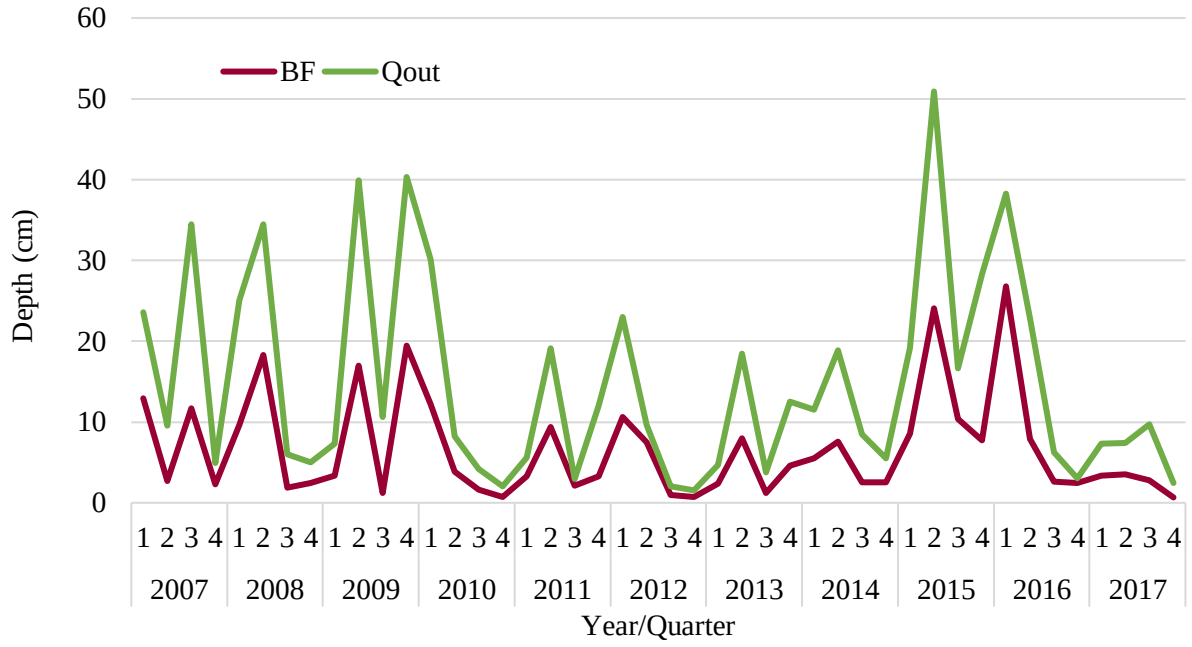

Figure 32: Trends of quarterly baseflow (BF) and streamflow out (Q_{out}). BF data from United States Geological Survey.

Estimated quarterly WWD are shown in Table 10 (ODEQ, 2018). WWD data was only available by water year from 2009-2017, so the period of record begins in 2008 Q4 and ends after 2017 Q3. On average, quarterly WWD accounted for just 1.5% of quarterly Q_{out}. While WWD volumes are far too small to make an impact on the overall SEWPR water balance, this data can be useful for identifying major water users in the SEWPR. Industrial facilities accounted for the largest percentage (74%) of the total WWD in the SEWPR on average, followed by commercial facilities (16%) and municipalities (11%) (Figure 33). One single paper mill facility accounted for over 64% of the total WWD on average, nearly 6 times greater than all municipalities combined.

Table 10: Quarterly wastewater discharge (WWD) depths within the Southeast Watershed Planning Region of Oklahoma. Data from Oklahoma Department of Environmental Quality.

	Quarterly WWD Depths (cm)			
Year	Q1	Q2	Q3	Q4
2007	-	-	-	-
2008	-	-	-	0.080
2009	0.094	0.127	0.106	0.119
2010	0.115	0.097	0.096	0.098
2011	0.090	0.112	0.091	0.096
2012	0.123	0.104	0.096	0.090
2013	0.096	0.114	0.104	0.125
2014	0.102	0.104	0.118	0.106
2015	0.120	0.147	0.109	0.133
2016	0.136	0.144	0.108	0.106
2017	0.114	0.116	0.120	-
Avg.	0.110	0.118	0.105	0.106

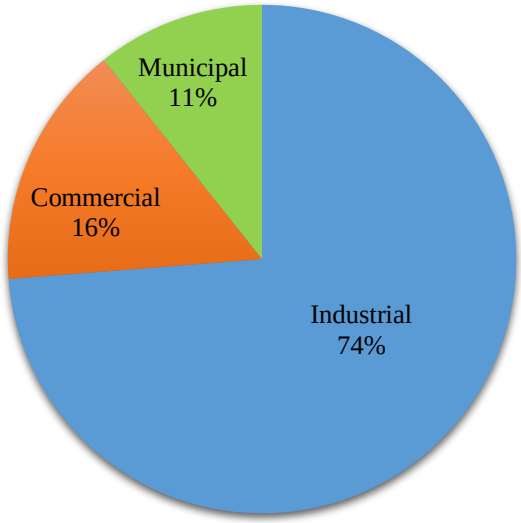

Figure 33: Percentage of total quarterly wastewater discharge (WWD) in the Southeast Watershed Planning Region of Oklahoma from different water use sectors (ODEQ, 2018).

Quarterly RD for the SEWPR are shown in Table 11 (USACE, 2020). The three reservoirs that contribute to the RD volumes are located in the lower portion of the SEWPR, so their discharges contributed largely to the quarterly Q_{out} component of the WBM. On average, RD accounted for over 62% of quarterly Q_{out}, and the two had a strong positive correlation (Table 8). The quarterly trends of RD and Q_{out} are shown in Figure 34 and follow an almost identical pattern. These similarities in the quarterly trends of the two components are a positive sign for the accuracy of the Q_{out} estimation methods, since the RD data is from a reliable source (USACE, 2020).

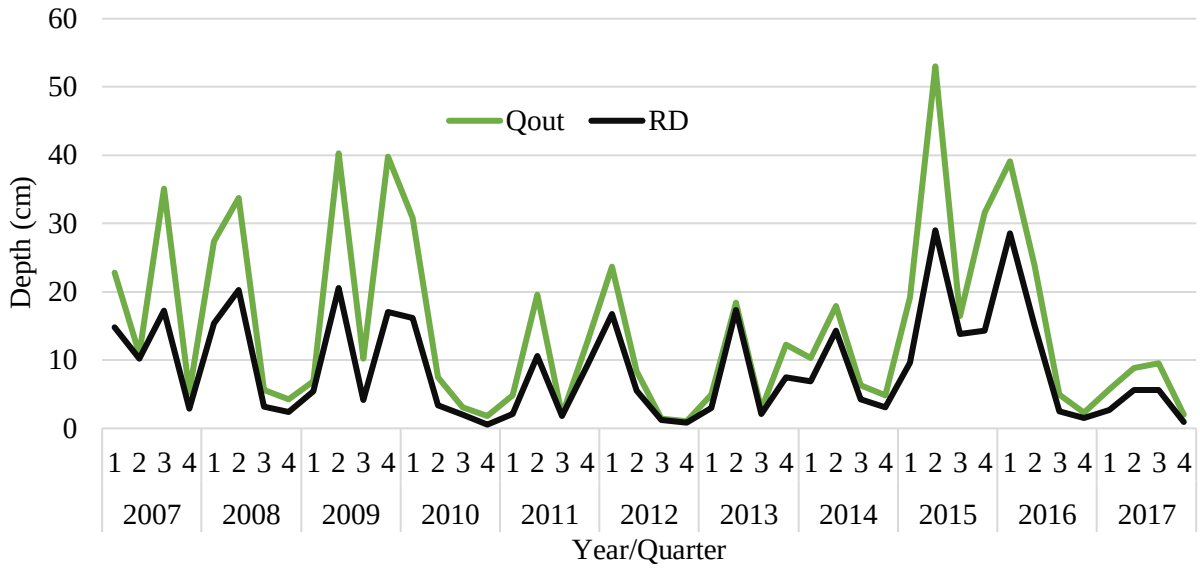

Figure 34: Trends of quarterly streamflow out (Q_{out}) and reservoir discharges (RD). RD data from the United States Army Corps of Engineers.

Table 11: Quarterly reservoir discharge (RD) depths from Broken Bow Lake, Hugo Lake, and Pine Creek Lake. Data from United States Army Corps of Engineers.

	Quarterly RD Depths (cm)			
Year	Q1	Q2	Q3	Q4
2007	14.8	10.2	17.2	2.9
2008	15.3	20.3	3.2	2.4
2009	5.4	20.5	4.1	17.1
2010	16.2	3.4	2.0	0.5
2011	2.1	10.6	1.9	9.3
2012	16.7	5.5	1.3	0.8
2013	2.9	17.3	2.1	7.5
2014	6.9	14.3	4.2	3.1
2015	9.6	29.0	13.9	14.3
2016	28.6	15.0	2.5	1.5
2017	2.7	5.6	5.6	1.0
Avg.	11.0	13.8	5.3	5.5

5.5 Consumptive Use

Using the quarterly WBM component results from Section 5.1 as inputs for Equation 5, quarterly consumptive use (*C*) from 2007-2017 was estimated for the SEWPR. The results of the WBM are shown in Table 12 and Figure 35. The range of estimated *C* depths is 61.8 cm with a maximum depth of 32.6 cm (2015 Q4) and a minimum depth of -29.2 cm (2015 Q3). Since *C* was estimated as the remaining volume of water unaccounted for in the other WBM components, the possibility of *C* being negative exists, and this was the case for 22 out of 44 quarters. However, *C* is defined in this study as the volume of water removed from a watershed by human activities, so it does not make practical sense for this volume to be negative over a 3-month period. For example, for the *C* estimate of -5.3 cm for 2007 Q1 to be correct, a volume of water that was 5.3 cm greater than the volume of water consumed would have to have been imported into the SEWPR, which is extremely unlikely.

If all quarters with negative *C* are ignored, the average *C* would be 7.0 cm for all quarters combined, and 5.9 cm, 6.6 cm, 2.7 cm, and 8.5 cm for Q1, Q2, Q3, and Q4 respectively. While these values do seem more reasonable than negative values, it is still highly unlikely that such a large volume of water could be consumed in the SEWPR during any given quarter. The average annual *C* depth for 2007-2017 was estimated to be 23.7 cm if negative *C* values are ignored. This is 79 times greater than the 2015 *C* depth (0.3 cm) in the SEWPR from irrigation and thermoelectric power that was estimated from the 2015 USGS water use study (Dieter et al., 2018). While the USGS estimate only includes *C* from irrigation and thermoelectric uses, it is extremely unlikely that an additional 23.4 cm of *C* came from other water use sectors. The WBM appears to be considerably overestimating quarterly *C* in the SEWPR. The overestimated and negative *C* volumes are likely due to large, mostly unknown uncertainty associated with the

other WBM components which are discussed in Section 5.2. Since this uncertainty makes up a considerable portion of the estimated *C* volumes, it is not appropriate to refer to the estimates as consumptive use. Instead, the results of the WBM are referred to as consumptive use + error (C_{+err}).

Table 12: Estimated quarterly consumptive use + error (C_{+err}) depths from the Southeast Watershed Planning Region of Oklahoma water balance model.

	C_{+err} (cm)			
Year	Q1	Q2	Q3	Q4
2007	-5.3	5.6	-12.0	4.7
2008	2.7	4.7	-13.5	3.8
2009	1.3	3.2	-18.4	3.1
2010	1.1	-2.2	-2.1	4.4
2011	-5.0	12.3	-18.0	10.5
2012	7.6	-3.3	-7.4	-4.9
2013	11.2	4.4	-15.0	6.2
2014	-3.4	-2.5	-7.1	1.9
2015	-2.3	-5.9	-29.2	32.6
2016	-8.8	9.6	-9.0	-2.2
2017	11.3	-2.1	2.7	9.4
Avg.	0.9	2.2	-11.7	6.3

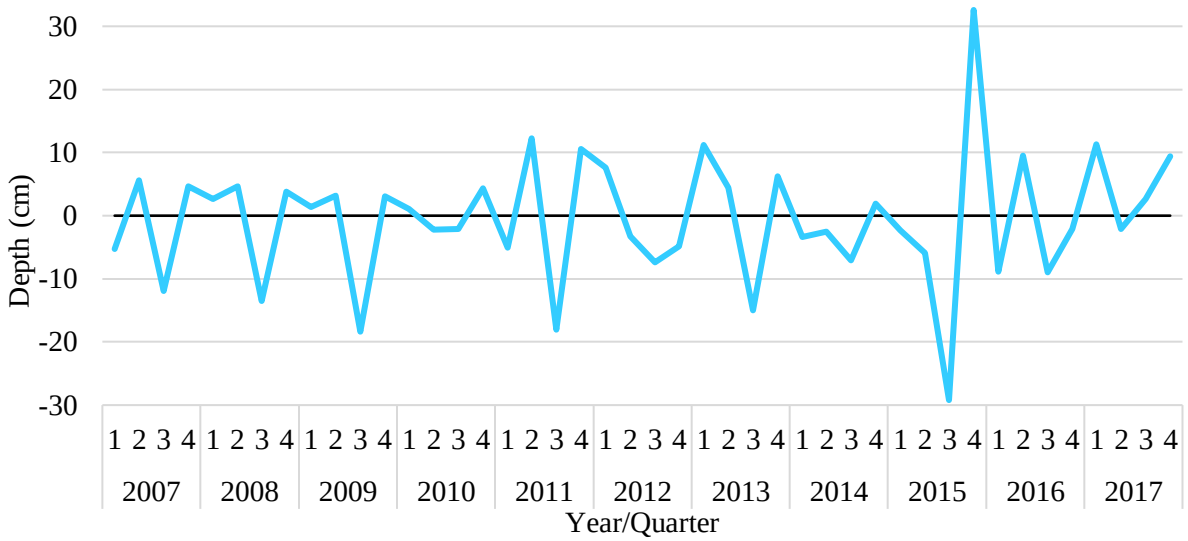

Figure 35: Trends of quarterly consumptive use + error (C_{+err}) depths.

To understand why the WBM estimates such large, and sometimes negative, quarterly C_{+err} volumes, the volumes and quarterly trends among the other WBM components were compared to C_{+err}. The CC between each WBM component and C_{+err} are shown in Table 13. For individual quarters, only *P* in Q4 and ΔS_{surf} in Q3 and Q4 showed correlation that was significant at the 95% confidence level (Table 13) with C_{+err}, with both components showing positive correlation with C_{+err}. *P* and ΔS_{surf} also showed significant positive correlation with C_{+err} among all quarters, along with *ET* which showed significant negative correlation with C_{+err} among all quarters (Table 13). These relationships can also be seen by comparing the quarterly trends of C_{+err} with ΔS_{surf} (Figure 36), *P* (Figure 37), and *ET* (Figure 38). In quarters with higher *P* than *ET*, C_{+err} was typically also higher (e.g. 2013 Q1, 2015 Q4), and when *P* was less than *ET*, C_{+err} tends to be lowest (e.g. 2011 Q3, 2015 Q3). This relationship is shown in Figure 39, where C_{+err} is compared to net *P* (*P* minus *ET*). The quarter with the highest average C_{+err} (Q4) was also the quarter with the highest net *P*, and the quarter with the lowest C_{+err} (Q3) was the quarter with the lowest net *P*. C_{+err} and net *P* also showed a strong positive correlation (0.71) that was significant at the 95% confidence level.

Table 13: Correlation coefficients between consumptive use + error (C_{+err}) and each of the other water balance model components for each of the four annual quarters, and for all quarters combined. The WBM components include precipitation (P), evapotranspiration (ET), streamflow out (Q_{out}), surface storage change (ΔS_{surf}), and sub-surface storage change (ΔS_{sub}). * denotes significance at the 95% confidence level.

	P	Q_{out}	ET	ΔS_{surf}	ΔS_{sub}
Q1	0.39	-0.40	-0.10	0.56	-0.14
Q2	0.12	-0.06	-0.02	-0.15	-0.24
Q3	0.39	-0.23	0.27	0.62*	-0.45
Q4	0.88*	0.55	-0.23	0.93*	0.05
All Quarters	0.43*	0.14	-0.43*	0.60*	0.06

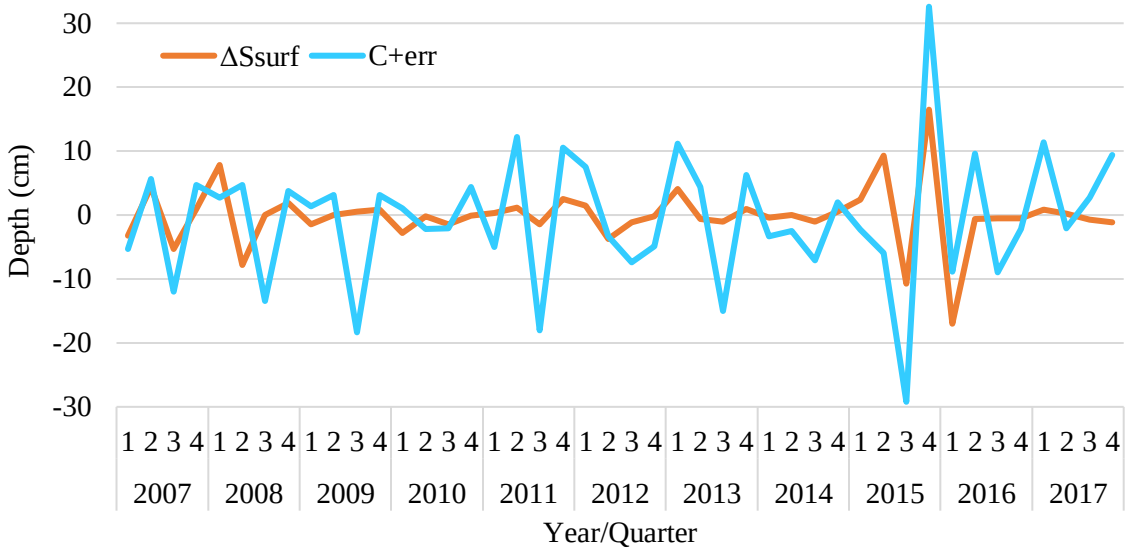

Figure 36: Trends of quarterly consumptive use + error (C_{+err}) and surface storage (ΔS_{surf}) depths.

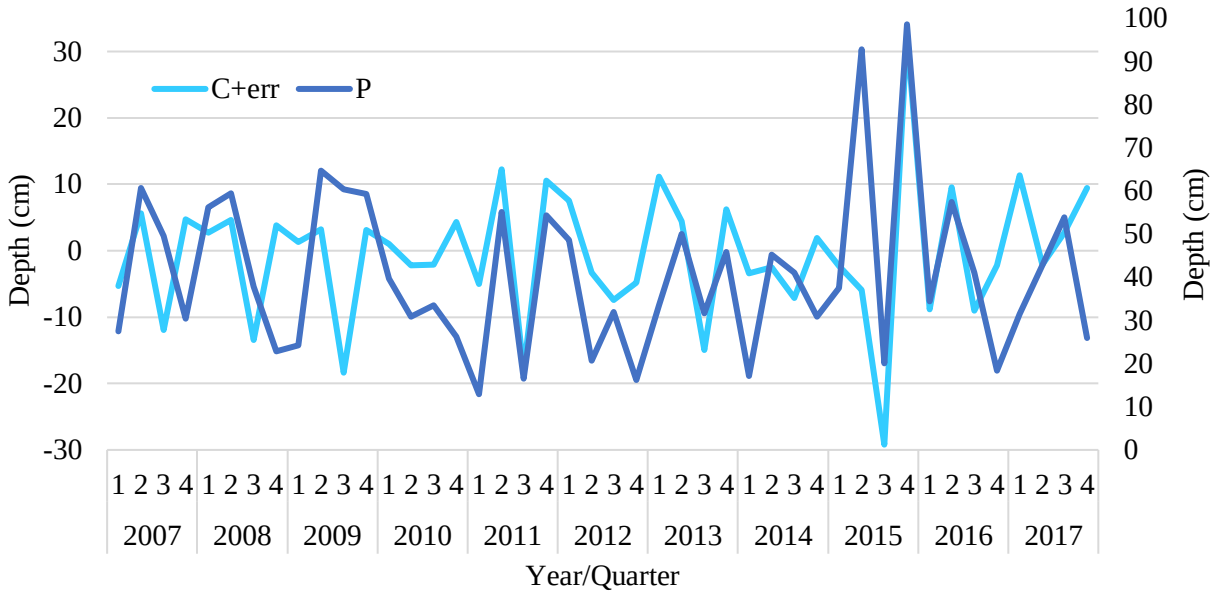

Figure 37: Trends of quarterly consumptive use + error (C_{+err}) (left axis) and precipitation (P) (right axis) depths. *P* data from the National Centers for Environmental Prediction Stage IV Quantitative Precipitation Estimates.

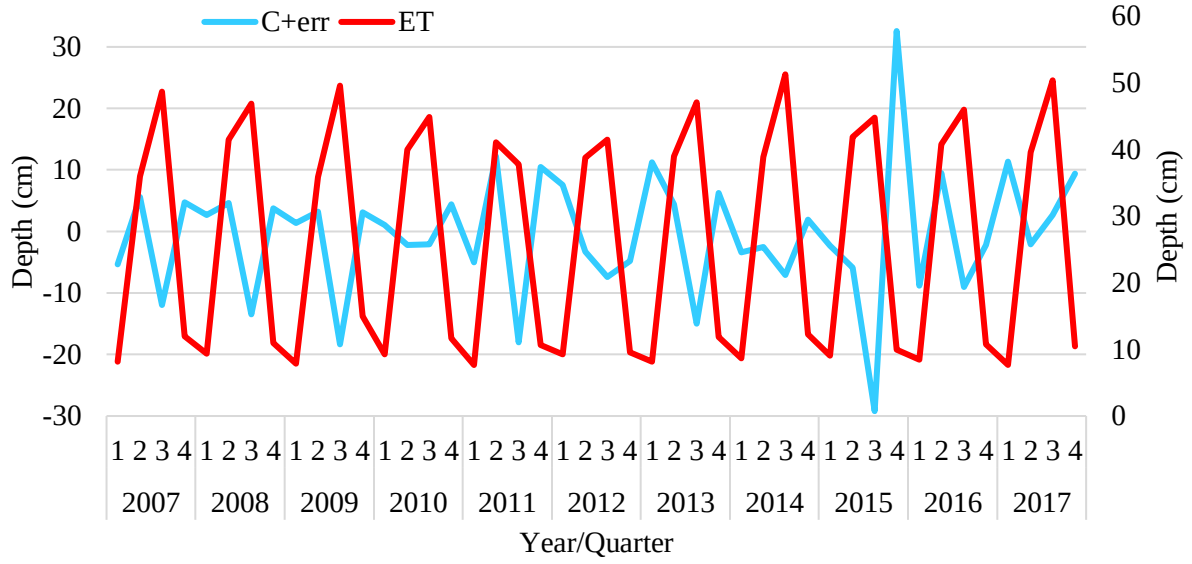

Figure 38: Trends of quarterly consumptive use + error (C_{+err}) (left axis) and evapotranspiration (*ET*) (right axis) depths. *ET* data from the Famine Early Warning Systems Network.

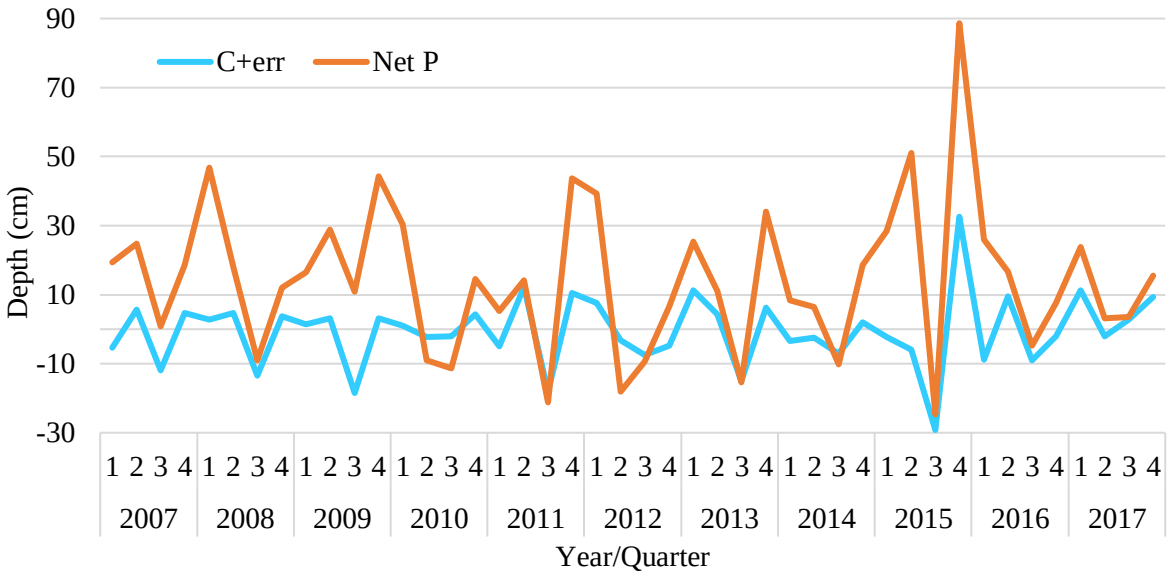

Figure 39: Trends of quarterly consumptive use + error (C_{+err}) and net precipitation (Net P) (precipitation – evapotranspiration) depths.

These results indicate that the unrealistic quarterly C_{+err} volumes estimated using a WBM are likely caused by uncertainties associated with the estimates of the natural hydrologic components in the SEWPR on a quarterly basis. The total combined uncertainty of each WBM component contributes to the total uncertainty of the C_{+err} calculation. The total uncertainty is discussed in the following section.

5.6 Total Water Balance Model Uncertainty

The uncertainty of each WBM component estimation method that was estimated in Section 5.2 contributes to the total uncertainty of the WBM, and the C_{+err} estimation. Because much of the uncertainty is still unknown, the known uncertainty estimation must be referred to as minimum uncertainty, as the true uncertainty value is likely higher. The quarterly C_{+err} volumes along with minimum uncertainty are given in Table 14. Quarterly minimum uncertainty ranged from 2.0 to 18.7 cm and 23% to 724%. The average quarterly uncertainty was 8.0 cm and 181%.

Table 14: Quarterly consumptive use + error (C_{+err}) volumes with minimum uncertainty given in both cm and relative percent.

	Quarterly C_{+err} with Minimum Uncertainty (cm)			
Year	Q1	Q2	Q3	Q4
2007	-5.3 ± 6.1 115%	5.6 ± 9.4 167%	-12.0 ± 16.3 136%	4.7 ± 3.3 71%
2008	2.7 ± 7.7 287%	4.7 ± 15.0 322%	-13.5 ± 9.9 74%	3.8 ± 3.1 82%
2009	1.3 ± 2.9 219%	3.2 ± 14.1 442%	-18.4 ± 11.3 62%	3.1 ± 10.1 328%
2010	0.9 ± 7.7 724%	-2.2 ± 9.0 413%	-2.1 ± 9.3 443%	4.4 ± 2.6 59%
2011	-5.0 ± 2.4 48%	12.3 ± 11.5 94%	-18.0 ± 7.7 43%	10.5 ± 4.6 44%
2012	7.6 ± 6.2 82%	-3.3 ± 9.4 282%	-7.4 ± 8.3 112%	-4.9 ± 2.0 42%
2013	11.2 ± 3.0 27%	4.4 ± 10.8 246%	-15.0 ± 9.6 64%	6.2 ± 4.6 74%
2014	-3.4 ± 3.6 106%	-2.5 ± 10.6 422%	-7.1 ± 11.0 154%	1.9 ± 3.3 167%
2015	-2.3 ± 5.5 240%	-5.9 ± 18.7 317%	-29.2 ± 12.9 44%	32.6 ± 9.7 30%
2016	-8.8 ± 10.9 123%	9.6 ± 12.1 127%	-9.0 ± 9.7 108%	-2.2 ± 2.5 117%
2017	11.3 ± 2.6 23%	-2.1 ± 9.1 438%	2.7 ± 11.4 422%	9.4 ± 2.5 26%

Even with most of the WBM uncertainty unaccounted for, the uncertainty values for C_{+err} are considerably high. These values would increase greatly in all likelihood if the remaining uncertainty for the WBM were quantifiable. These high uncertainty values are surely a major factor causing the extreme over/underestimation of quarterly C_{+err} volumes in the SEWPR.

5.7 Annual Water Balance Model

While the quarterly time scale of the WBM allows for analysis of seasonal variation and trends between the different WBM components, using a longer time period for the WBM

analysis provides additional useful information about both the relationships between the different WBM components, and C_{+err} estimates. A separate analysis was performed using an annual rather than quarterly time scale for the WBM. All parameters were kept the same as the quarterly WBM, including the analysis period of 2007-2017. The only variation was that WBM components were converted from quarterly to annual volumes and then used in Equation 5 to estimate C_{+err}. The quarterly volumes P, Q_{out}, and ET were simply summed for each year to calculate their annual volumes. For ΔS_{surf} and ΔS_{sub}, Equation 7 was used as it was for the quarterly WBM, but instead using storage volumes from the first day or month of each year, depending on the temporal resolution of the data. The results of the annual WBM are given in Table 15 and annual trends for each component are shown in Figure 40 for P, Q_{out} and ET, and Figure 41 for ΔS_{surf} and ΔS_{sub}. Trends of estimated annual C_{+err} are shown in Figure 42.

Table 15: Results of the annual water balance model (WBM) analysis. Annual volumes for each WBM component and consumptive use + error (C_{+err}) are given in cm along with the average annual volumes for 2007-2017. WBM components include precipitation (P), streamflow out (Q_{out}), evapotranspiration (ET), surface storage change (ΔS_{surf}), and sub-surface storage change (ΔS_{sub}).

	WBM Component Volumes (cm)					
Year	P	Q_{out}	ET	ΔS_{surf}	ΔS_{sub}	C_{+err}
2007	168.3	74.0	104.7	-3.1	-0.3	-7.0
2008	176.4	71.0	108.6	1.9	-2.8	-2.3
2009	208.7	97.2	108.3	-0.1	14.1	-10.8
2010	130.5	43.1	105.8	-4.6	-15.0	1.2
2011	138.9	39.0	97.1	2.7	0.4	-0.3
2012	117.4	34.5	99.1	-3.7	-4.4	-8.0
2013	161.0	38.3	105.9	3.4	6.5	6.8
2014	134.4	39.3	111.1	-0.8	-4.1	-11.1
2015	249.1	120.3	105.6	17.6	10.4	-4.8
2016	151.3	70.2	105.9	-18.7	4.3	-10.4
2017	154.0	25.9	108.0	-0.8	-0.5	21.4
Avg.	162.7	59.3	105.5	-0.6	0.8	-2.3

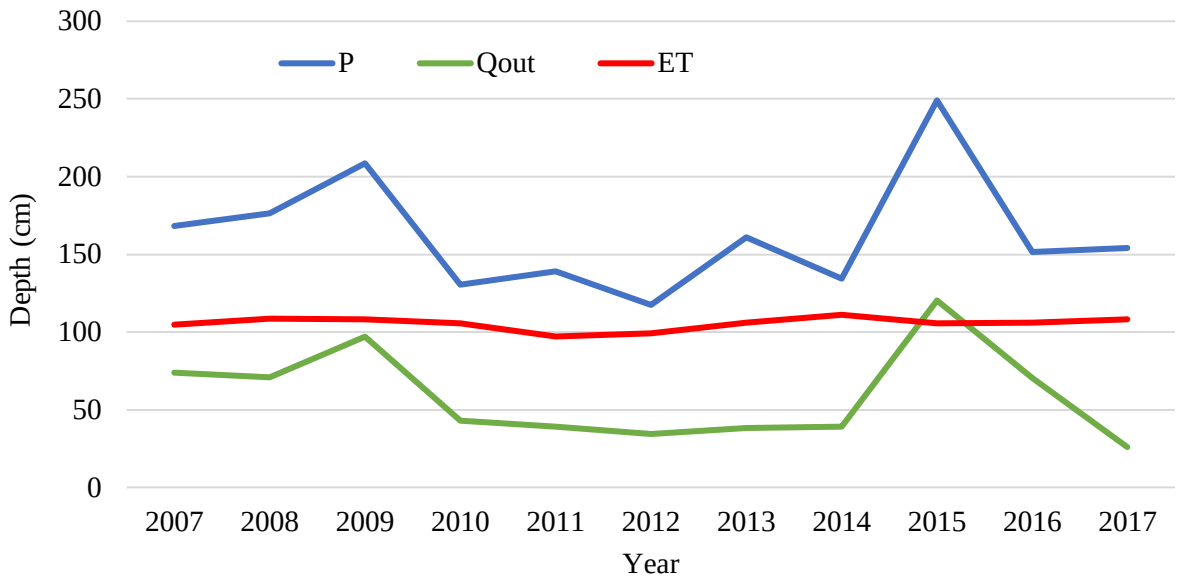

Figure 40: Trends of annual precipitation (*P*), streamflow out (Q_{out}) and evapotranspiration (*ET*) depths. *P* data from the National Centers for Environmental Prediction Stage IV Quantitative Precipitation Estimates. *ET* data from the Famine Early Warning Systems Network.

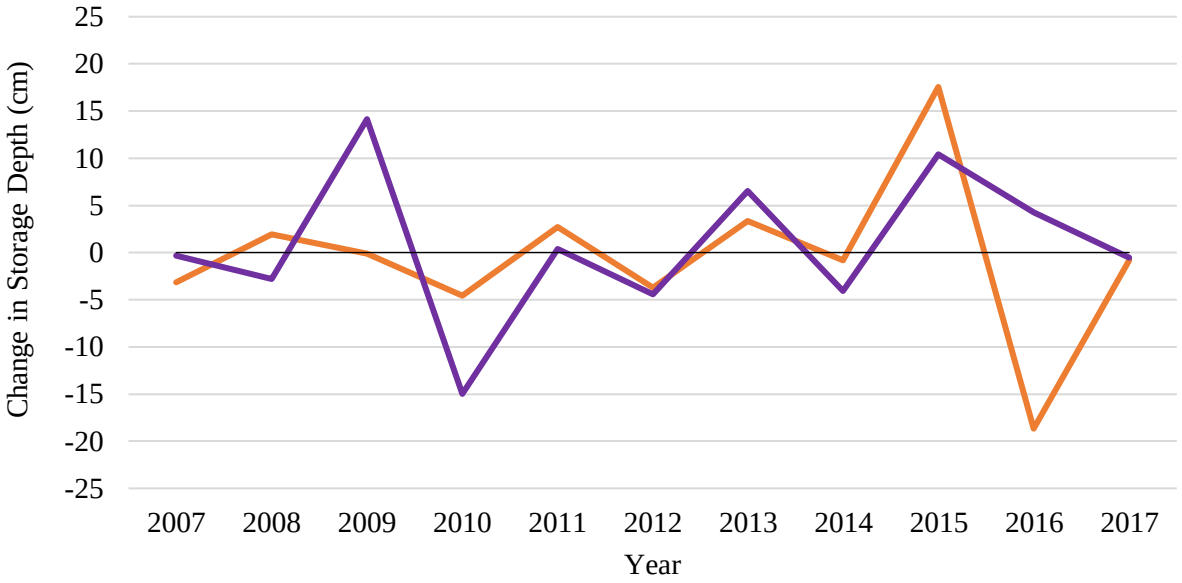

Figure 41: Trends of annual surface storage change (ΔS_{surf}) and sub-surface storage change (ΔS_{sub}) depths. ΔS_{sub} data from the Gravity Recovery and Climate Experiment satellite mission.

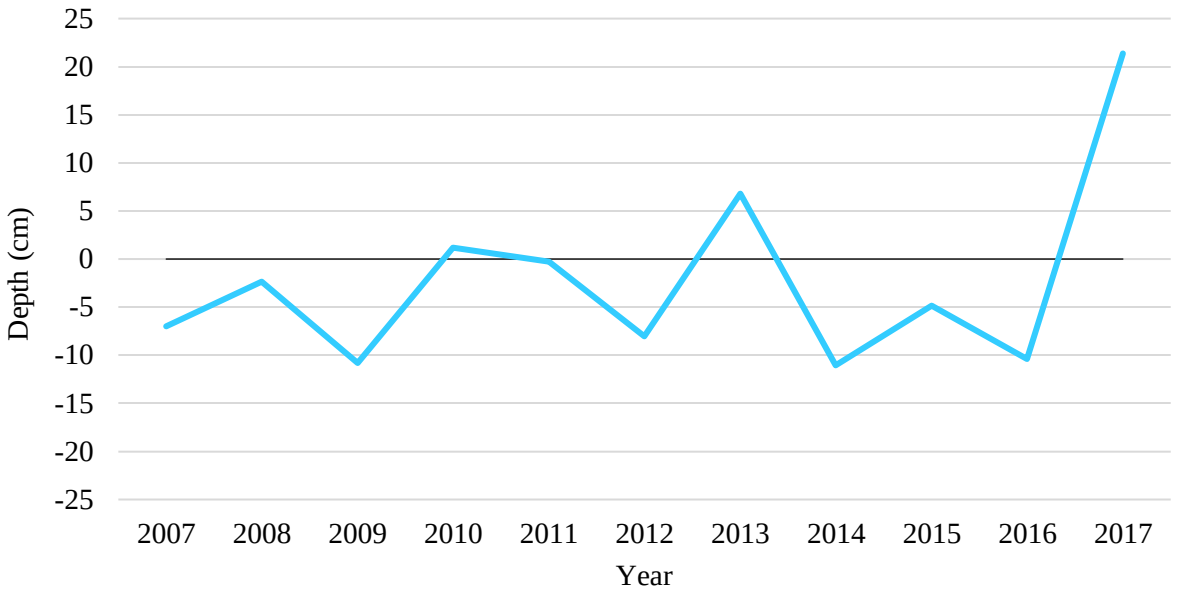

Figure 42: Trends of annual consumptive use + error (C_{+err}) depths.

The variability of each annual WBM was calculated using the coefficient of variation (CV), as was done for the quarterly WBM analysis (Table 16). The CV for ΔS_{surf} and ΔS_{sub} was again omitted from the CV calculations due to misleading CV values caused by the negative change in storage values. The CV for total annual surface storage (S_{surf}) from the first day of each year was used to represent ΔS_{surf} variability, and the standard deviation (σ) was used for ΔS_{sub} since no total sub-surface storage estimates were available. The increased time scale from quarterly to annual reduced the temporal variability of each WBM component, except for S_{surf}. This lower variability may have contributed to a reduction in the range of C_{+err} from 61.8 cm for the quarterly WBM to 32.5 cm for the annual WBM. Theoretically, annual C_{+err} should be greater than quarterly C_{+err}, because humans will consume more water in a year than in 3 months. In this case however, the negative quarterly C_{+err} values offset many of the positive C_{+err} values which led to a decreased range of values and a similar average magnitude of both quarterly (7.2 cm) and annual (7.4 cm) C_{+err}.

Table 16: Average annual coefficient of variation (CV) values for the annual water balance model (WBM) component's, and average quarterly CV values for the quarterly WBM components. WBM components include precipitation (P), streamflow out (Q_{out}), evapotranspiration (ET), surface storage change (ΔS_{surf}), and sub-surface storage change (ΔS_{sub}). Total surface storage (S_{surf}) was used to represent ΔS_{surf} variability. * standard deviation was used to represent ΔS_{sub} variability.

	Coefficients of Variation	
WBM Component	Average Annual	Average Quarterly
P	0.2	0.5
Q_{out}	0.5	0.9
ET	<0.1	0.6
S_{surf}	0.3	0.2
ΔS_{sub}*	7.6*	10.0*

Unfortunately, the annual WBM still produced unrealistic C_{+err} values. 8 out of 11 years had negative volumes, and the maximum positive volume was 21.4 cm, almost 73 times greater than the estimated 2015 consumptive use estimation the from USGS study (Dieter et al., 2018). This suggests that the extremely large and unrealistic C_{+err} values produced by both the quarterly and annual WBMs are caused by the large unknown uncertainty associated with the current WBM methodology.

Chapter 6 – Conclusions & Future Research

The main objective of this study was to develop a method for quantifying C_{+err} without the need for accurate withdrawal and return flow data. Quantifying C_{+err} provides highly useful information for designing and tracking progress towards water conservation initiatives like Oklahoma's Water for 2060. The method for quantifying C_{+err} developed in this study was a WBM designed to estimate C_{+err} as the residual volume of water unaccounted for in the natural hydrologic balance. The model was designed for the SEWPR and tested on a quarterly basis from 2007-2017. The results showed that the SEWPR WBM estimated extremely large, and sometimes negative, volumes for quarterly C_{+err} that were significantly larger than the one previously estimated C_{+err} volume for the region. Even after the time scale of the WBM was increased from quarterly to annual to determine if seasonal variability impacted the WBM output, the C_{+err} volumes were still unrealistic and relatively unaffected by the four-fold time scale increase.

The most likely explanation for the extreme C_{+err} volumes is the unquantifiable uncertainty associated with the WBM component estimation methods. The components that likely contribute the largest uncertainty are Q_{out}, ΔS_{surf} and ΔS_{sub} because, unlike P and ET, reliable datasets for these components are not available. Another possibility is that the use of a WBM with natural hydrologic components may not be an appropriate method for estimating C_{+err}. Human consumption of water may be independent of the natural hydrologic processes to some extent, and even more so in the SEWPR than other regions since there is an abundance of water availability and very little demand. When C_{+err} is considered as a part of the natural water balance, the possibility of imbalances between the other hydrologic components causing negative or extremely large C_{+err} estimates exists. However, there is currently too much unknown

uncertainty associated with the WBM to determine if it is an appropriate method for estimating C_{+err} or not.

While the WBM is currently unsuitable for estimating quarterly C_{+err} volumes in the SEWPR, the analysis of the WBM components conducted in this study offers useful information regarding hydrologic patterns and relationships within the SEWPR. Some of the noteworthy findings from the WBM component analysis are listed below:

- Precipitation (*P*) was the largest component in terms of total depth across the SEWPR in 34 of 44 quarters from 2007-2017. Evapotranspiration (*ET*) was the largest in the remaining 10 quarters.

- *ET* followed a very cyclical pattern of being much higher in Q2 and Q3 than in Q1 and Q4. Mean quarterly depth across the SEWPR was significantly lower in both Q1 and Q4 than in Q2 and Q3 for *ET* ($p < 0.01$), but not for *P* ($p = 0.10$). *ET* and *P* also showed weak correlation for all quarters from 2007-2017 (CC = 0.25), which suggested that the amount of *ET* each quarter was not dependent on the amount of *P*.

- Solar radiation (R) showed strong positive correlation (CC = 0.95) with *ET* for all quarters from 2007-2017, and R was significantly lower in both Q1 and Q4 than in Q2 and Q3 ($p < 0.01$), as was the case with *ET*. This suggested that ET was dependent on the amount of R rather than on *P*.

- Streamflow out (Q_{out}) showed positive correlation with *P* (CC = 0.69) which is typical for a rainfall-streamflow relationship. However, several quarters showed an opposite trend where *P* increased while Q_{out} decreased, or vice versa. This was likely due to delayed releases from reservoirs following periods of heavy rainfall to mitigate flooding in areas downstream of the reservoirs.

- For the storage change components, sub-surface storage change (ΔS_{sub}) was greater than surface storage change (ΔS_{surf}) in magnitude for 36 of 44 quarters from 2007-2017, and the average quarterly magnitude was greater for ΔS_{sub} than for ΔS_{surf} ($p < 0.01$). This could suggest there is greater sub-surface storage capacity than surface storage capacity, but there is too much unknown uncertainty associated with the estimation methods to test that theory.

- Streams that flow out of the SEWPR had a fairly even mix of baseflow (BF) and runoff on average, with average quarterly baseflow index (BFI) for each quarter ranging from 0.47 in Q2 to 0.51 in Q1, with an average of 0.49 for all quarters from 2007-2017.

- Industrial facilities accounted for the largest portion of quarterly wastewater discharges (WWD) in the SEPWR on average (74%), followed by commercial facilities (16%), and municipalities (11%). A single paper mill facility accounted for over 64% of the average quarterly WWD, which was nearly 6 times greater than the average WWD from all municipalities combined.

- Quarterly reservoir discharges (RD) from major reservoirs in the lower portion of the SEWPR (Broken Bow Lake, Hugo Lake, and Pine Creek Lake) showed strong positive correlation with Q_{out} (0.95) and followed nearly identical quarterly trends to Q_{out}. This is a positive sign for the accuracy of the Q_{out} estimation methods, since the RD data is from a reliable database (USACE, 2020).

In addition to the highlighted findings above, the innovative estimation methods that were developed for certain WBM components were notable achievements of this study. The methods for estimating both Q_{out} and ΔS_{surf} were not only crucial to the function of the WBM approach to estimate consumptive use, but also have potential applications reaching far beyond this study. If the uncertainty of the Q_{out} methodology for estimating temporal variations of

streamflow at ungauged sites can be further quantified and reduced, the methods could be incredibly useful for hydrologic and environmental research. The ΔS_{surf} methodology for estimating storage volumes of unmapped waterbodies from surface area could provide similar benefits if further research is done to improve its performance. This study also provides estimates for other important hydrologic variables (BF, WWD, and RD) which could be useful information for water managers and researchers.

Although the estimates for consumptive use provided in this study were not as promising as expected, the more important objective of developing the methodology and establishing the framework for the WBM was achieved. The data gathered, the methodologies developed, and the valuable insights gained from this study lay the groundwork for future research. The first step for this study moving forward would be to quantify any remaining unknown uncertainty if it is feasible to do so. There is currently far too much unknown uncertainty to determine the appropriateness of the WBM for C_{+err} estimation. Further research should also be done on the current methodologies for WBM component estimation to explore ways to alter and improve their performance by reducing uncertainty. Table 17 describes the current limitations of each WBM component estimation method, and the next steps that must be taken to improve the WBM.

Another suggestion for future work would be to explore model automation for the WBM component estimation methods, possibly within a single programming language. This would allow for faster computations and more advanced model improvements like calibration and optimization. Automation would also make it easier to apply the WBM to other Watershed Planning Regions (WPR) in Oklahoma. Obtaining additional results from other regions will allow for a better determination of the appropriateness of the WBM for estimating C_{+err} volumes

in Oklahoma. The WBM should be applied next to a WPR with a higher water demand than the SEWPR, such as the Central or Panhandle WPR. Consumptive use in these regions should be more than the SEWPR or other WPRs with low demand estimates. Analyzing C_{+err} results for a WPR with higher demand could help to identify more ways to improve the WBM to be applicable to all WPRs across Oklahoma.

Table 17: Limitations and suggestions for how to improve and reduce uncertainty for each water balance model (WBM) component estimation method. WBM components include precipitation (P), streamflow out (Q_{out}), evapotranspiration (ET), surface storage change (ΔS_{surf}), and sub-surface storage change (ΔS_{sub}). Some limitations are specific to the Southeast Watershed Planning Region of Oklahoma (SEWPR).

WBM Component	Limitations	How to Improve
P	4 km spatial resolution of pixels	Find data product with smaller spatial resolution, if possible
Q_{out}	Lack of stream gauge stations on small streams exiting the SEWPR	Install stream gauge stations on small streams exiting the SEWPR to collect multiple years of discharge observations
ET	Uncertainty of the SSEBop ET_a model and USACE reservoir evaporation	Search for an improved ET_a product and quantify USACE reservoir uncertainty
ΔS_{surf}	Lack of aerial image availability for waterbody digitization, and lack of up-to-date bathymetric data of lentic waterbodies	Gain access to historical aerial imagery at no greater than quarterly time steps, and conduct additional bathymetric surveys with more advanced equipment
ΔS_{sub}	GRACE satellite data has very large spatial resolution that is not suitable for regions at the scale of the SEWPR	Install a network of piezometers and soil moisture probes to record multiple years of groundwater and soil moisture fluxes

References

Alemaw, B. F., & Chaoka, T. R. (2003). A continental scale water balance model: a GIS-approach for Southern Africa. *Physics and Chemistry of the Earth, Parts A/B/C*, *28*(20-27), 957-966.

Andales, A. A., Chávez, J. L., Bauder, T. A., & Broner, I. (2011). Irrigation scheduling: the water balance approach. *Service in action; no. 4.707*.

Arnell, N. W. (1999). A simple water balance model for the simulation of streamflow over a large geographic domain. *Journal of Hydrology*, *217*(3-4), 314-335.

Barker, S. (2012). Oklahoma State and County Population Projections Through 2075. *2012 Demographic State of the State Report.*

Brock, F. V., K. C. Crawford, R. L. Elliott, G. W. Cuperus, S. J. Stadler, H. L. Johnson, and M. D. Eilts, 1995: The Oklahoma Mesonet: A technical overview. *J. Atmos. Oceanic Technol., 12*, 5-19.

Chen, S., Gourley, J. J., Hong, Y., Kirstetter, P. E., Zhang, J., Howard, K., ... & Qi, Y. (2013). Evaluation and uncertainty estimation of NOAA/NSSL next-generation National Mosaic Quantitative Precipitation Estimation product (Q2) over the continental United States. *Journal of Hydrometeorology*, *14*(4), 1308-1322.

Chen, M., Senay, G. B., Singh, R. K., & Verdin, J. P. (2016). Uncertainty analysis of the Operational Simplified Surface Energy Balance (SSEBop) model at multiple flux tower sites. *Journal of Hydrology, 536*, 384-399.

Dieter, C. A., Maupin, M. A., Caldwell, R. R., Harris, M. A., Ivahnenko, T. I., Lovelace, J. K., ... & Linsey, K. S. (2018). *Estimated use of water in the United States in 2015* (No. 1441). US Geological Survey.

Enrolled House Bill No. 3055, 82 O.S. 2011 Section 108.11, (Oklahoma, 2011).

Environmental Systems Research Institute (ESRI), (2018). ArcGIS Desktop version 10.6.

Esralew, R. A., & Smith, S. J. (2010). *Methods for estimating flow-duration and annual mean-flow statistics for ungaged streams in Oklahoma*. US Department of the Interior, US Geological Survey.

European Commission (2015). Guidance document on the application of water balances for supporting the implementation of the WFD *Technical Report-2015-9-090* (Version 6.1).

Famine Early Warning Systems Network. (2019). Actual Evapotranspiration data available on the World Wide Web at URL [https://earlywarning.usgs.gov/fews/datadownloads/]

Ferguson, B. K. (1996). Estimation of direct runoff in the Thornthwaite water balance. *The Professional Geographer*, *48*(3), 263-271.

Gleick, P. H. (1987). The development and testing of a water balance model for climate impact assessment: modeling the Sacramento basin. *Water Resources Research*, *23*(6), 1049-1061.

Guo, S., Wang, J., Xiong, L., Ying, A., & Li, D. (2002). A macro-scale and semi-distributed monthly water balance model to predict climate change impacts in China. *Journal of Hydrology*, *268*(1-4), 1-15.

Harrell Jr, F.E., with contributions from Charles Dupont and many others. (2019). Hmisc: Harrell Miscellaneous. R package version 4.2-0. [https://CRAN.R-project.org/package=Hmisc]

Harwell, G. R. (2012). Estimation of Evaporation from Open Water: A Review of Selected Studies, Summary of US Army Corps of Engineers Data Collection and Methods, and Evaluation of Two Methods for Estimation of Evaporation from Five Reservoirs in Texas. *US Geological Survey*. Scientific Investigations Report 2012-5202.

Healy, R. W., Winter, T. C., LaBaugh, J. W., & Franke, O. L. (2007). Water budgets: foundations for effective water-resources and environmental management (Vol. 1308). *Reston, Virginia: US Geological Survey*.

Landerer F.W. and S. C. Swenson. (2012). Accuracy of scaled GRACE terrestrial water storage estimates. Water Resources Research, Vol 48, W04531, 11 PP.

Liebe, J., Van De Giesen, N., & Andreini, M. (2005). Estimation of small reservoir storage capacities in a semi-arid environment: A case study in the Upper East Region of Ghana. *Physics and Chemistry of the Earth, Parts A/B/C*, *30*(6-7), 448-454.

Martinez, G. F., & Gupta, H. V. (2010). Toward improved identification of hydrological models: A diagnostic evaluation of the “abcd” monthly water balance model for the conterminous United States. *Water Resources Research*, *46*(8).

Maupin, M. A., Kenny, J. F., Hutson, S. S., Lovelace, J. K., Barber, N. L., & Linsey, K. S. (2014). *Estimated use of water in the United States in 2010* (No. 1405). US Geological Survey.

McPherson, R. A., C. Fiebrich, K. C. Crawford, R. L. Elliott, J. R. Kilby, D. L. Grimsley, J. E. Martinez, J. B. Basara, B. G. Illston, D. A. Morris, K. A. Kloesel, S. J. Stadler, A. D. Melvin, A.J. Sutherland, and H. Shrivastava, 2007: Statewide monitoring of the mesoscale environment: A technical update on the Oklahoma Mesonet. *J. Atmos. Oceanic Technol.*, *24*, 301–321.

National Agricultural Imagery Program. (2018). United States Department of Agriculture, Farm Service Agency, Aerial Photography Field Office. Salt Lake City, Utah.

Oklahoma Department of Environmental Quality. (2018). National Pollutant Discharge Elimination System. Discharge Monitoring Report. Data from https://gis.deq.ok.gov/maps/

Oklahoma Water Resources Board. (2011). 2012 OCWP Executive Report. Published by the Oklahoma Water Resources Board under the authority of the Oklahoma State Legislature as the principal report for the official update of the Oklahoma Comprehensive Water Plan. Available online at [http://www. owrb.ok.gov/ocwp] (October 2011).

Oklahoma Water Resources Board. (2011). Southeast Watershed Planning Region Report. Published by the Oklahoma Water Resources Board under the authority of the Oklahoma State Legislature as an ancillary report for the official update of the Oklahoma Comprehensive Water Plan. Available online at http://www.owrb.ok.gov/ocwp (October 2011).

R Core Team (2018). R: A language and environment for statistical computing. R Foundation for Statistical Computing, Vienna, Austria. URL [https://www.R-project.org/]

Rodell, M., Chen, J., Kato, H., Famiglietti, J. S., Nigro, J., & Wilson, C. R. (2007). Estimating groundwater storage changes in the Mississippi River basin (USA) using GRACE. *Hydrogeology Journal*, *15*(1), 159-166.

Rodrigues, L. N., Sano, E. E., Steenhuis, T. S., & Passo, D. P. (2012). Estimation of small reservoir storage capacities with remote sensing in the Brazilian Savannah Region. *Water Resources Management*, *26*(4), 873-882.

Rokni, K., Ahmad, A., Selamat, A., & Hazini, S. (2014). Water feature extraction and change detection using multitemporal Landsat imagery. *Remote sensing*, *6*(5), 4173-4189.

Rutledge, A. T. (1998). Computer programs for describing the recession of ground-water discharge and for estimating mean ground-water recharge and discharge from streamflow records: Update. US Geological Survey, 98, 4148.

Saravanane, R., Ranade, V. V., Bhandari, V. M., & Rao, A. S. (2014). Urban Wastewater Treatment for Recycling and Reuse in Industrial Applications: Indian Scenario. *Industrial Wastewater Treatment, Recycling and Reuse*, 283-322.

Senay, G. B., Bohms, S., Singh, R. K., Gowda, P. H., Velpuri, N. M., Alemu, H., & Verdin, J. P. (2013). Operational evapotranspiration mapping using remote sensing and weather datasets: A new parameterization for the SSEB approach. *JAWRA Journal of the American Water Resources Association*, *49*(3), 577-591.

Senay, G. B., Budde, M., Verdin, J. P., & Melesse, A. M. (2007). A coupled remote sensing and simplified surface energy balance approach to estimate actual evapotranspiration from irrigated fields. *Sensors*, *7*(6), 979-1000.

Scanlon, B. R., Longuevergne, L., & Long, D. (2012). Ground referencing GRACE satellite estimates of groundwater storage changes in the California Central Valley, USA. *Water Resources Research*, *48*(4).

Schaake, J. C., Koren, V. I., Duan, Q. Y., Mitchell, K., & Chen, F. (1996). Simple water balance model for estimating runoff at different spatial and temporal scales. *Journal of Geophysical Research: Atmospheres*, *101*(D3), 7461-7475.

Shaffer, K. (2008). Consumptive water use in the Great Lakes Basin. US Department of the Interior, US Geological Survey.

Shaffer, K., & Runkle, D. L. (2007). *Consumptive Water, Use Coefficients for the Great Lakes Basin and Climatically Similar Areas*. Reston, VA: US Geological Survey.

Swenson, S.C. (2012). GRACE monthly land water mass grids NETCDF RELEASE 5.0. Ver. 5.0. PO.DAAC, CA, USA. Dataset accessed [2019-10-01] at [http://dx.doi.org/10.5067/TELND-NC005]

Swenson, S., Famiglietti, J., Basara, J., & Wahr, J. (2008). Estimating profile soil moisture and groundwater variations using GRACE and Oklahoma Mesonet soil moisture data. *Water Resources Research*, *44*(1).

Swenson, S. C. and J. Wahr. (2006). Post-processing removal of correlated errors in GRACE data, Geophys. Res. Lett., 33, L08402.

Thornthwaite, C. W., and J. R. Mather. (1955). The Water Balance, *Publications in Climatology* VIII(1): 1-104, Drexel Institute of Climatology, Centerton, New Jersey.

Tidwell, V. C., Moreland, B. D., Zemlick, K. M., Roberts, B. L., Passell, H. D., Jensen, D., ... & Larsen, S. (2014). Mapping water availability, projected use and cost in the western United States. *Environmental Research Letters*, *9*(6), 064009.

United States Army Corps of Engineers (2013). Hydrographic Surveying. *EM 1110-2-1003*.

United States Army Corps of Engineers (2020). Tulsa District. Monthly Charts of Reservoir Data. Retrieved from [https://www.swt-wc.usace.army.mil/].

United States Census Bureau (2011). *Census Blocks with Population and Housing Counts*. Retrieved from [https://www.census.gov/geographies/mapping-files/time-series/geo/tiger-line-file.2010.html]

United States Geological Survey (2017). Water Science Glossary of Terms. *U.S. Department of the Interior*.

United States Geological Survey, 2019, Earth Resources Observation and Science (EROS) Center data available on the World Wide Web at URL [https://earthexplorer.usgs.gov/]

United States Geological Survey, 2019, National Water Information System data available on the World Wide Web (USGS Water Data for the Nation) at URL [https://waterdata.usgs.gov/nwis/]

Wahr, J., Molenaar, M., & Bryan, F. (1998). Time variability of the Earth's gravity field: Hydrological and oceanic effects and their possible detection using GRACE. Journal of Geophysical Research: Solid Earth, 103(B12), 30205-30229.

Wang, D. (2012). Evaluating interannual water storage changes at watersheds in Illinois based on long-term soil moisture and groundwater level data. *Water Resources Research*, *48*(3).

Wang, G., Xia, J., & Chen, J. (2009). Quantification of effects of climate variations and human activities on runoff by a monthly water balance model: a case study of the Chaobai River basin in northern China. *Water Resources Research*, *45*(7).

Westenbroek, S. M., Kelson, V. A., Dripps, W. R., Hunt, R. J., & Bradbury, K. R. (2010). SWB--a modified Thornthwaite-Mather soil-water-balance code for estimating groundwater recharge (p. 60). Reston, VA: *US Department of the Interior, US Geological Survey, Ground Resources Program.*

Woods, A.J., Omernik, J.M., Butler, D.R., Ford, J.G., Henley, J.E., Hoagland, B.W., Arndt, D.S., and Moran, B.C., 2005, Ecoregions of Oklahoma (color poster with map, descriptive text, summary tables, and photographs): *Reston, Virginia, U.S. Geological Survey* (map scale 1:1,250,000).

Wyatt, B. M., Ochsner, T. E., Fiebrich, C. A., Neel, C. R., & Wallace, D. S. (2017). Useful drainage estimates obtained from a large-scale soil moisture monitoring network by applying the unit-gradient assumption. *Vadose Zone Journal*, *16*(6).

Xu, C. Y., & Chen, D. (2005). Comparison of seven models for estimation of evapotranspiration and groundwater recharge using lysimeter measurement data in Germany. *Hydrological Processes: An International Journal*, *19*(18), 3717-3734.

Xu, C. Y., & Singh, V. P. (1998). A review on monthly water balance models for water resources investigations. *Water Resources Management*, *12*(1), 20-50.

Xu, H. (2006). Modification of normalized difference water index (NDWI) to enhance open water features in remotely sensed imagery. *International Journal of Remote Sensing*, *27*(14), 3025-3033.

Yang, L., Jin, S., Danielson, P., Homer, C., Gass, L., Bender, S. M., ... & Funk, M. (2018). A new generation of the United States National Land Cover Database: Requirements, research priorities, design, and implementation strategies. *ISPRS journal of photogrammetry and remote sensing*, *146*, 108-123.

Appendix

Table A1: Quarterly streamflow coefficients (SC) representing the proportion of long-term average (1971-2017) to observed net flow gain from 2007-2017 for the Little River and Red River. Data from the United States Geological Survey.

	Little River				Red River			
Year	Q1	Q2	Q3	Q4	Q1	Q2	Q3	Q4
2007	1.47	0.75	0.64	0.28	1.83	0.22	4.17	0.31
2008	2.23	2.51	0.60	0.37	2.16	2.45	0.31	0.29
2009	0.76	3.20	0.77	3.30	0.30	3.17	0.85	3.15
2010	2.82	0.74	0.27	0.26	2.21	0.66	0.18	0.13
2011	0.64	2.28	0.05	0.95	0.19	1.04	0.10	0.60
2012	2.24	0.43	0.09	0.04	1.31	0.73	0.12	0.07
2013	0.11	0.50	0.19	0.70	0.24	1.38	0.12	0.65
2014	0.49	0.64	0.43	0.39	0.67	1.33	0.31	0.26
2015	2.09	3.00	0.40	1.75	1.30	4.82	2.11	2.21
2016	1.85	2.18	0.34	0.00	3.35	1.46	0.32	0.17
2017	0.63	0.73	0.82	0.10	0.18	0.56	0.85	0.15

Table A2: StreamStats average annual flow in cubic feet per second (cfs), and drainage area in square kilometers (km^2) for each outflow stream in the Southeast Watershed Planning Region of Oklahoma. Streams are organized in ascending order by drainage area. Data from the United States Geological Survey.

Outflow Stream	StreamStats Average Flow (cfs)	Drainage Area (km^2)	Receiving River
Ash Creek	17.2	23.4	Little River
South Caney Creek	16.1	28.0	Little River
Garland Creek	16.5	34.2	Red River
Doaksville Creek	17.6	36.3	Red River
Buck Creek	23.3	36.7	Little River
Pine Creek	21.1	42.3	Red River
Buzzard Creek	20.8	43.9	Red River
Holly Branch	25.3	47.9	Red River
Boss Creek	24.3	49.0	Red River
Waterfall Creek	28.2	56.4	Red River
North Caney Creek	37.6	64.2	Little River
Clear Creek	39.2	78.8	Red River
Robinson Creek	66.2	84.0	Little River
McKinney Creek	47.1	93.1	Red River
Rock Creek	86.9	131	Little River
Waterhole Creek	90.5	184	Red River
Norwood Creek	111	189	Red River
Kiamichi River	2,450	4,720	Red River
Little River	4,150	5,920	-

Table A3: Quarterly storage in cm for United States Army Corps of Engineers (USACE) managed reservoirs within the Southeast Watershed Planning Region of Oklahoma, including Broken Bow Lake, Hugo Lake, Pine Creek Lake, and Sardis Lake. The first day of each quarter was used as the storage depth. Data from USACE Tulsa District.

Year	Quarter	Broken Bow	Hugo	Pine Creek	Sardis	Total
2007	1	10.7	3.5	1.4	3.4	18.9
	2	9.9	2.0	0.7	3.0	15.6
	3	11.2	4.1	1.6	3.5	20.4
	4	9.5	1.7	0.6	3.0	14.8
2008	1	9.6	2.0	0.7	3.0	15.3
	2	13.2	4.0	2.9	3.5	23.6
	3	10.5	1.9	0.8	3.0	16.2
	4	10.3	2.0	0.6	3.0	15.9
2009	1	9.9	1.9	3.0	3.0	17.8
	2	10.1	2.1	0.8	3.0	16.0
	3	10.3	2.3	0.8	3.0	16.3
	4	10.7	2.0	0.6	3.0	16.3
2010	1	10.5	2.7	1.1	3.1	17.4
	2	9.8	1.8	0.6	2.9	15.2
	3	10.1	1.5	0.6	2.9	15.0
	4	8.9	1.2	0.4	2.8	13.2
2011	1	9.0	1.2	0.4	2.7	13.3
	2	8.7	1.6	0.4	2.7	13.4
	3	10.1	1.9	0.4	2.9	15.3
	4	8.7	1.2	0.2	2.6	12.8
2012	1	9.9	2.1	0.4	3.0	15.4
	2	11.1	2.7	1.0	3.0	17.7
	3	9.4	1.3	0.3	2.9	13.8
	4	8.7	0.9	0.2	2.7	12.5
2013	1	8.3	0.8	0.1	2.6	11.9
	2	10.2	2.2	0.6	3.1	16.1
	3	10.3	2.0	0.6	2.9	15.9
	4	9.3	1.5	0.5	2.8	14.1
2014	1	10.0	2.0	0.6	3.0	15.5
	2	9.8	1.8	0.5	3.0	15.1
	3	10.2	1.7	0.5	3.0	15.4
	4	9.1	1.5	0.5	2.9	14.0
2015	1	9.1	1.7	0.5	3.0	14.3
	2	10.6	2.2	0.6	3.0	16.3
	3	11.3	9.5	2.1	4.1	27.0

	4	9.6	1.5	0.4	2.9	14.4
2016	1	14.3	8.7	4.7	4.2	31.9
	2	10.0	1.6	0.4	3.0	15.0
	3	9.8	1.6	0.4	2.9	14.8
	4	9.1	1.3	0.7	2.9	14.1
2017	1	8.3	1.2	0.7	2.8	13.1
	2	8.9	1.6	0.6	2.9	14.0
	3	9.6	1.6	0.5	3.0	14.6
	4	9.1	1.4	0.4	2.9	13.8

Table A4: Estimated quarterly storage in cm for reservoirs within the Southeast Watershed Planning Region with bathymetric data from the Oklahoma Water Resources Board (OWRB) including Lake Carl Albert, Lake Nanih Waiya, Ozzie Cobb Lake, and Schooler Lake. Storage depth was estimated on the day closest to the beginning of each quarter that a suitable Landsat image was available to estimate surface area, using equations in Table 3.

Year	Quarter	Carl Albert	Nanih Waiya	Ozzie Cobb	Schooler	Total
2007	1	0.029	0.008	0.003	0.002	0.042
	2	0.027	0.007	0.003	0.001	0.038
	3	0.026	0.007	0.003	0.002	0.038
	4	0.025	0.007	0.003	0.002	0.037
2008	1	0.031	0.008	0.003	0.002	0.044
	2	0.030	0.008	0.003	0.002	0.043
	3	0.026	0.007	0.002	0.002	0.038
	4	0.025	0.006	0.002	0.002	0.035
2009	1	0.028	0.007	0.003	0.001	0.039
	2	0.028	0.007	0.003	0.002	0.039
	3	0.025	0.006	0.003	0.002	0.036
	4	0.028	0.007	0.003	0.002	0.039
2010	1	0.030	0.007	0.003	0.002	0.041
	2	0.028	0.006	0.003	0.001	0.039
	3	0.024	0.006	0.002	0.002	0.033
	4	0.022	0.006	0.002	0.001	0.031
2011	1	0.021	0.006	0.002	0.001	0.031
	2	0.029	0.007	0.003	0.001	0.040
	3	0.024	0.006	0.002	0.002	0.034
	4	0.031	0.009	0.003	0.002	0.045
2012	1	0.031	0.008	0.004	0.002	0.045
	2	0.026	0.008	0.002	0.002	0.038
	3	0.025	0.006	0.003	0.002	0.036
	4	0.026	0.009	0.003	0.004	0.041
2013	1	0.029	0.008	0.003	0.002	0.043
	2	0.028	0.008	0.003	0.002	0.041
	3	0.028	0.008	0.002	0.002	0.040
	4	0.031	0.009	0.004	0.003	0.047
2014	1	0.032	0.010	0.004	0.002	0.048
	2	0.027	0.008	0.003	0.002	0.040
	3	0.027	0.008	0.003	0.002	0.040
	4	0.033	0.009	0.003	0.002	0.047
2015	1	0.031	0.010	0.004	0.002	0.047
	2	0.030	0.010	0.004	0.003	0.047

	3	0.027	0.008	0.003	0.002	0.040
	4	0.030	0.010	0.004	0.003	0.046
2016	1	0.034	0.009	0.004	0.002	0.049
	2	0.027	0.008	0.003	0.002	0.040
	3	0.027	0.008	0.003	0.002	0.040
	4	0.029	0.008	0.003	0.001	0.041
2017	1	0.026	0.008	0.003	0.002	0.040
	2	0.028	0.008	0.003	0.002	0.041
	3	0.028	0.008	0.003	0.002	0.040
	4	0.029	0.008	0.003	0.003	0.042

Table A5: Surface area in acres (ac) and storage volume in acre-feet (ac-ft) for 17 small lentic waterbodies in the Southeast Watershed Planning Region of Oklahoma, based on bathymetric data that was collected between July and October, 2019. Each waterbody also includes the area and volume for each contour interval below the actual shoreline, which provided additional area-volume data to build regression equations (Table 5).

Waterbody	Area (ac)	Volume (ac-ft)
Waterbody 1 (full)	3.55	14.10
2 ft contour	2.60	7.86
4 ft contour	1.41	3.85
6 ft contour	0.81	2.68
8 ft contour	0.30	0.41
10 ft contour	0.06	0.03
Waterbody 2 (full)	0.81	3.41
2 ft contour	0.67	2.24
3 ft contour	0.60	2.00
4 ft contour	0.50	0.71
5 ft contour	0.37	0.24
6 ft contour	0.05	0.01
Waterbody 3 (full)	0.37	1.94
4 ft contour	0.26	0.67
6 ft contour	0.14	0.21
8 ft contour	0.03	0.06
10 ft contour	0.01	0.02
Waterbody 4 (full)	0.40	2.08
2 ft contour	0.34	1.33
4 ft contour	0.28	0.70
6 ft contour	0.16	0.25

8 ft contour	0.05	0.04
Waterbody 5 (full)	0.25	0.89
2 ft contour	0.17	0.47
4 ft contour	0.09	0.20
6 ft contour	0.04	0.07
8 ft contour	0.01	0.01
Waterbody 6 (full)	0.25	1.53
4 ft contour	0.18	0.66
6 ft contour	0.12	0.35
8 ft contour	0.07	0.15
10 ft contour	0.03	0.03
Waterbody 7 (full)	0.35	0.91
1 ft contour	0.30	0.58
2 ft contour	0.25	0.29
3 ft contour	0.14	0.08
4 ft contour	0.01	0.01
Waterbody 8 (full)	0.73	2.75
1 ft contour	0.60	2.09
2 ft contour	0.52	1.52
3 ft contour	0.45	1.02
4 ft contour	0.35	0.60
5 ft contour	0.21	0.32
6 ft contour	0.11	0.13
7 ft contour	0.06	0.04
Waterbody 9 (full)	0.97	4.52
3 ft contour	0.81	1.84
4 ft contour	0.74	1.05
5 ft contour	0.40	0.43
6 ft contour	0.10	0.15
7 ft contour	0.03	0.06
Waterbody 10 (full)	0.76	2.48
1 ft contour	0.54	1.75
2 ft contour	0.44	1.22
3 ft contour	0.35	0.81
4 ft contour	0.28	0.48
5 ft contour	0.18	0.23
6 ft contour	0.09	0.07
Waterbody 11 (full)	0.18	0.65
2 ft contour	0.12	0.36
3 ft contour	0.10	0.24

4 ft contour	0.08	0.15
5 ft contour	0.05	0.08
6 ft contour	0.03	0.04
Waterbody 12 (full)	5.24	14.76
2 ft contour	2.80	7.25
3 ft contour	2.20	4.64
4 ft contour	1.68	2.60
5 ft contour	0.86	1.02
Waterbody 13 (full)	0.09	0.18
1 ft contour	0.06	0.11
2 ft contour	0.04	0.06
3 ft contour	0.03	0.02
Waterbody 14 (full)	0.05	0.08
1 ft contour	0.03	0.04
2 ft contour	0.02	0.01
Waterbody 15 (full)	8.78	46.17
2 ft contour	6.97	30.28
4 ft contour	3.78	19.51
6 ft contour	2.67	13.09
8 ft contour	2.08	8.26
10 ft contour	1.36	4.66
12 ft contour	0.90	2.38
14 ft contour	0.52	0.92
16 ft contour	0.19	0.15
Waterbody 16 (full)	7.24	60.27
3 ft contour	5.48	41.13
6 ft contour	3.89	26.53
9 ft contour	2.59	16.46
12 ft contour	1.72	9.79
15 ft contour	1.06	5.50
18 ft contour	0.68	2.74
21 ft contour	0.39	1.06
Waterbody 17 (full)	1.01	5.95
3 ft contour	0.70	3.38
6 ft contour	0.45	1.64
9 ft contour	0.21	0.56
12 ft contour	0.06	0.07

Table A6: Estimated total quarterly unmapped waterbody storage within the Southeast Watershed Planning Region of Oklahoma. Quarters in **bold** had available imagery from the United States Department of Agriculture National Agricultural Imagery Program used to calculate waterbody surface area.

	Total Unmapped Waterbody Storage (cm)			
Year	Q1	Q2	Q3	Q4
2007	0.83	0.99	0.60	0.82
2008	1.31	**0.86**	0.43	0.70
2009	0.78	1.07	0.78	1.29
2010	1.02	0.42	**0.38**	0.75
2011	0.58	0.82	0.20	1.26
2012	1.18	0.26	0.41	0.61
2013	0.93	0.76	**0.38**	1.10
2014	0.64	0.68	0.42	0.83
2015	0.99	1.48	**0.09**	2.05
2016	0.95	0.86	0.49	0.63
2017	0.91	**1.00**	0.66	0.77

Table A7: Estimated quarterly change in equivalent water thickness (EWT) in cm for the Southeast Watershed Planning Region of Oklahoma (SEWPR). EWT represents the total amount of surface water, groundwater, and soil moisture across the SEWPR. Quarters in *italics* were estimated using linear interpolation (Equation 14). 2017 Q3 and Q4 (denoted with *) were estimated using a regression model (Equation 15) due to a lack of available data for those quarters. Data from the Gravity Recovery and Climate Experiment satellite mission.

	Change in EWT (cm)			
Year	Q1	Q2	Q3	Q4
2007	2.2	7.9	-22.0	8.7
2008	16.7	-20.4	-1.2	4.0
2009	8.1	-14.3	18.7	1.3
2010	-1.2	-14.2	-12.7	8.9
2011	4.9	-16.6	-6.8	21.7
2012	8.8	-24.4	-3.2	10.0
2013	9.8	-11.5	-3.6	15.4
2014	1.6	-8.9	-9.3	11.8
2015	11.8	3.8	-13.9	27.8
2016	-6.0	-16.1	-1.2	7.2
2017	7.1	-3.5	-8.7*	5.3*

Table A8: Quarterly depths in cm for all water balance model components including precipitation (*P*), streamflow out (Q_{out}), evapotranspiration (*ET*), surface storage change (ΔS_{surf}), and sub-surface storage change (ΔS_{sub}). Negative depths for ΔS_{surf} and ΔS_{sub} indicate a decrease in total storage from the previous quarter. Maximum values for each component are written in **bold**, minimum values are written in *italics*.

Year	Quarter	P	Q_{out}	ET	ΔS_{surf}	ΔS_{sub}
2007	1	27.5	22.8	8.2	-3.2	5.0
	2	60.7	10.9	35.9	4.4	3.9
	3	49.6	35.1	48.7	-5.3	-16.9
	4	30.5	5.2	11.9	1.0	7.6
2008	1	56.2	27.4	9.4	7.8	8.9
	2	59.5	33.8	41.5	-7.8	-12.6
	3	37.9	5.7	46.8	0.0	-1.1
	4	22.9	4.2	10.9	1.9	2.0
2009	1	24.3	6.9	7.9	-1.5	9.6
	2	64.8	40.3	35.8	0.0	-14.5
	3	60.4	10.2	49.6	0.5	**18.5**
	4	59.2	39.8	15.0	0.9	0.5
2010	1	39.7	30.8	9.3	-2.8	1.4
	2	30.9	7.5	39.9	-0.2	-14.0
	3	33.5	3.0	44.9	-1.4	-10.9
	4	26.3	1.8	11.7	-0.1	8.5
2011	1	12.9	4.9	7.7	0.4	5.0
	2	55.2	19.6	41.1	1.2	-18.9
	3	16.5	1.9	37.7	-1.4	-3.7
	4	54.3	12.6	10.6	2.5	18.0
2012	1	48.6	23.7	9.3	1.5	6.6
	2	20.7	8.3	38.8	-3.8	-19.4
	3	32.0	1.5	41.4	-1.2	-2.3
	4	16.2	1.0	9.6	-0.2	10.7
2013	1	33.5	5.0	8.2	4.0	5.1
	2	50.0	18.4	38.9	-0.6	-11.1
	3	31.6	2.8	47.0	-1.1	-2.2
	4	45.9	12.2	11.8	1.0	14.7
2014	1	17.1	10.3	8.7	-0.4	1.8
	2	45.3	17.9	38.9	0.0	-9.0
	3	41.1	6.3	**51.3**	-1.0	-8.3
	4	30.9	4.8	12.3	0.5	11.4
2015	1	37.5	19.2	9.0	2.4	9.1
	2	92.9	**53.0**	41.8	9.3	-5.4

	3	20.1	16.5	44.8	-10.7	-1.3
	4	**98.6**	31.6	10.0	**16.5**	8.0
2016	1	34.4	39.1	8.4	-17.0	12.7
	2	57.5	23.8	40.8	-0.7	-16.0
	3	41.1	4.9	46.0	-0.5	-0.3
	4	18.3	2.3	10.7	-0.5	7.9
2017	1	31.5	5.7	7.7	0.8	6.0
	2	42.8	8.8	39.6	0.2	-3.8
	3	53.8	9.5	50.4	-0.7	-8.0
	4	25.9	2.0	10.4	-1.2	5.3
Mean of 2007-2017	1	33.0	17.8	8.5	-0.7	6.5
	2	52.7	22.0	39.4	0.2	-11.0
	3	38.0	8.8	46.2	-2.1	-3.3
	4	39.0	10.7	11.4	2.0	8.6